Journal Pre-proofs

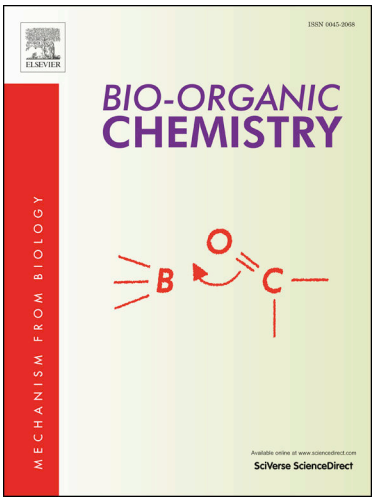

Design, synthesis and biological evaluation of new series of hexahydroquinoline and fused quinoline derivatives as potent inhibitors of wild-type EGFR and mutant EGFR (L858R and T790M)

Mennatallah A. Shaheen, Ali A. El-Emam, Nadia S. El-Gohary

PII: S0045-2068(20)31572-8
DOI: https://doi.org/10.1016/j.bioorg.2020.104274
Reference: YBIOO 104274

To appear in: *Bioorganic Chemistry*

Received Date: 4 July 2020
Revised Date: 6 September 2020
Accepted Date: 9 September 2020

Please cite this article as: M.A. Shaheen, A.A. El-Emam, N.S. El-Gohary, Design, synthesis and biological evaluation of new series of hexahydroquinoline and fused quinoline derivatives as potent inhibitors of wild-type EGFR and mutant EGFR (L858R and T790M), *Bioorganic Chemistry* (2020), doi: https://doi.org/10.1016/j.bioorg.2020.104274

Design, synthesis and biological evaluation of new series of hexahydroquinoline and fused quinoline derivatives as potent inhibitors of wild-type EGFR and mutant EGFR (L858R and T790M)

Mennatallah A. Shaheen[a,b], Ali A. El-Emam[a], Nadia S. El-Gohary[a,*]

[a]*Department of Medicinal Chemistry, Faculty of Pharmacy, Mansoura University, Mansoura 35516, Egypt*
[b]*Department of Pharmaceutical Chemistry, Faculty of Pharmacy, Horus University, New Damietta, Egypt*

[*]Corresponding author: dr.nadiaelgohary@yahoo.com, el_gohary@mans.edu.eg

ABSTRACT: New series of hexahydroquinoline and fused quinoline derivatives were designed and synthesized. The thirty seven new compounds were screened for *in vitro* antitumor activity over HepG2, HCT-116 and MCF-7 cancer cell lines. Results indicated that compounds **2e, 2h, 5b, 5c, 6a, 7d** and **9b** have the strongest potency over the three cancer cells, and they were further screened for *in vitro* antitumor activity over NSCLC cell lines (A431 and H1975), as well as cytotoxicity against WI38 and WISH normal cell lines. Results revealed that **7d** potently inhibited the growth of H1975 cells harboring $EGFR^{T790M}$ mutation (IC_{50} = 1.32±0.2 μM) over A431 cells overexpressing $EGFR^{WT}$ (IC_{50} = 4.96±0.3 μM). Moreover, the seven compounds displayed low cytotoxicity against the tested normal cells. The seven potent antitumor compounds were examined for their ability to inhibit the activity of $EGFR^{WT}$. The attained data manifested that **7d** has remarkable $EGFR^{WT}$ inhibitory activity (IC_{50} = 0.083±0.002 μM) compared to erlotinib (IC_{50} = 0.067±0.002 μM). Compound **7d** was further studied for its enzymatic inhibitory activity against other eight human kinases, and it displayed outstanding inhibitory activity against $EGFR^{L858R}$ and $EGFR^{T790M}$ mutants (IC_{50} = 0.053±0.002, 0.026±0.001 μM, respectively), as well as JAK3 (IC_{50} = 0.069±0.003 μM). Analysis of cell cycle evidenced that **7d** induces cell cycle arrest in G2/M and pre-G1 phases in the tested cancer cells. In addition, cancer cell death induced by **7d** was evidenced to take place *via* apoptosis supported by elevated Bax/Bcl-2 ratio in the tested cancer cells. Moreover, docking results confirmed the good binding interactions of **7d** with $EGFR^{WT}$, $EGFR^{L858R}$, $EGFR^{T790M}$ and JAK3, which came in agreement with the results of *in vitro* enzyme assay. Further, **7d** is predicted to have good oral absorption, good drug-likeness properties and low toxicity risks in human.

Keywords: Hexahydroquinolines, Fused quinolines, Antitumor, EGFR inhibition, Cell cycle analysis, Apoptosis, Computational studies.

1. Introduction

Cancer is a hazardous disease affecting human in developed and developing countries [1]. Currently, treatment strategies include surgery [2], chemotherapy [3] and radiotherapy [4]. Despite the extensive research and rapid progress in cancer treatment, there is an urgent need for new therapies, and it is important to recognize new agents and new targets for cancer treatment. Receptor tyrosine kinases play a substantial role in signal transduction pathways that control cell division and differentiation. Epidermal growth factor receptor tyrosine kinase (EGFR-TK) belongs to a family of receptor tyrosine kinases that includes three other members (erbB2/HER-2, erbB3/HER-3 and erbB4/HER-4) [5,6].

EGFR-TK is an essential enzyme for intracellular signaling and cell transformation, and anomalous expression of this enzyme was reported in a variety of human malignancies, including non-small cell lung cancer (NSCLC) [7], hepatocellular [8], colorectal [9] and breast [10] cancers. As such, inhibition of EGFR-TK provides a rational basis for a class of targeted therapies, EGFR-TK inhibitors (EGFR-TKIs). EGFR-TKIs compete with ATP for ATP-binding site on EGFR. The ATP-binding site (Fig. 1) has the following characteristic features: Adenine binding region that contains two principal hydrogen bonds formed through interaction of N1 and N6 of the adenine ring with the corresponding amino acids. Lots of EGFR-TKIs use one of the two hydrogen bonds. Sugar pocket that represents a hydrophilic region. Hydrophobic binding regions and channels, though not used by ATP but play an important role in binding affinity and inhibitor selectivity. Phosphate binding region which is largely solvent exposed, and can be used for improving inhibitor selectivity [11].

In the last few years, the oncogenic role of EGFR has been more finely characterized due to the improved understanding of the mechanisms of receptor activation, the finding of somatic mutations of the receptor as well as mutations in the components of the signaling pathway, and in a great measure due to the excellent success of anti-EGFR therapies in clinic [12]. First-generation EGFR-TKIs such as gefitinib [13] and erlotinib [14] (Fig. 2) were proved to be effective in treatment of NSCLC; however, drug resistance rapidly develops. Hence, there is still an urgent need for effective clinical medicines that could overcome drug resistance in patients with advanced NSCLC harboring EGFR-mutations

Studies revealed that T790M ‘gatekeeper’ mutation in EGFR was the most common mechanism of resistance to the first-generation EGFR-TKIs [15,16]. Also, L858R mutation was reported as another mechanism of resistance to first-generation EGFR-TKIs [17]. To overcome resistance to first-generation EGFR-TKIs, the second-generation EGFR-TKIs (e.g., pelitinib

[18] and neratinib [19]) (Fig 2) were developed; however, acquired resistance to these agents invariably develops. Studies proved that T790M mutation in EGFR gene was also a common mechanism of resistance to the second-generation EGFR-TKIs [20]. Accordingly, third-generation EGFR-TKIs (e.g., osimertinib [21] and olmutinib [22]) (Fig. 2) were developed to overcome resistance to first- and second-generations EGFR-TKIs, and they enabled the irreversible binding to Cys797 residue in the ATP-binding site. In particular, osimertinib showed great selectivity toward the drug-resistant mutant $EGFR^{T790M}$ over the wild-type EGFR ($EGFR^{WT}$), which made it an efficacious medical regimen for patients harboring $EGFR^{T790M}$ mutation [20,23-25]. Because T790M [15,16] and L858R [17] are the frequent mutations that lead to resistance to EGFR-TKIs, we found it interesting to develop new drugs targeting $EGFR^{L858R}$ and $EGFR^{T790M}$ mutants to overcome resistance to first- and second-generation EGFR-TKIs in patients with advanced NSCLC harboring EGFR-mutations.

2. Rational and design

Quinoline is an important scaffold for a variety of anticancer agents that target a diverse range of receptor tyrosine kinases. The most widely studied of these receptors is EGFR-TK. Pelitinib (Figs. 2 and 3), a quinoline-3-carbonitrile derivative, is an anticancer agent with irreversible EGFR-TK inhibitory activity [18]. Furthermore, neratinib (Figs. 2 and 3) is an EGFR-TK inhibitor that could be used as an adjuvant therapy in patients with early stage breast cancer in which HER2 is overexpressed [19]. Moreover, quinoline-3-carbonitriles **A** [26] (Figs. 2 and 3) and **B** [26] (Fig. 2) displayed potent antitumor activity against human epidermoid (A431), breast (SKBR3) and colon (SW620) cancer cells, as well as potent EGFR-TK inhibitory activity. The quinoline-3-carboxamide derivative **C** [27] (Figs. 2 and 3) was found to elicit outstanding antitumor activity against MCF-7 cancer cells through targeting EGFR-TK. Further, the hexahydroquinoline-3-carboxylate **D** [28] (Figs. 2 and 3) was described as promising antitumor agent against human alveolar basal epithelial (A549) and small cell lung (H446) cancer cells through targeting EGFR-TK. All these quinoline derivatives were proved to act *via* competing with ATP for binding at the catalytic domain of EGFR-TK, and they share the essential pharmacophoric features required for EGFR-TK inhibition, including quinoline or hexahydroquinoline as a central heteroaromatic ring (occupies the adenine binding region), cyano, carboxamide or ester substitution for H-bond formation with the ATP-binding site, hydrophobic head (occupies the hydrophobic binding region I) and hydrophobic tail (occupies the hydrophobic binding region II). Taking these literature findings into consideration, and as an

attempt to prepare new antitumor EGFR-TKIs, the hexahydroquinoline scaffold was introduced as a central heteroaromatic ring similarly to the hexahydroquinoline EGFR-TKI **D**, and the cyano group or carboxylic (bioisostere of carboxamide) was retained at 3-postion. Further, the hydrophobic head at 4-position was replaced with various hydrophobic aromatic moieties (substituted with halogens as lipophilic electron-withdrawing groups); in addition, two methyl substituents were introduced at 7-position of hexahydroquinoline scaffold as a hydrophobic tail in order to prepare three new series of hexahydroquinolines **2a-j, 3a-c** and **4a-h** that could target EGFR-TK (Fig. 3).

Furthermore, the bioactive pyrimidine **E** [29] (Figs. 4 and 5) possessed potent antitumor activity against the NSCLC cells (H3255, A431, HCC827, H1975 and PC-9) through targeting $EGFR^{WT}$ and $EGFR^{L858R}$. Additionally, the pyrimidines **F** [30] (Figs. 4 and 5) and **G** [30] (Fig. 4) were established to display prominent antitumor activity against breast (MCF-7), colon (HCT-116) and human alveolar basal epithelial (A549) cancer cells through targeting EGFR-TK. Besides, several benzylideneamine derivatives **H** [31] (Figs. 4 and 5) were described as promising antitumor agents against human kidney epithelial (293T) cancer cells and EGFR-TKIs. Moreover, the phenylthiourea derivatives **I** [32] (Figs. 4 and 5) were proved to exhibit outstanding antitumor efficacy over MCF-7 cancer cells through targeting EGFR-TK. Furthermore, [1,2,4]triazole **J** [33] (Figs. 4 and 5) displayed interesting antitumor efficacy over HepG2, MCF-7 and HCT-116 cancer cells, as well as potent EGFR-TK inhibitory activity, whereas the [1,2,4]triazole derivatives **K** [34] (Figs. 4 and 5) were established as promising antitumor agents against A549 and small cell lung (H446) cancer cells *via* targeting EGFR-TK. Inspired by these findings and as an attempt to study the effect of replacement of the bicyclic quinoline scaffold in the small-molecule inhibitors with large tricyclic or tetracyclic scaffolds on the antitumor and EGFR-TK inhibitory activities, the concept of molecular hybridization was followed to prepare new series of fused quinoline derivatives. Molecular hybridization involves the combination of different pharmacophoric moieties with pertinent biological activities to obtain new hybrid compounds with improved activity, selectivity and safety [35,36]. Accordingly, new series of tetrahydropyrimidoquinolines **5a-f**, hexahydropyrimidoquinolines **6a,b**, and tetrahydro[1,2,4]triazolopyrimidoquinolines **9a,b** were designed through incorporation of pyrimidine and [1,2,4]triazole rings into the hexahydroquinoline scaffold (Fig. 5). Further, the manipulation strategy embraced the incorporation of benzylideneamine and phenylthiourea moieties into the hexahydropyrimidoquinoline scaffold (series **7a-d** and **8a,b**, respectively) (Fig. 5) in order to verify the importance of these moieties for the antitumor and EGFR-TK inhibitory activities.

The designed new analogs were prepared and screened for antitumor and EGFR-TK inhibitory activities. However, inhibition of EGFR-TK activity is not sufficient to eradicate tumors, meaning that a single-target chemotherapeutic agent is not enough to treat the symptoms. Since single-targeted chemotherapeutics have limited antitumor activity, researchers have done their best to find out other better strategies for cancer remedy, for instance, the multi-target drug design strategy, which is based on the design and synthesis of several bioactive molecules that direct multiple targets to induce different alterations of cellular function [37-39]. Multitargeting chemotherapeutics have the potential to demonstrate additive or synergistic effects compared to the single-targeted ones; therefore, they attained an increasing interest in combating resistant cancer cells [40].

Structure-activity relationship study revealed that the 4-imino-3-(4-(dimethylamino)benzylidene)amino)hexahydropyrimidoquinoline derivative **7d** has the most potent antitumor and $EGFR^{WT}$ inhibitory activities, the promising potency of **7d** might be attributed to presence of 4-(dimethylamino)benzylidene)amino moiety that offers an extra hydrophobic site, and an extra hydrogen bond acceptor site for binding interactions with the target. Additionally, compound **7d** was evaluated for its ability to inhibit other eight enzymes from different classes of human tyrosine kinases ($EGFR^{L858R}$, $EGFR^{T790M}$, TYK2, JAK3, BTK, VEGFR-2, mTOR and HER-4) to ensure its multi-targeted activity, and hence good curative effect. Also, its capability to induce cell cycle arrest and cell apoptosis, as well as its effect on Bax/Bcl-2 ratio in HepG2, HCT-116 and MCF-7 cancer cells were assessed. Further, molecular docking studies utilizing the crystal structures of $EGFR^{WT}$, $EGFR^{L858R}$, $EGFR^{T790M}$ and JAK3 were performed to investigate the possible binding patterns of the potent compound **7d** with these target kinases.

3. Results and discussion

3.1. Chemistry

A general approach to synthesize the designed compounds is outlined in Schemes 1-3. The arylidenemalononitriles **1a-j** [41-48] were synthesized *via* reaction of araldehydes with malononitrile in ethanol [41,48]. In Scheme 1, 2-amino-4-aryl-7,7-dimethyl-5-oxo-5,6,7,8-tetrahydroquinoline-3-carbonitriles **2a-j** were prepared *via* reaction of arylidinemalononitriles **1a-j** with dimedone in refluxing ethanol in presence of ammonium acetate adopting the literature

procedure [49]. The structures of **2a-j** were confirmed on the basis of IR, ^{1}H NMR, ^{13}C NMR, mass spectra and X-ray crystallography (Fig. 6).

Referring to Scheme 2, heating *ortho* aminonitriles **2a, 2b** and **2f** with sulfuric acid 70% at 70 °C for 1-2 h afforded the corresponding *ortho* aminocarboxylic acid derivatives **3a-c**. Refluxing *ortho* aminonitriles **2a-d**, **2f-h** and **2j** with excess triethyl orthoformate afforded the corresponding ethyl formimidates **4a-h** following the literature procedure [49,50]. Compounds **4a-e** and **4h** were used as precursors for the synthesis of new pyrimidoquinoline derivatives. Adopting the reported method [49,50], compounds **4a-e** and **4h** were refluxed with ammonia solution 35% in ethanol to give the corresponding 4-aminopyrimidoquinoline derivatives **5a-f**. Furthermore, the hexahydropyrimidoquinolines **6a,b** were synthesized *via* reaction of **4a,b** with hydrazine hydrate in ethanol at room temperature according to the reported procedure [51]. With respect to Scheme 3, the 3-amino-4-iminohexahydropyrimidoquinoline **6a** was allowed to react with benzaldehyde derivatives in refluxing ethanol in presence of a catalytic amount of piperidine to produce the corresponding 3-(4-(un)substituted benzylidene)amino)hexahydropyrimidoquinolines **7a-d**. The 3-(4-substituted phenyl)-1-(substituted hexahydropyrimidoquinolin-3-yl)thioureas **8a,b** were synthesized *via* refluxing 3-amino-4-iminohexahydropyrimidoquinoline **6a** with the appropriate phenyl isothiocyanate in ethanol. Upon heating 3-amino-4-iminohexahydropyrimidoquinolines **6a,b** with triethyl orthoformate, the corresponding tetrahydrotriazolopyrimidoquinolines **9a,b** were attained. The structures of the new compounds were ascertained by spectral and elemental analyses.

3.2. Biology

3.2.1. Cytotoxicity testing

3.2.1.1. In vitro antitumor testing

MTT assay was followed to assess the antitumor activity of the thirty seven new derivatives over hepatocellular (HepG2), colorectal (HCT-116) and breast (MCF-7) cancer cell lines [52-54], utilizing doxorubicin, erlotinib and osimertinib as reference drugs. Doxorubicin is one of the most effective chemotherapeutic agents against several types of human cancers, including HepG2 [55], HCT-116 [56] and MCF-7 [55] cancers. Two different mechanisms of action have been proposed for doxorubicin, (i) intercalation of DNA and inhibition of topoisomerase II leading to changes in chromatin structure, (ii) generation of free radicals and oxidative damage to biomolecules [57]. However, doxorubicin resistance is a serious problem

and several mechanisms such as reduction of drug uptake, activation of drug detoxification, increased drug efflux and DNA repair capacity, and deflecting apoptotic pathway [58,59] have been proposed.

Concentrations of compounds that induce 50% inhibition of cell viability (IC_{50}, μM) were determined (Table 1). Results showed that **2e, 2h, 5b, 5c, 6a, 7d** and **9b** are the most potent members against all selected cancer cells (IC_{50} = 2.91-10.35 μM) in comparison to the doxorubicin (IC_{50} = 4.17-5.23 μM), erlotinib (IC_{50} = 4.16-11.21 μM), and osimertinib (IC_{50} = 8.44-9.72 μM). Also, compounds **4d, 4h** and **8b** were proved to have strong activity against HCT-116 cells (IC_{50} = 3.85-9.82 μM). Further, compounds **4g** and **7b** manifested strong activity against HepG2 cells (IC_{50} = 10.17±0.9 and 9.50±0.8 μM, respectively). Additionally, **4g** exhibited high potency over MCF-7 cells (IC_{50} = 7.92 μM). On the other hand, **2f** and **5d** demonstrated moderate efficacy over the three cancer cells (IC_{50} = 13.64-20.61 μM), whereas **8b** was proved to have moderate activity over HepG2 and MCF-7 cells (IC_{50} = 14.49 and 12.57 μM, respectively). Furthermore, compounds **4b, 4g, 7a** and **7b** were found to be moderately active over HCT-116 cells (IC_{50} = 12.10-19.32 μM). The rest of the tested compounds displayed moderate to weak activity over the three cancer cells.

3.2.1.1.1. Analysis of structure-activity relationship

*Concerning the hexahydroquinolines **2a-j***

With regard to analogs carrying substituted phenyl moiety at 4-position of hexahydroquinoline ring **2a-g**, it is evident that presence of 2,4-difluorophenyl moiety at 4-position of hexahydroquinoline ring led to promising antitumor potency over the three cancer cells (compound **2e**). Replacement of 2,4-difluorophenyl moiety with 2,6-difluorophenyl resulted in decreased activity over the three cancer cells (compound **2f** versus **2e**), and this might be due to the steric hindrance caused by the 2,6-difluoro substituents on the phenyl moiety in **2f**. Replacement of 2,6-difluorophenyl moiety in **2f** with 2-chloro-6-fluorophenyl resulted in decreased activity over the three cancer cells (compound **2d**), and this might be attributed to the increased lipophilicity of **2d** (LogP = 2.32) compared to **2f** (LogP = 1.80). Replacing 2-chloro-6-fluorophenyl moiety in **2d** with 2,6-dichlorophenyl resulted in decreased potency over the three cancer cells (compound **2c** versus **2d**), and this might be attributed to the increased lipophilicity of **2c** (LogP = 2.83) compared to **2d** (LogP = 2.32). Replacing 2,6-dichlorophenyl moiety in **2c** with 2,3-dichlorophenyl resulted in decreased potency over all cancer cells (compound **2a** versus **2c**), while its replacement with 3,4-dichlorophenyl resulted in improved activity over HCT-116

and MCF-7 cells, and decreased activity over HepG2 (compound **2b** versus **2c**). Further, replacement of 2,4-difluorophenyl moiety in **2e** with biphenyl led to weak activity over the three cancer cells (compound **2g**). On the other hand, presence of [1,3]benzodioxol-4-yl moiety at 4-position of hexahydroquinoline resulted in high potency over the three cancer cells (compound **2h**). Replacement of [1,3]benzodioxol-4-yl moiety with naphthalen-2-yl led to weak activity over all cancer cells (compound **2i** versus **2h**). Contrariwise, replacement of naphthalen-2-yl moiety in **2i** with anthracen-9-yl resulted in improved potency over all cancer cells (compound **2j** versus **2i**).

*Concerning the 2-aminohexahydroquinoline-3-carboxylic acid analogs **3a-c***

Presence of 3,4-dichlorophenyl moiety at 4-position of hexahydroquinoline-3-carboxylic acid led to moderate activity over HepG2, and weak activity over HCT-116 and MCF-7 cells (compound **3b**). Replacement of 3,4-dichlorophenyl moiety in **3b** with 2,3-dichlorophenyl or 2,6-difluorophenyl resulted in weak or no activity over all cancer cells (compounds **3a** and **3c**, respectively).

*Considering the structures of the ethyl formimidates **4a-h***

With respect to the analogs carrying substituted phenyl moiety at 4-position of hexahydroquinoline ring **4a-f**, it is obvious that presence of 2-chloro-6-fluorophenyl moiety at 4-position of hexahydroquinoline ring led to the highest activity over the three cancer cells (compound **4d**). Replacing 2-chloro-6-fluorophenyl moiety in **4d** with 2,6-dichlorophenyl or 2,6-difluorophenyl resulted in decreased activity over all tested cancer cells (compounds **4c** and **4e**, respectively). Replacing 2,6-dichlorophenyl moiety in **4c** with 2,3-dichlorophenyl counterpart resulted in mild increase in activity over all cancer cells (compound **4a** versus **4c**), while its replacement with 3,4-dichlorophenyl resulted in apparent increase in activity over all selected cancer cells (compound **4b** versus **4c**), and we can conclude that the activity of the dichlorophenyl analogs **4a-c** is influenced by the positions of the two chloro substituents, whereas the decreased activity in **4c** compared to **4a** and **4b** might be due to the steric hinderance caused by the 2,6-dichloro substituents in **4c**. On the other hand, the *N*-(4-((1,1'-biphenyl)-4-yl)hexahydroquinolin-2-yl)formimidate **4f** showed the lowest activity amongst all tested *N*-(4-(substituted phenyl)hexahydroquinolin-2-yl)formimidates, and this might be attributed to the increased lipophilicity of **4f** (LogP = 4.64) in comparison to **4a-e** (LogP = 2.60-4.13). From another point of view, presence of the bicyclic [1,3]benzodioxol-4-yl moiety at 4-position of hexahydroquinoline ring led to eminent potency over all selected cancer cells (compound **4g**). Replacement of [1,3]benzodioxol-4-yl in **4g** with anthracen-9-yl resulted in

mild increase in activity over HCT-116, and mild decrease in activity over HepG2 and MCF-7 cells (compound **4h** versus **4g**).

*With respect to the hexahydropyrimidoquinolines **5a-f***

Presence of 3,4-dichlorophenyl moiety at 5-position of hexahydroquinoline ring led to high potency over the three cancer cells (compound **5b**). Replacement of 3,4-dichlorophenyl moiety in **5b** with 2,3-dichlorophenyl resulted in weak activity over the three cancer cells (compound **5a**), while its replacement with 2,6-dichlorophenyl led to mild increase in activity over HCT-116, and mild decrease in activity over HepG2 and MCF-7 cancer cells (compound **5c** versus **5b**). Replacement of 2,6-dichlorophenyl moiety with 2,6-difluorophenyl resulted in decreased activity over all cancer cells (compound **5e** versus **5c**), and this might be attributed to the decreased lipophilicity of **5e** (LogP = 2.70) compared to **5c** (LogP = 3.73). Replacement of 3,4-dichlorophenyl moiety in **5b** with the polycyclic anthracen-9-yl resulted in decreased activity over the three cancer cells (compound **5f**), and this might be attributed to the bulkiness of the anthracene moiety.

*Referring to the hexahydropyrimidoquinolines **6a,b***

It is obvious that presence of 2,3-dichlorophenyl moiety at 5-position of hexahydropyrimidoquinoline nucleus led to high potency over the three cancer cells (compound **6a**), while its replacement with 3,4-dichlorophenyl led to weak activity over all cancer cells (compound **6b** versus **6a**).

*Considering the structures of the hexahydropyrimidoquinoline derivatives **7a-d***

Presence of unsubstituted benzylideneamino moiety at 3-position of hexahydropyrimidoquinoline scaffold led to moderate activity over the three cancer cells (compound **7a**). Replacement of unsubstituted benzylideneamino moiety in **7a** with 4-chlorobenzylideneamino led to increased activity over HepG2 and HCT-116 cells, and decreased activity over MCF-7 cells (compound **7b**). Replacement of 4-chlorobenzylideneamino moiety in **7b** with 4-bromobenzylideneamino led to apparent decrease in activity over the three cancer cells (compound **7c**), and this might be attributed to the increased lipophilicity of **7c** (LogP = 4.78) compared to **7b** (LogP = 4.65). Contrariwise, replacement of 4-chlorobenzylidene moiety in **7b** with 4-(dimethylamino)benzylidene led to compound **7d** with close potency to doxorubicin and higher potency than erlotinib and osimertinib over the three cancer cells, and this confirms that presence of phenyl substituted with electron-donating group in **7d** led to

higher potency than the unsubstituted phenyl (compound **7a**) or phenyl substituted with electron-withdrawing group (compounds **7b,c**).

*Regarding the activity of 1-(substituted hexahydropyrimidoquinolin-3-yl)-3-(4-substituted phenyl)thiourea derivatives **8a,b***

Presence of 3-(4-chlorophenyl)thiourea moiety at 3-position of hexahydropyrimidoquinoline nucleus led to moderate activity over the three cancer cells (compound **8a**). Replacement of 3-(4-chlorophenyl)thiourea moiety in **8a** with 3-(4-methoxyphenyl)thiourea led to evident increase in activity over all cancer cells (compound **8b** versus **8a**), and this confirms that presence of phenyl substituted with electron-donating group improves the antitumor potency.

*Referring to the tetrahydrotriazolopyrimidoquinolines **9a,b***

Presence of 2,3-dichlorophenyl moiety at 12-position of tetrahydrotriazolopyrimidoquinoline nucleus led to moderate activity over HepG2 and HCT-116 cells, and weak activity over MCF-7 cells (compound **9a**). Replacement of 2,3-dichlorophenyl moiety in **9a** with 3,4-dichlorophenyl led to high potency over the three cancer cells (compound **9b** versus **9a**).

3.2.1.2. Cytotoxicity testing against NSCLC cell lines that overexpress $EGFR^{WT}$ (A431) and mutant $EGFR^{T790M}$ (H1975), as well as normal cell lines (WI38 and WISH)

Cytotoxicity of compounds **2e, 2h, 5b, 5c, 6a, 7d** and **9b** against NSCLC cell lines (A431, overexpressing $EGFR^{WT}$) and (H1975, harboring mutant $EGFR^{T790M}$), as well as lung fibroblast (WI38) and amnion epithelial (WISH) normal cell lines was assessed adopting MTT assay [52-54]. IC_{50} values (μM) were determined, and results are compared to doxorubicin, erlotinib and osimertinib (Table 2). Compound **7d** exhibited potent activity against H1975 cells (IC_{50} = 1.32±0.2 μM) with 3.8-fold selectivity over A431 cells (IC_{50} = 4.96±0.3 μM). The potency of **7d** over A431 cells was proved to be higher that of osimertinib (IC_{50} = 5.63±0.3 μM), whereas its potency over H1975 was half that of osimertinib (IC_{50} = 0.69±0.1 μM), and 6.45 times higher than that of erlotinib (IC_{50} = 8.52±0.5 μM). Similarly, compounds **2e, 2h** and **5c** were proved to be more selective toward H1975 cells (IC_{50} = 7.13±0.6, 3.89±0.4 and 4.46±0.4 μM, respectively) compared to A431 cells (IC_{50} = 9.82±1.0, 5.78±0.5 and 9.10±1.1 μM, respectively). On contrary, compounds **5b, 6a** and **9b** showed higher activity against A431 cells (7.89±0.6, 10.62±1.5 and 9.67±1.3 μM, respectively) over H1975 cells (8.75±0.6, 12.31±1.7 and 10.11±1.3 μM, respectively). Referring to results of cytotoxicity against normal cells (Table 2), the seven tested compounds showed lower cytotoxicity against WI38 (IC_{50} = 39.26-86.42 μM) and WISH (IC_{50} =

19.78-63.37 μM) normal cells than doxorubicin (IC_{50} = 6.72±0.5 and 3.18±0.2 μM, respectively). In addition, the selectivity index (SI) values of **2e, 2h, 5b, 5c, 6a, 7d** and **9b** toward HepG2, HCT-116, MCF-7, A431 and H1975 cancer cells versus WI38 and WISH normal cells were calculated (Table 3). The SI values more than 2 are considered as high selectivity [60,61]. Results indicated that the seven compounds have high SI values toward the five cancer cells versus the two normal cells (SI = 2.09-48.69), and they are expected to be safe antitumor agents. In addition, compound **7d** displayed the highest SI values toward all tested cancer cells (except HCT-116) with the highest SI values toward H1975 NSCLC cells harboring $EGFR^{T790M}$ mutation (SI = 48.69 and 35.14) versus WI38 and WISH normal cells, respectively.

3.2.2. Mechanistic studies

3.2.2.1. Tyrosine kinase assay

The potent antitumor agents in the current study were subjected to further studies to investigate their potential mechanism of action. $EGFR^{WT}$ inhibitory activity of the potent antitumor compounds **2e, 2h, 5b, 5c, 6a, 7d** and **9b** was studied [62], and results are displayed as % inhibition of $EGFR^{WT}$ (at 10 μM) (Fig. 7) and IC_{50} (μM) (Table 4), and they are compared to erlotinib and osimertinib as reference drugs. Compound **7d** demonstrated the highest $EGFR^{WT}$ inhibitory activity (IC_{50} = 0.083±0.002 μM) close to that of erlotinib (IC_{50} = 0.067±0.002 μM) and about 6 times higher than that of osimertinib (IC_{50} = 0.48±0.009 μM), and this result comes in accordance with the antitumor screening results. In addition, compounds **2e, 2h** and **5b** displayed promising $EGFR^{WT}$ inhibitory activity (IC_{50} = 0.153±0.003, 0.129±0.003 and 0.143±0.003 μM, respectively). Additionally, compounds **5c**, **6a** and **9b** exhibited good $EGFR^{WT}$ inhibitory activity (IC_{50} = 0.216±0.005, 0.347±0.007 and 0.459±0.009 μM, respectively). Further, compound **7d** was assessed for its inhibitory activity against $EGFR^{L858R}$ and $EGFR^{T790M}$ mutants [62]. Results are displayed as % inhibition (at 10 μM) (Fig. 8) and IC_{50} (μM) (Table 5), and compared to erlotinib and osimertinib as reference drugs. Compound **7d** displayed potent inhibitory activity against the drug-sensitive $EGFR^{L858R}$ and the drug-resistant $EGFR^{T790M}$ (IC_{50} = 0.053±0.002 and 0.026±0.001 μM, respectively) compared to that of erlotinib (IC_{50} = 0.045±0.001 and 0.443±0.002 μM, respectively) and osimertinib (IC_{50} = 0.025±0.001 and 0.022±0.001 μM, respectively). Actually, the activity of **7d** was close to that of erlotinib over $EGFR^{L858R}$ and 17 times higher than that of erlotinib over $EGFR^{T790M}$. Additionally, **7d** displayed similar activity to that of osimertinib over $EGFR^{T790M}$ and half the activity of

osimertinib over $EGFR^{L858R}$, and we can conclude that **7d** has high selectivity toward mutant forms of EGFR over the wild-type form, and hence it might overcome resistance to EGFR-TKIs that develops due to L858R and T790M mutations of EGFR gene.

Compound **7d** was subjected to further studies against other six different human kinases containing SH2 domain (TYK2) or both SH2 and SH3 domains (JAK3 and BTK) and other human protein or lipid kinases (VEGFR-2, mTOR and HER-4) adopting the kinase profile assay [62], and using erlotinib as a reference drug. Results are expressed as % inhibition (at 10 μM) (Fig. 8) and IC_{50} (μM) (Table 5). Compound **7d** exhibited potent enzymatic inhibitory activity against JAK3 (IC_{50} = 0.069±0.003 μM) which was proved to be 2 times higher than that of erlotinib (IC_{50} = 0.146±0.003 μM). In addition, it showed promising enzymatic inhibitory activity against the other tested human kinases (IC_{50} = 0.089-0.298 μM). Taking together, compound **7d** is considered to be a promising multi-kinase inhibitor (with the highest selectivity toward $EGFR^{T790M}$ mutant) that might prevent drug resistance by interfering with intracellular signaling pathways or by inhibiting mutated binding sites or genes, and hence it could be used as a promising candidate compound for treatment of patients with advanced NSCLC harboring $EGFR^{T790M}$ mutation.

3.2.2.1.1. Analysis of structure-activity relationship

With respect to $EGFR^{WT}$ inhibitory activity, the 3-((4-(dimethylamino)benzylidene)amino)hexahydropyrimidoquinoline **7d** demonstrated the highest $EGFR^{WT}$ inhibitory activity (IC_{50} = 0.083±0.002 μM), the potent inhibitory activity of **7d** might be related to presence of 4-(dimethylamino)benzylidene moiety that carries an extra site for hydrophobic interaction as well as an extra hydrogen bond acceptor site. On the other hand, the 4-amino-5-(3,4-dichlorophenyl)tetrahydropyrimidoquinoline **5b** showed good inhibitory activity (IC_{50} = 0.143±0.003 μM). Replacing 3,4-dichlorophenyl moiety in **5b** with 2,6-dichlorophenyl resulted in decreased inhibitory activity (compound **5c**, IC_{50} = 0.216±0.005 μM), the decreased activity of **5c** in comparison to **5b** might be due to the steric hinderence caused by the 2,6-dichloro substituents on the phenyl moiety in **5c**. Replacing 4-aminotetrahydropyrimidoquinoline in **5b,c** with 3-amino-4-iminohexahydropyrimidoquinoline resulted in obvious decrease in activity (compound **6a**, IC_{50} = 0.347±0.007 μM), and this might be attributed to the possibility of intramolecular hydrogen bonding interaction between 3-amino and 4-imino groups in **6a** that hinders its bonding interaction with $EGFR^{WT}$. Further, replacing hexahydropyrimidoquinoline scaffold in **7d** with hexahydroquinoline led to decreased activity (compounds **2e** and **2h**, IC_{50} =

0.153±0.003 and 0.129±0.003 μM, respectively). Comparing the activity of compounds **2e** and **2h**, it is evident that presence of 3,4-difluorophenyl moiety at 4-position of hexahydroquinoline led to good $EGFR^{WT}$ inhibitory activity (compound **2e**, IC_{50} = 0.153±0.003 μM). Replacing 3,4-difluorophenyl moiety in **2e** with [1,3]benzodioxol-4-yl led to increased potency (compound **2h**, IC_{50} = 0.129±0.003 μM), and this might be attributed to presence of two extra hydrogen bond acceptor sites in **2h**. On contrary, replacing the hexahydropyrimidoquinoline scaffold in **7d** with tetrahydrotriazolopyrimidoquinoline resulted in obvious decrease in activity (compound **9b**, IC_{50} = 0.459±0.009 μM), and this might be attributed to the decreased number of hydrogen bond acceptor and donor sites in **9b** as well as the absence of the extra hydrophobic site present in **7d**.

3.2.2.2. Analysis of cell cycle by flow cytometry assay

Several studies evidenced that EGFR-TKIs are capable of inducing cell cycle arrest and cellular apoptosis [63-66]. To further understand the antitumor mechanism of compound **7d**, its effects on cell cycle progression in HepG2, HCT-116 and MCF-7 cells were examined (at the IC_{50} of the corresponding cell line) [67-69]. Analysis of cell cycle in HepG2 showed that **7d** decreased % cells in G0/G1 phase (from 51.88% to 36.22%), and increased % cells in S phase (from 34.03% to 38.12%), G2/M phase (from 14.09% to 25.66%) and pre-G1 phase (from 1.44% to 17.85%) (Figs. 9 and 10). Analysis of cell cycle in HCT-116 illustrated that **7d** decreased % cells in G0/G1 phase (from 48.52% to 34.05%) and S phase (from 35.61% to 27.44%), and increased % cells in G2/M phase (from 15.87% to 38.51%) and pre-G1 phase (from 1.19% to 22.49%) (Figs. 9 and 10). Regarding results of cell cycle analysis in MCF-7, **7d** decreased % cells in G0/G1 phase (from 56.14% to 28.99%) and S phase (from 32.91% to 29.41%), and increased % cells in G2/M phase (from 10.95% to 41.6%) and pre-G1 phase (from 1.78% to 32.11%) (Figs. 9 and 10). From the attained results, we can conclude that **7d** demonstrated considerable elevation in cell population of the three tested cancer cells in G2/M phase but at different intensities, and induced cellular apoptosis in pre-G1 phase (Figs. 9 and 10), and accordingly stopped the mitotic cycle.

3.2.2.3. Induction of cellular apoptosis

Cancer is one of the diseases where little cellular apoptosis develops leading to growth of malignant cells that will not die. Apoptosis is a well-known target in cancer therapeutics [70]. The mechanism of apoptosis is complex and involves different pathways [70]. Therefore, compound **7d** was examined for its capability to induce apoptosis in HepG2, HCT-116 and

MCF-7 cancer cells adopting the flow cytometry assay [67-69]. The flow cytometry assay results of cells pigmented with propidium iodide (PI) and annexin V-fluorescein isothiocyanate (annexin V-FITC) are shown in Fig. 11. The annexin V/PI double staining disclosed that after 24 h of exposure, **7d** (at the IC_{50} of the corresponding cell line) induced early and late apoptosis in the three cancer cells compared to the untreated cells. Compound **7d** induced higher percentage of total apoptosis in MCF-7 cells compared to HepG2 and HCT-116 cells (Figs. 11 and 12). On contrary, it induced weak necrosis in the three treated cancer cells (Figs. 11 and 12) affirming that cell death induced by **7d** takes place mainly *via* apoptosis.

3.2.2.4. Analysis of levels of Bax and Bcl-2 proteins

Bcl-2 (B-cell lymphoma 2) family members are significant regulators of apoptosis that can be classified into three groups of proteins [71]. The first group protects against apoptosis (Bcl-2 itself) [71]. The second group is represented by Bax (Bcl-2 associated protein X) and Bak (Bcl-2 antagonist), which are the key activators of the apoptosis machinery in response to cellular stress stimuli [71]. The third group is comprised of different categories of proteins such as Bid (BH3 interacting death domain), Bim (Bcl-2 interacting mediator) and others [71]. Overexpression of the antiapoptotic protein Bcl-2 leads to antagonism of apoptosis and development of resistance of tumor cells to common chemotherapeutic agents. Thus, development of new drugs that can inhibit the antiapoptotic action of Bcl-2 is a very attractive strategy in the design of anticancer agents [72]. The effect of compound **7d** on the expression levels of Bax and Bcl-2 proteins was determined after treatment of HepG2, HCT-116 and MCF-7 cancer cells with compound **7d** (at 10 μM) [72] (Fig. 13). Compound **7d** showed 5.71, 8.15 and 16.51-fold up-regulation in the level of the proapoptotic protein Bax in HepG2, HCT-116 and MCF-7 cells, respectively compared to the untreated cells, while it markedly down-regulated the level of the antiapoptotic protein Bcl-2 in HepG2, HCT-116 and MCF-7 cells up to 0.72, 0.53 and 0.31-fold compared to the untreated cells. These findings proved that induction of apoptosis by the active compound **7d** was achieved through up-regulation of Bax and down-regulation of Bcl-2.

4. Computational studies

4.1. Binding mode of compound 7d to $EGFR^{WT}$, $EGFR^{L858R}$, $EGFR^{T790M}$ and JAK3

In order to provide a deep insight into the binding mode of compound **7d** (potent $EGFR^{WT}$, $EGFR^{L858R}$, $EGFR^{T790M}$ and JAK3 inhibitor) to $EGFR^{WT}$, $EGFR^{L858R}$, $EGFR^{T790M}$ and JAK3, a

study based on the crystal structures of $EGFR^{WT}$ (PDB code: 3W2S) [73], $EGFR^{L858R}$ (PDB code: 4LQM) [74], $EGFR^{T790M}$ (PDB code: 2JIV) [75] and JAK3 (PDB code: 5TTV) [76] was accomplished applying "molecular operating environment (MOE) version 2014.0901" Chemical Computing Group Inc. software [77]. Results of docking of **7d** into the ATP-binding pocket of $EGFR^{WT}$ illustrated that it interacts with $EGFR^{WT}$ through two hydrogen bonding interactions, one formed between NH of pyrimidoquinoline and Asp800, and the second one formed between oxygen atom of C=O and Ser720, as well as one arene-H interaction between the phenyl of benzylidene moiety and Leu844 (Fig. 14). Results of docking of **7d** into $EGFR^{L858R}$ revealed that it forms one hydrogen bonding interaction between the Cl at 3-position of phenyl ring and Met793, as well as two arene-H interactions, one formed between the phenyl of benzylidene moiety and Leu718, and the second one formed between the 5-phenyl moiety and Val726 (Fig. 15). Docking results of **7d** into $EGFR^{T790M}$ showed that it forms two hydrogen bonding interactions through N1 and N3 of pyrimidoquinoline with Met793, as well as one arene-H interaction between the phenyl of benzylidene moiety and Gly796 (Fig. 16). Further, docking results of **7d** into the binding site of JAK3 indicated that it binds to JAK3 through two hydrogen bonding interactions, one formed between the C=NH group and Arg911, and the second one formed between N1 and Lys830, as well as one arene-H interaction between the 5-phenyl moiety and Arg953 (Fig. 17). Summary of residues involved in arene-H interaction, number of hydrogen bonds, residues involved in hydrogen bonding interaction and docking interaction energy (kcal/mol) of compound **7d** with $EGFR^{WT}$, $EGFR^{L858R}$, $EGFR^{T790M}$ and JAK3 is presented in Table 6. These results came in agreement with the results of *in vitro* enzyme assay, and gave a preliminary conception of the binding mode of the new analogs.

4.2. *In silico* studies

In silico studies have a significant rule in discovery of new drugs, since they are of great importance in predicting the physicochemical properties, pharmacokinetics, and toxicity of drugs of biological interest [78]. For the new compounds, Lipinski's rule [79] and Veber's parameters [80] were analyzed using Molinspiration software [81]. Further, ADME properties were predicted using PreADMET software [82]. Likewise, toxicity risks in human and drug-likeness were prophesied applying Osiris property explorer software [83].

4.2.1. Molinspiration calculations

Lipinski's rule helps to predict whether a biologically active compound is likely to have the chemical and physical properties that ensure good oral absorption or not [79]. Likewise, topological polar surface area (TPSA) and number of rotatable bonds (Nrotb) affect the extent of drug absorption [80]. Molinspiration software [81] was applied for analysis of TPSA, Nrotb and Lipinski's rule parameters of the new compounds. Results (Table 7) illustrated that all of the new compounds agreed with the adequate criteria of TPSA, Nrotb and Lipinski's rule with zero or one violation of Lipinski's rule, hence they are predicted to have good oral absorption.

4.2.2. ADME prediction

PreADMET software [82] was utilized to analyze the ADME characteristics of the new compounds. Blood-brain barrier (BBB) penetration, plasma protein binding (%PPB) and human intestinal absorption (%HIA) were predicted, and results are listed in Table 8. It was reported that drugs with BBB (C_{brain}/C_{blood}) values more than 1 are predicted to be CNS-active candidates, whereas those with BBB (C_{brain}/C_{blood}) values less than 1 are foreseen to be CNS-inactive candidates [84]. Compounds **2a, 2c, 5a, 5c, 6a,b, 7a-d, 8a,b** and **9a** are foreseen to be CNS-active candidates (BBB penetration = 1.05-6.24). On contrary, the remaining compounds are foreseen to be CNS-inactive candidates (BBB penetration = 0.05-0.89). Additionally, all of the analyzed compounds are predicted to display excellent plasma protein binding (%PPB = 62.55-100.00%), and excellent human intestinal absorption (%HIA = 88.79-97.22%).

4.2.3. Prediction of toxicity risks in human and drug-likeness

The new derivatives were analyzed for prediction of various toxicity risks in human (tumorigenicity, irritancy and mutagenicity) and drug-likeness using Osiris software [83]. Results (Table 9) manifested that all of the analyzed compounds are expected to be non-tumorigenic (except **2j, 4h** and **5f**), non-irritating (except **2j, 4h** and **5f**) and non-mutagenic (except **2j, 4h** and **5f**).

Drug-likeness rules are used for studying the drug-like properties of a molecule. A positive value indicates that the compound has fragments which are frequently present in commercial drugs [85]. Results (Table 9) showed that **3a,b, 5a-c, 6a,b, 7a-d, 8a,b** and **9a,b** have acceptable drug-likeness values.

5. Conclusion

Results of antitumor assay assured that compounds **2e, 2h, 5b, 5c, 6a, 7d** and **9b** are the most potent members over HepG2, HCT-116 and MCF-7 cancer cells (IC_{50} = 2.91-10.13 μM). Moreover, compound **7d** exhibited enhanced inhibitory potency over H1975 NSCLC cells harboring mutated $EGFR^{T790M}$ (IC_{50} = 1.32±0.2 μM) over A431 cells overexpressing $EGFR^{WT}$ (IC_{50} = 4.96±0.3 μM), and hence **7d** is considered to be a promising and selective candidate for effective treatment of patients with $EGFR^{T790M}$-mutated NSCLC cell lines. In addition, the seven active antitumor compounds displayed low cytotoxicity over WI38 and WISH normal cells (IC_{50} = 19.78-86.42 μM), and they might be utilized as potent and safe antitumor agents. Results of $EGFR^{WT}$ inhibitory activity revealed that **7d** has the strongest inhibitory activity (IC_{50} = 0.083±0.002 μM). Further, compound **7d** showed potent inhibitory activity against $EGFR^{L858R}$ and $EGFR^{T790M}$ mutants (IC_{50} = 0.053±0.002 and 0.026±0.001 μM, respectively), and hence it might overcome resistance to EGFR-TKIs. Additionally, **7d** exhibited outstanding inhibitory activity against JAK3 (IC_{50} = 0.069±0.003 μM) which was proved to be 2-fold higher than that of erlotinib (IC_{50} = 0.146±0.005 μM). Analysis of cell cycle demonstrated that **7d** induces cell cycle arrest in G2/M and pre-G1 phases in HepG2, HCT-116 and MCF-7 cancer cells. Furthermore, death of cancer cells induced by **7d** was affirmed to occur mainly *via* apoptosis supported by elevation of Bax/Bcl-2 ratio. Docking results affirmed the precise fit of **7d** into the binding site of $EGFR^{WT}$, $EGFR^{L858R}$, $EGFR^{T790M}$ and JAK3 enzymes. Moreover, results of Molinspiration and Osiris calculations proved that **7d** is predicted to have good oral absorption, good drug-likeness properties and low toxicity risks in human. An overview on the attained results emphasized that **7d** is a new potent multi-kinase inhibitor with promising antitumor activity against H1975 NSCLC cells harboring $EGFR^{T790M}$ mutation. These advantages together with the low cytotoxicity of **7d** against normal cells indicate that **7d** is considered to be an auspicious lead compound for future evolution of new more potent and more selective antitumor agents against resistant NSCLC cells harboring EGFR mutations.

.

6. Experimental

6.1. Chemistry

Stuart melting point (SMP30) apparatus was utilized for determining the melting points (°C). IR spectra were recorded in KBr disc on Unicam SP 1000 IR spectrometer (ν in cm^{-1}). ^1H

and ^{13}C NMR spectra were recorded on Bruker Avance III HD FT-high resolution (400 MHz) and (500 MHz). Chemical shifts are expressed in δ ppm with reference to tetramethylsilane. Mass spectra were recorded on Triple Quad Tandem spectrometer (ESI) at 4.0 and 3.5 kV for positive and negative ion modes, respectively, and on direct probe controller inlet part of thermo scientific ISQ single quadrupole GC-MS spectrometer (ISQ LT) utilizing X-calibur software, Regional Center of Mycology and Biotechnology (RCMB), Al-Azhar University, Nasr city, Cairo, Egypt. Elemental analyses (% C, H, N) were achieved, and they were in harmony with the predicted structures within ±0.4% of the calculated values. Reaction times were monitored by TLC plates (Silica gel 60 F254), and spots were visualized by UV (366 nm). Hexane/ethyl acetate (9:1) was used for elution. The arylidenemalononitriles **1a-j** were synthesized adopting the previously reported procedure [41,48].

6.1.1. Synthesis of 2-amino-4-aryl-7,7-dimethyl-5-oxo-1,4,5,6,7,8-hexahydroquinoline-3-carbonitriles 2a-j

A mixture of dimedone (0.7 g, 0.005 mol), ammonium acetate (1.93 g, 0.025 mol) and arylidenemalononitrile **1a–j** (0.005 mol) in absolute ethanol (10 mL) was refluxed for 5-7 h. The precipitate formed was filtered, dried and crystallized from ethanol to yield the hexahydroquinoline derivatives **2a-j**.

*6.1.1.1. 2-Amino-4-(2,3-dichlorophenyl)-7,7-dimethyl-5-oxo-1,4,5,6,7,8-hexahydroquinoline-3-carbonitrile **(2a)***

Pale yellow powder, yield 85%, m.p. 253-255 °C. IR: 3445, 3323 (NH_2); 3204 (NH); 2191 (C≡N); 1663 (C=O). ^1H NMR (500 MHz, DMSO-d_6): δ 0.97 (s, 3H, CH_3), 1.03 (s, 3H, CH_3), 2.07 (d, J = 16.5 Hz, 1H, CH), 2.24 (d, J = 16.0 Hz, 1H, CH), 2.50-2.52 (m, 2H, CH_2), 4.77 (s, 1H, C_4-H), 7.12 (s, 2H, NH_2, D_2O-exchangeable), 7.15 (d, J = 8.0 Hz, 1H, Ar-H), 7.29 (t, J = 7.5 Hz, 1H, Ar-H), 7.45-7.47 (dd, J = 1.5, 1.5 Hz, 1H, Ar-H). ^{13}C NMR: δ 26.9, 28.3, 31.8, 33.7, 49.9, 56.3, 111.6, 119.1, 128.3, 128.5, 128.8, 130.2, 131.8, 144.4, 158.7, 163.3, 195.7. ESI-MS, *m/z*: 362.10 $[M+H]^+$, 360.30 $[M-H]^+$. Anal. Calcd. (Found) for $C_{18}H_{17}Cl_2N_3O$ (361.07): C, 59.68 (59.35); H, 4.73 (4.44); N, 11.60 (11.92).

*6.1.1.2. 2-Amino-4-(3,4-dichlorophenyl)-7,7-dimethyl-5-oxo-1,4,5,6,7,8-hexahydroquinoline-3-carbonitrile **(2b)*** [86]

White crystals, yield 85%, m.p. 243-245 °C [86]. IR: 3531, 3473 (NH_2); 3327 (NH); 2187 (C≡N); 1687 (C=O). ^1H NMR (500 MHz, DMSO-d_6): δ 0.99 (s, 3H, CH_3), 1.04 (s, 3H, CH_3), 2.06 (d, J = 16.0 Hz, 1H, CH), 2.28 (d, J = 16.0 Hz, 1H, CH), 2.36 (d, J = 20.0 Hz, 1H, CH),

2.54 (d, *J* = 20.0 Hz, 1H, CH), 5.20 (s, 1H, C_4-H), 7.14 (s, 2H, NH_2, D_2O-exchangeable), 7.25 (t, *J* = 8.0 Hz, 1H, Ar-H), 7.34-7.36 (dd, *J* = 0.8, 0.8 Hz, 1H, Ar-H), 7.42-7.45 (dd, *J* = 1.2, 1.2 Hz, 1H, Ar-H). ^{13}C NMR: δ 24.1, 27.2, 35.9, 45.8, 53.7, 53.9, 106.5, 113.5, 123.9, 124.0, 125.3, 130.2, 130.7, 132.0, 153.9, 158.5, 191.4. ESI-MS, *m/z*: 362.10 $[M+H]^+$, 360.30 $[M-H]^+$. Anal. Calcd. (Found) for $C_{18}H_{17}Cl_2N_3O$ (361.07): C, 59.68 (59.92); H, 4.73 (4.96); N, 11.60 (11.22).

6.1.1.3. 2-Amino-4-(2,6-dichlorophenyl)-7,7-dimethyl-5-oxo-1,4,5,6,7,8-hexahydroquinoline-3-carbonitrile ***(2c)*** [87]

Pale yellow powder, yield 85%, m.p. 240-242 °C [87]. IR: 3473, 3323 (NH_2); 3175 (NH); 2189 (C≡N); 1684 (C=O). ^{1}H NMR (500 MHz, DMSO-d_6): δ 0.98 (s, 3H, CH_3), 1.04 (s, 3H, CH_3), 2.06-2.07 (m, 1H, CH), 2.25-2.34 (m, 1H, CH), 2.34-2.38 (m, 1H, CH), 2.52 (m, 1H, CH), 5.19 (s, 1H, C_4-H), 7.11 (s, 2H, NH_2, D_2O-exchangeable), 7.23 (t, *J* = 7.5 Hz, 1H, Ar-H), 7.33-7.35 (dd, *J* = 1.5, 1.5 Hz, 1H, Ar-H), 7.43-7.45 (dd, *J* = 1.5, 1.0 Hz, 1H, Ar-H). ^{13}C NMR: δ 26.9, 31.6, 32.6, 41.3, 49.9, 56.0, 110.0, 119.0, 128.5, 129.0, 134.1, 135.8, 159.4, 163.8, 195.7. ESI-MS, *m/z*: 362.10 $[M+H]^+$, 360.40 $[M-H]^+$. Anal. Calcd. (Found) for $C_{18}H_{17}Cl_2N_3O$ (361.07): C, 59.68 (59.31); H, 4.73 (4.65); N, 11.60 (11.42).

6.1.1.4. 2-Amino-4-(2-chloro-6-fluorophenyl)-7,7-dimethyl-5-oxo-1,4,5,6,7,8-hexahydroquinoline-3-carbonitrile ***(2d)***

White powder, yield 72%, m.p. 197-199 °C. IR: 3415, 3331 (NH_2); 3212 (NH); 2197 (C≡N); 1683 (C=O). ^{1}H NMR (500 MHz, DMSO-d_6): δ 0.93 (s, 3H, CH_3), 1.04 (s, 3H, CH_3), 2.06 (d, *J* = 16.0 Hz, 1H, CH), 2.26 (d, *J* = 16.5 Hz, 1H, CH), 2.35 (d, *J* = 18.0 Hz, 1H, CH), 2.55 (d, *J* = 18.0 Hz, 1H, CH), 4.87 (s, 1H, C_4-H), 7.12 (s, 2H, NH_2, D_2O-exchangeable), 7.13-7.25 (m, 3H, Ar-H). ^{13}C NMR: δ 26.3, 28.6, 29.5, 31.7, 49.8, 56.0, 114.7, 115.1, 119.2, 125.2, 125.5 (d, *J* = 3.5 Hz), 129.2 (d, *J* = 9.2 Hz), 133.6 (d, *J* = 4.1 Hz), 158.2, 159.3, 163.5, 195.7. ESI-MS, *m/z*: 346.10 $[M+H]^+$. Anal. Calcd. (Found) for $C_{18}H_{17}ClFN_3O$ (345.10): C, 62.52 (62.34); H, 4.96 (4.69); N, 12.15 (12.35).

6.1.1.5. 2-Amino-4-(2,4-difluorophenyl)-7,7-dimethyl-5-oxo-1,4,5,6,7,8-hexahydroquinoline-3-carbonitrile ***(2e)***

Pale green powder, yield 70%, m.p. 187-189 °C. IR: 3424, 3333 (NH_2); 3227 (NH); 2179 (C≡N); 1685 (C=O). ^{1}H NMR (500 MHz, DMSO-d_6): δ 0.91 (s, 3H, CH_3), 1.03 (s, 3H, CH_3), 2.06 (d, *J* = 16.0 Hz, 1H, CH), 2.28 (d, *J* = 16.0 Hz, 1H, CH), 2.34 (d, *J* = 17.5 Hz, 1H, CH), 2.54-2.58 (dd, *J* = 1.5, 1.0 Hz, 1H, CH), 4.62 (s, 1H, C_4-H), 7.01 (t, *J* = 8.5 Hz, 2H, Ar-H), 7.12 (s, 2H, NH_2, D_2O-exchangeable), 7.26-7.32 (m, 1H, Ar-H). ^{13}C NMR: δ 25.0, 26.0, 28.7, 31.8, 49.8, 54.3, 110.2, 111.7 (d, *J* = 25.0 Hz), 119.1 (t, *J* = 15.5 Hz), 119.5, 129.1 (t, *J* = 9.5 Hz), 159.3, 159.7 (d,

J = 9.5 Hz), 161.7 (d, *J* = 10.0 Hz), 163.5, 195.7. EI-MS, *m/z*: 329.30 (2.19, M^+), 83.10 (100.00). Anal. Calcd. (Found) for $C_{18}H_{17}F_2N_3O$ (329.35): C, 65.64 (65.35); H, 5.20 (5.46); N, 12.76 (12.43).

6.1.1.6. 2-Amino-4-(2,6-difluorophenyl)-7,7-dimethyl-5-oxo-1,4,5,6,7,8-hexahydroquinoline-3-carbonitrile ***(2f)***

White crystals, yield 70%, m.p. 255-257 °C. IR: 3408, 3333 (NH_2); 3217 (NH); 2199 (C≡N); 1685 (C=O). ^{1}H NMR (500 MHz, DMSO-d_6): δ 0.91 (s, 3H, CH_3), 1.03 (s, 3H, CH_3), 2.06 (d, *J* = 16.5 Hz, 1H, CH), 2.26-2.36 (m, 2H, CH_2), 2.57 (d, *J* = 17.5 Hz, 1H, CH), 4.62 (s, 1H, C_4-H), 7.01 (t, *J* = 16.0 Hz, 2H, Ar-H), 7.13 (s, 2H, NH_2, D_2O-exchangeable), 7.25-7.31 (m, 1H, Ar-H). ^{13}C NMR: δ 25.0, 26.0, 28.7, 31.8, 49.8, 54.4, 110.2, 111.7 (d, *J* = 25.0 Hz), 119.1 (t, *J* = 15.5 Hz), 119.5, 129.1 (t, *J* = 10.8 Hz), 159.3, 159.6 (d, *J* = 7.4 Hz), 161.6 (d, *J* = 7.1 Hz), 163.5, 195.7. ESI-MS, *m/z*: 328.40 $[M-H]^+$. Anal. Calcd. (Found) for $C_{18}H_{17}F_2N_3O$ (329.13): C, 65.64 (65.34); H, 5.20 (5.41); N, 12.76 (12.43).

6.1.1.7. 2-Amino-4-((1,1'-biphenyl)-4-yl)-7,7-dimethyl-5-oxo-1,4,5,6,7,8-hexahydroquinoline-3-carbonitrile ***(2g)***

White crystals, yield 90%, m.p. 242-244 °C. IR: 3384, 3318 (NH_2); 3208 (NH); 2193 (C≡N); 1682 (C=O). ^{1}H NMR (500 MHz, DMSO-d_6): δ 0.97 (s, 3H, CH_3), 1.04 (s, 3H, CH_3), 2.12 (d, *J* = 16.0 Hz, 1H, CH), 2.26 (d, *J* = 15.5 Hz, 1H, CH), 2.53 (s, 2H, CH_2), 4.21 (s, 1H, C_4-H), 7.05 (s, 2H, NH_2, D_2O-exchangeable), 7.22 (d, *J* = 8.5 Hz, 2H, Ar-H), 7.33 (t, *J* = 7.5 Hz, 1H, Ar-H), 7.44 (t, *J* = 7.5 Hz, 2H, Ar-H), 7.58 (d, *J* = 8.5 Hz, 2H, Ar-H), 7.62 (d, *J* = 7.5 Hz, 2H, Ar-H). ^{13}C NMR: δ 26.9, 28.4, 31.9, 35.3, 50.0, 58.1, 112.6, 119.8, 126.6, 126.7, 127.3, 127.8, 128.9, 138.5, 139.9, 144.0, 158.5, 162.5, 195.8. ESI-MS, *m/z*: 367.70 $[M-H]^+$. Anal. Calcd. (Found) for $C_{24}H_{23}N_3O$ (369.18): C, 78.02 (78.32); H, 6.27 (6.40); N, 11.37 (11.64).

6.1.1.8. 2-Amino-4-([1,3]benzodioxol-4-yl)-7,7-dimethyl-5-oxo-1,4,5,6,7,8-hexahydroquinoline-3-carbonitrile ***(2h)***

Greyish green crystals, yield 65%, m.p. 231-233 °C. IR: 3392, 3330 (NH_2); 3216 (NH); 2190 (C≡N); 1686 (C=O). ^{1}H NMR (500 MHz, DMSO-d_6): δ 0.94 (s, 3H, CH_3), 1.03 (s, 3H, CH_3), 2.06 (d, *J* = 15.5 Hz, 1H, CH), 2.26 (d, *J* = 15.5 Hz, 1H, CH), 2.39 (d, *J* = 17.0 Hz, 1H, CH), 2.50-2.58 (m, 1H, CH), 4.24 (s, 1H, C_4-H), 5.83 (s, 1H, Dioxole-H), 6.02 (s, 1H, Dioxole-H), 6.58-6.62 (m, 1H, Ar-H), 6.70-6.74 (m, 2H, Ar-H), 6.98 (s, 2H, NH_2, D_2O-exchangeable). ^{13}C NMR: δ 26.3, 28.7, 31.8, 32.1, 50.0, 57.6, 100.7, 107.1, 110.9, 119.7, 121.3, 121.5, 126.2, 144.5, 147.1, 150.2, 163.0, 195.7. EI-MS, *m/z*: 338.18 (100.00, M^++1), 337.25 (63.10, M^+). Anal. Calcd. (Found) for $C_{19}H_{19}N_3O_3$ (337.38): C, 67.64 (67.41); H, 5.68 (5.48); N, 12.46 (12.22).

*6.1.1.9. 2-Amino-7,7-dimethyl-4-(naphthalen-2-yl)-5-oxo-1,4,5,6,7,8-hexahydroquinoline-3-carbonitrile **(2i)*** [88]

White powder, yield 75%, m.p. 255-257 °C [88]. IR: 3348, 3312 (NH_2); 3172 (NH); 2190 (C≡N); 1684 (C=O). ^{1}H NMR (500 MHz, DMSO-d_6): δ 0.95 (s, 3H, CH_3), 1.03 (s, 3H, CH_3), 2.07 (d, J = 16.5 Hz, 1H, CH), 2.25 (d, J = 16.0 Hz, 1H, CH), 2.54 (d, J = 4.5 Hz, 2H, CH_2), 4.35 (s, 1H, C_4-H), 7.07 (s, 2H, NH_2, D_2O-exchangeable), 7.26-7.28 (dd, J = 1.5, 2.0 Hz, 1H, Ar-H), 7.44-7.49 (m, 2H, Ar-H), 7.66 (s, 1H, Ar-H), 7.83-7.85 (m, 2H, Ar-H), 7.88 (d, J = 7.5 Hz, 1H, Ar-H). ^{13}C NMR: δ 26.7, 28.4, 31.8, 35.9, 50.0, 58.1, 112.5, 119.8, 125.5, 125.6, 125.7, 126.2, 127.5, 127.7, 128.1, 132.0, 132.8, 142.1, 158.5, 162.6, 195.8. ESI-MS, *m/z*: 344.30 $[M+H]^+$, 341.90 $[M-H]^+$. Anal. Calcd. (Found) for $C_{22}H_{21}N_3O$ (343.17): C, 76.94 (76.72); H, 6.16 (6.34); N, 12.24 (12.52).

*6.1.1.10. 2-Amino-4-(anthracen-9-yl)-7,7-dimethyl-5-oxo-1,4,5,6,7,8-hexahydroquinoline-3-carbonitrile **(2j)***

Dark orange crystals, yield 56%, m.p. 227-228 °C. ^{1}H NMR (500 MHz, DMSO-d_6): δ 0.86 (s, 3H, CH_3), 1.02 (s, 3H, CH_3), 1.88 (d, J = 16.0 Hz, 1H, CH), 2.13 (d, J = 16.0 Hz, 1H, CH), 2.53 (d, J = 17.5 Hz, 1H, CH), 2.62 (d, J = 18.0 Hz, 1H, CH), 5.98 (s, 1H, C_4-H), 7.05 (s, 2H, NH_2, D_2O-exchangeable), 7.41-7.46 (m, 2H, Ar-H), 7.57-7.70 (m, 2H, Ar-H), 8.06-8.09 (m, 3H, Ar-H), 8.52 (s, 1H, Ar-H), 8.65 (d, J = 9.0 Hz, 1H, Ar-H). ^{13}C NMR: δ 27.5, 28.5, 29.4, 31.5, 50.0, 58.3, 113.9, 119.3, 124.5, 126.0, 126.8, 128.8, 129.8, 130.8, 131.5, 134.6, 158.1, 162.0, 195.7. EI-MS, *m/z*: 395.19 (18.65, M^++2), 394.27 (42.81, M^++1), 393.38 (49.91, M^+), 83.20 (100.00). Anal. Calcd. (Found) for $C_{26}H_{23}N_3O$ (393.49): C, 79.36 (79.66); H, 5.89 (5.79); N, 10.68 (10.29).

6.1.2. Synthesis of 2-amino-7,7-dimethyl-5-oxo-4-(substituted phenyl)-1,4,5,6,7,8-hexahydroquinoline-3-carboxylic acids 3a-c

The appropriate *ortho* aminonitrile **2a, 2b** and **2f** (0.002 mol) was heated with sulfuric acid 70% (6 mL) at 70 °C for 1-2 h. The reaction mixture was cooled and neutralized with 10% NaOH. The precipitated solid was filtered and crystallized from ethanol/water (1:1) to afford the corresponding *ortho* aminocarboxylic acids **3a-c**.

*6.1.2.1. 2-Amino-4-(2,3-dichlorophenyl)-7,7-dimethyl-5-oxo-1,4,5,6,7,8-hexahydroquinoline-3-carboxylic acid **(3a)***

White powder, yield 60%, m.p. 192-194 °C. IR: 3452 (CO<u>O</u>H); 3216, 3123 (NH_2, NH); 1692 (<u>CO</u>OH); 1640 (C=O). ^{1}H NMR (400 MHz, DMSO-d_6): δ 0.99 (s, 3H, CH_3), 1.07 (s, 3H, CH_3),

2.16-2.27 (dd, *J* = 16.0, 16.0 Hz, 2H, CH_2), 2.44 (d, *J* = 29.6 Hz, 2H, CH_2), 2.95 (s, 1H, NH, D_2O-exchangeable), 4.17 (s, 1H, C_4-H), 7.12 (d, *J* = 7.2 Hz, 1H, Ar-H), 7.37 (s, 1H, Ar-H), 7.57 (d, *J* = 7.6 Hz, 1H, Ar-H), 10.21 (s, 1H, COOH, D_2O-exchangeable). ^{13}C NMR: δ 28.9, 32.9, 33.4, 38.2, 50.4, 94.0, 112.0, 127.3, 129.2, 129.6, 131.3, 131.5, 144.7, 153.8, 170.4, 180.7, 195.0. EI-MS, *m/z*: 381.31 (35.12, M^+), 353.28 (100.00). Anal. Calcd. (Found) for $C_{18}H_{18}Cl_2N_2O_3$ (381.25): C, 56.71 (56.49); H, 4.76 (4.44); N, 7.35 (7.72).

6.1.2.2. 2-Amino-4-(3,4-dichlorophenyl)-7,7-dimethyl-5-oxo-1,4,5,6,7,8-hexahydroquinoline-3-carboxylic acid ***(3b)***

White powder, yield 65%, m.p. 207-209 °C. IR: 3449 (CO<u>OH</u>); 3218, 3124 (NH_2, NH); 1693 (<u>CO</u>OH); 1641 (C=O). ^{1}H NMR (500 MHz, DMSO-d_6): δ 0.96 (s, 3H, CH_3), 1.04 (s, 3H, CH_3), 2.17-2.24 (m, 2H, CH_2), 2.41-2.49 (m, 2H, CH_2), 2.96 (s, 1H, NH, D_2O-exchangeable), 4.14 (s, 1H, C_4-H), 7.09 (d, *J* = 7.5 Hz, 1H, Ar-H), 7.34 (s, 1H, Ar-H), 7.55 (d, *J* = 8.0 Hz, 1H, Ar-H), 10.20 (s, 1H, COOH, D_2O-exchangeable). ^{13}C NMR: δ 28.5, 32.4, 32.9, 37.7, 49.9, 78.0, 111.5, 126.8, 128.7, 128.8, 130.8, 131.0, 144.2, 153.3, 170.0, 173.1, 194.5. Anal. Calcd. (Found) for $C_{18}H_{18}Cl_2N_2O_3$ (381.25): C, 56.71 (56.43); H, 4.76 (4.39); N, 7.35 (7.55).

6.1.2.3. 2-Amino-4-(2,6-difluorophenyl)-7,7-dimethyl-5-oxo-1,4,5,6,7,8-hexahydroquinoline-3-carboxylic acid ***(3c)***

Pale green powder, yield 62%, m.p. 245-246 °C. IR: 3453 (CO<u>OH</u>); 3220 (NH); 3160, 3126 (NH_2); 1710 (<u>CO</u>OH); 1630 (C=O). ^{1}H NMR (500 MHz, DMSO-d_6): δ 0.88 (s, 3H, CH_3), 1.01 (s, 3H, CH_3), 2.01 (d, *J* = 16.0 Hz, 1H, CH), 2.16 (d, *J* = 16.0 Hz, 1H, CH), 2.25-2.30 (m, 2H, CH_2), 3.08 (s, 1H, NH, D_2O-exchangeable), 4.48 (s, 1H, C_4-H), 6.98 (s, 2H, Ar-H), 7.25 (s, 1H, Ar-H), 10.19 (s, 1H, COOH, D_2O-exchangeable). ^{13}C NMR: δ 26.5, 28.7, 32.2, 35.6, 50.1, 78.0, 108.5, 111.6 (d, *J* = 25.0 Hz), 119.7 (t, *J* = 17.9 Hz), 128.6 (t, *J* = 9.5 Hz), 153.0, 159.6 (d, *J* = 8.4 Hz), 161.5 (d, *J* = 9.5 Hz), 169.3, 194.3. EI-MS, *m/z*: 348.23 (28.79, M^+), 231.30 (100.00). Anal. Calcd. (Found) for $C_{18}H_{18}F_2N_2O_3$ (348.35): C, 62.06 (62.41); H, 5.21 (5.50); N, 8.04 (8.42).

6.1.3. Synthesis of ethyl *N*-(4-aryl-3-cyano-7,7-dimethyl-5-oxo-1,4,5,6,7,8-hexahydroquinolin-2-yl)formimidates 4a-h

A solution of *ortho* aminonitrile **2a-d, 2f-h** and **2j** (0.001 mol) in triethyl orthoformate (10 mL) was refluxed for 7-10 h. Excess triethyl orthoformate was evaporated under reduced pressure and the solid attained was crystallized from ethanol to produce the ethyl formimidates **4a-h**.

6.1.3.1. Ethyl N-(4-(2,3-dichlorophenyl)-3-cyano-7,7-dimethyl-5-oxo-1,4,5,6,7,8-hexahydroquinolin-2-yl)formimidate ***(4a)***

Pink crystals, yield 60%, m.p. 204-206 °C. ^{1}H NMR (500 MHz, DMSO-d_6): δ 0.99 (s, 3H, CH_3), 1.04 (s, 3H, CH_3), 1.28 (t, *J* = 7.5 Hz, 3H, $OCH_2C\underline{H_3}$), 2.12 (d, *J* = 16.5 Hz, 1H, CH), 2.25 (d, *J* = 16.0 Hz, 1H, CH), 2.58 (s, 2H, CH_2), 4.27-4.30 (q, *J* = 7.5 Hz, 2H, $OC\underline{H_2}CH_3$), 5.00 (s, 1H, C_4-H), 7.28 (d, *J* = 7.5 Hz, 1H, Ar-H), 7.34 (t, *J* = 7.5 Hz, 1H, Ar-H), 7.53-7.54 (dd, *J* = 1.5, 1.5 Hz, 1H, Ar-H), 8.56 (s, 1H, N=CH). ^{13}C NMR: δ 14.1, 27.1, 28.2, 31.9, 33.3, 49.9, 64.2, 80.4, 110.7, 116.6, 128.6, 129.5, 129.6, 130.5, 132.1, 156.6, 162.3, 163.3, 163.8, 195.7. EI-MS, *m/z*: 422.22 (42.81, M^++4), 420.21 (18.88, M^++2), 418.25 (29.43, M^+), 83.13 (100.00). Anal. Calcd. (Found) for $C_{21}H_{21}Cl_2N_3O_2$ (418.32): C, 60.30 (60.54); H, 5.06 (5.39); N, 10.05 (10.44).

6.1.3.2. Ethyl N-(4-(3,4-dichlorophenyl)-3-cyano-7,7-dimethyl-5-oxo-1,4,5,6,7,8-hexahydroquinolin-2-yl)formimidate ***(4b)***

Pink crystals, yield 63%, m.p. 205-207 °C. ^{1}H NMR (500 MHz, DMSO-d_6): δ 0.98 (s, 3H, CH_3), 1.04 (s, 3H, CH_3), 1.28 (t, *J* = 7.0 Hz, 3H, $OCH_2C\underline{H_3}$), 2.11 (d, *J* = 16.0 Hz, 1H, CH), 2.25 (d, *J* = 16.5 Hz, 1H, CH), 2.56 (s, 2H, CH_2), 4.28-4.29 (q, *J* = 7.0 Hz, 2H, $OC\underline{H_2}CH_3$), 4.89 (s, 1H, C_4-H), 7.33 (d, *J* = 8.0 Hz, 1H, Ar-H), 7.40 (d, *J* = 7.5 Hz, 1H, Ar-H), 7.59 (s, 1H, Ar-H), 8.55 (s, 1H, N=CH). Anal. Calcd. (Found) for $C_{21}H_{21}Cl_2N_3O_2$ (418.32): C, 60.30 (60.19); H, 5.06 (5.36); N, 10.05 (10.31).

6.1.3.3. Ethyl N-(4-(2,6-dichlorophenyl)-3-cyano-7,7-dimethyl-5-oxo-1,4,5,6,7,8-hexahydroquinolin-2-yl)formimidate ***(4c)***

White crystals, yield 72%, m.p. 215-216 °C. ^{1}H NMR (500 MHz, DMSO-d_6): δ 0.99 (s, 3H, CH_3), 1.04 (s, 3H, CH_3), 1.28 (t, *J* = 7.0 Hz, 3H, $OCH_2C\underline{H_3}$), 2.09 (d, *J* = 15.5 Hz, 1H, CH), 2.24-2.28 (dd, *J* = 5.0, 5.5 Hz, 1H, CH), 2.45 (d, *J* = 17.5 Hz, 1H, CH), 2.50 (d, *J* = 18.0 Hz, 1H, CH), 4.28-4.32 (q, *J* = 7.0 Hz, 2H, $OC\underline{H_2}CH_3$), 5.41 (s, 1H, C_4-H), 7.28-7.33 (m, 1H, Ar-H), 7.38-7.45 (m, 1H, Ar-H), 7.49-7.52 (m, 1H, Ar-H), 8.57 (s, 1H, N=CH). ^{13}C NMR: δ 14.3, 27.6, 28.7, 32.4, 37.2, 50.4, 64.7, 80.8, 111.2, 117.1, 128.9, 129.9, 131.0, 132.5, 157.1, 162.8, 164.3, 196.3. Anal. Calcd. (Found) for $C_{21}H_{21}Cl_2N_3O_2$ (418.32): C, 60.30 (60.50); H, 5.06 (5.41); N, 10.05 (10.32).

6.1.3.4. Ethyl N-(4-(2-chloro-6-fluorophenyl)-3-cyano-7,7-dimethyl-5-oxo-1,4,5,6,7,8-hexahydroquinolin-2-yl)formimidate ***(4d)***

Pink crystals, yield 63%, m.p. 196-197 °C. IR: 3448 (NH); 2209 (C≡N); 1668 (C=O). ^{1}H NMR (500 MHz, DMSO-d_6): δ 0.95 (s, 3H, CH_3), 1.04 (s, 3H, CH_3), 1.29 (t, *J* = 7.0 Hz, 3H, $OCH_2C\underline{H_3}$), 2.08-2.12 (d, *J* = 16.5 Hz, 1H, CH), 2.28 (d, *J* = 15.5 Hz, 1H, CH), 2.43-2.46 (m,

1H, CH), 2.59 (d, *J* = 17.5 Hz, 1H, CH), 4.28-4.32 (q, *J* = 7.0 Hz, 2H, OC<u>H</u>$_2$CH$_3$), 5.08 (s, 1H, C$_4$-H), 7.18-7.36 (m, 3H, Ar-H), 8.58 (s, 1H, N=CH). ^{13}C NMR: δ 13.8, 26.3, 28.5, 31.1, 31.8, 49.8, 56.0, 64.2, 78.2, 108.2, 109.8, 114.8 (d, 100.0 Hz), 116.7, 126.1 (d, 120.0 Hz), 130.0 (d, 10.7 Hz), 133.9, 156.2-157.8 (m), 162.2, 163.9 (d, 11.0 Hz), 195.7. EI-MS, *m/z*: 404.32 (1.89, M$^+$+2), 401.69 (5.32, M$^+$), 55.13 (100.00). Anal. Calcd. (Found) for $C_{21}H_{21}ClFN_3O_2$ (401.87): C, 62.76 (62.42); H, 5.27 (5.36); N, 10.46 (10.30).

6.1.3.5. Ethyl N-(3-cyano-4-(2,6-difluorophenyl)-7,7-dimethyl-5-oxo-1,4,5,6,7,8-hexahydroquinolin-2-yl)formimidate ***(4e)***

White powder, yield 59%, m.p. 192-193 °C. IR: 3392 (NH); 2190 (C≡N); 1668 (C=O). ^{1}H NMR (500 MHz, DMSO-*d*$_6$): δ 0.93 (s, 3H, CH$_3$), 1.05 (s, 3H, CH$_3$), 1.29 (t, *J* = 7.5 Hz, 3H, OCH$_2$C<u>H</u>$_3$), 2.10 (d, *J* = 16.5 Hz, 1H, CH), 2.29 (d, *J* = 16.5 Hz, 1H, CH), 2.46 (d, *J* = 18.0 Hz, 1H, CH), 2.60 (d, *J* = 18.0 Hz, 1H, CH), 4.28-4.32 (q, *J* = 7.5 Hz, 2H, OC<u>H</u>$_2$CH$_3$), 4.85 (s, 1H, C$_4$-H), 7.07 (t, *J* = 9.0 Hz, 2H, Ar-H), 7.33-7.39 (m, 1H, Ar-H), 8.56 (s, 1H, N=CH). ^{13}C NMR: δ 13.8, 26.2, 28.5, 30.7, 31.9, 49.8, 64.3, 78.8, 109.3, 111.9 (d, *J* = 23.9 Hz), 116.9, 117.2 (t, *J* = 16.8 Hz), 130.0 (t, *J* = 10.8 Hz), 157.1, 159.7, 161.7, 162.2, 163.9, 195.7. EI-MS, *m/z*: 387.10 (1.78, M$^+$+2), 386.29 (7.45, M$^+$+1), 385.25 (32.80, M$^+$), 383.26 (100.00). Anal. Calcd. (Found) for $C_{21}H_{21}F_2N_3O_2$ (385.41): C, 65.44 (65.12); H, 5.49 (5.26); N, 10.90 (10.61).

6.1.3.6. Ethyl N-(4-((1,1'-biphenyl)-4-yl)-3-cyano-7,7-dimethyl-5-oxo-1,4,5,6,7,8-hexahydroquinolin-2-yl)formimidate ***(4f)***

Yellow crystals, yield 65%, m.p. 180-182 °C. ^{1}H NMR (500 MHz, DMSO-*d*$_6$): δ 0.99 (s, 3H, CH$_3$), 1.05 (s, 3H, CH$_3$), 1.29 (t, *J* = 6.5 Hz, 3H, OCH$_2$C<u>H</u>$_3$), 2.16 (d, *J* = 16.0 Hz, 1H, CH), 2.27 (d, *J* = 16.5 Hz, 1H, CH), 2.60 (s, 2H, CH$_2$), 4.28-4.32 (q, *J* = 7.0 Hz, 2H, OC<u>H</u>$_2$CH$_3$), 4.46 (s, 1H, C$_4$-H), 7.31-7.36 (m, 3H, Ar-H), 7.45 (t, *J* = 8.0 Hz, 2H, Ar-H), 7.61-7.64 (m, 4H, Ar-H), 8.56 (s, 1H, N=CH). ^{13}C NMR: δ 13.9, 27.1, 28.2, 31.8, 31.9, 50.0, 64.1, 82.3, 111.5, 117.3, 126.7, 126.9, 127.5, 128.4, 129.0, 139.1, 139.7, 142.0, 156.1, 162.0, 163.1, 195.8. EI-MS, *m/z*: 428.39 (4.07, M$^+$+2), 427.32 (21.08, M$^+$+1), 426.32 (100.00, M$^+$). Anal. Calcd. (Found) for $C_{27}H_{27}N_3O_2$ (425.53): C, 76.21 (76.50); H, 6.40 (6.20); N, 9.87 (9.50).

6.1.3.7. Ethyl N-(4-([1,3]benzodioxol-4-yl)-3-cyano-7,7-dimethyl-5-oxo-1,4,5,6,7,8-hexahydroquinolin-2-yl)formimidate ***(4g)***

White crystals, yield 60%, m.p. 220-221 °C. ^{1}H NMR (500 MHz, DMSO-*d*$_6$): δ 0.96 (s, 3H, CH$_3$), 1.04 (s, 3H, CH$_3$), 1.28 (t, *J* = 7.5 Hz, 3H, OCH$_2$C<u>H</u>$_3$), 2.11 (d, *J* = 15.5 Hz, 1H, CH), 2.26 (d, *J* = 16.5 Hz, 1H, CH), 2.58 (d, *J* = 17.5 Hz, 2H, CH$_2$), 4.27-4.31 (q, *J* = 7.5 Hz, 2H, OC<u>H</u>$_2$CH$_3$), 4.47 (s, 1H, C$_4$-H), 5.86 (s, 1H, Dioxole-H), 6.05 (s, 1H, Dioxole-H), 6.69-6.71 (dd,

J = 2.0, 1.5 Hz, 1H, Ar-H), 6.78-6.80 (m, 2H, Ar-H), 8.52 (s, 1H, N=CH). Anal. Calcd. (Found) for $C_{22}H_{23}N_3O_4$ (393.44): C, 67.16 (67.39); H, 5.89 (5.51); N, 10.68 (10.42).

6.1.3.8. Ethyl N-(4-(anthracen-9-yl)-3-cyano-7,7-dimethyl-5-oxo-1,4,5,6,7,8-hexahydroquinolin-2-yl)formimidate ***(4h)***

Orange crystals, yield 80%, m.p. 250-252 °C. ^{1}H NMR (500 MHz, DMSO-d_6): δ 0.87 (s, 3H, CH_3), 1.04 (s, 3H, CH_3), 1.27 (t, *J* = 7.5 Hz, 3H, $OCH_2C\underline{H}_3$), 1.92 (d, *J* = 16.0 Hz, 1H, CH), 2.14 (d, *J* = 16.5 Hz, 1H, CH), 2.63-2.65 (dd, *J* = 9.0, 9.0 Hz, 2H, CH_2), 4.26-4.31 (q, *J* = 7.5 Hz, 2H, $OC\underline{H}_2CH_3$), 6.24 (s, 1H, C_4-H), 7.45-7.47 (m, 2H, Ar-H), 7.53-7.61 (m, 2H, Ar-H), 8.09-8.13 (m, 3H, Ar-H), 8.58 (s, 1H, N=CH), 8.67-8.71 (m, 2H, Ar-H). ^{13}C NMR: δ 14.1, 26.9, 28.4, 31.6, 35.5, 50.0, 64.2, 82.7, 113.1, 116.8, 124.5, 124.6, 125.1, 128.9, 129.1, 130.9, 131.5, 132.6, 155.7, 161.9, 162.5, 195.6. EI-MS, *m/z*: 451.33 (5.32, M^++2), 450.36 (20.40, M^++1), 449.50 (20.40, M^+), 83.08 (100.00). Anal. Calcd. (Found) for $C_{29}H_{27}N_3O_2$ (449.55): C, 77.48 (77.22); H, 6.05 (6.32); N, 9.35 (9.63).

6.1.4. Synthesis of 4-amino-5-aryl-8,8-dimethyl-5,8,9,10-tetrahydropyrimido[4,5-*b*]quinolin-6(7*H*)-ones 5a-f

A mixture of compound **4a-e** and **4h** (0.005 mol) and ammonia solution 35% (10 mL) in absolute ethanol (15 mL) was refluxed for 10-12 h. The solvent was evaporated under reduced pressure, and the obtained solid was triturated with ice-water, filtered, washed with water, dried and crystallized from ethanol to yield the pyrimidoquinolines **5a-f**.

6.1.4.1. 4-Amino-5-(2,3-dichlorophenyl)-8,8-dimethyl-5,8,9,10-tetrahydropyrimido[4,5-b]quinolin-6(7H)-one ***(5a)***

White crystals, yield 89%, m.p. 227-228 °C. IR: 3478, 3300 (NH_2); 3152 (NH); 1659 (C=O). ^{1}H NMR (500 MHz, DMSO-d_6): δ 0.91 (s, 3H, CH_3), 1.05 (s, 3H, CH_3), 2.08 (d, *J* = 16.0 Hz, 1H, CH), 2.30 (d, *J* = 16.5 Hz, 1H, CH), 2.42-2.49 (m, 1H, CH), 2.66 (d, *J* = 17.5 Hz, 1H, CH), 5.20 (s, 1H, C_5-H), 6.36 (s, 1H, NH, D_2O-exchangeable), 7.02 (t, *J* = 9.0 Hz, 2H, Ar-H), 7.26-7.32 (m, 1H, Ar-H), 8.11 (s, 1H, Pyrimidine-H). ^{13}C NMR: δ 22.7, 26.1, 28.7, 31.9, 49.9, 94.3, 110.6, 117.0, 117.2, 129.5, 129.6, 129.7, 156.6, 159.7, 161.6, 162.8, 165.3, 195.7. EI-MS, *m/z*: 393.10 (1.52, M^++4), 391.10 (7.49, M^++2), 389.00 (11.43, M^+), 167.90 (100.00). Anal. Calcd. (Found) for $C_{19}H_{18}Cl_2N_4O$ (389.28): C, 58.62 (58.44); H, 4.66 (4.33); N, 14.39 (14.65).

6.1.4.2. 4-Amino-5-(3,4-dichlorophenyl)-8,8-dimethyl-5,8,9,10-tetrahydropyrimido[4,5-b]quinolin-6(7H)-one ***(5b)***

White crystals, yield 92%, m.p. 232-233 °C. IR: 3478, 3313 (NH_2); 3107 (NH); 1657 (C=O). ^{1}H NMR (500 MHz, DMSO-d_6): δ 0.89 (s, 3H, CH_3), 1.03 (s, 3H, CH_3), 2.12 (d, *J* = 15.5 Hz, 1H, CH), 2.31 (d, *J* = 16.0 Hz, 1H, CH), 2.55-2.65 (dd, *J* = 16.5, 16.0 Hz, 2H, CH_2), 4.92 (s, 1H, C_5-H), 7.05 (s, 2H, NH_2, D_2O-exchangeable), 7.15 (d, *J* = 6.0 Hz, 1H, Ar-H), 7.50 (d, *J* = 4.0 Hz, 1H, Ar-H), 7.72 (s, 1H, Ar-H), 8.09 (s, 1H, Pyrimidine-H). ^{13}C NMR: δ 26.9, 29.0, 31.8, 32.4, 50.4, 96.3, 113.9, 128.5, 129.8, 130.8, 130.9, 142.5, 144.3, 157.2, 161.5, 163.1, 164.9, 196.3. EI-MS, *m/z*: 390.60 (16.60, M^++2), 388.87 (29.82, M^+), 167.51 (100.00). Anal. Calcd. (Found) for $C_{19}H_{18}Cl_2N_4O$ (389.28): C, 58.62 (58.46); H, 4.66 (4.39); N, 14.39 (14.79).

6.1.4.3. 4-Amino-5-(2,6-dichlorophenyl)-8,8-dimethyl-5,8,9,10-tetrahydropyrimido[4,5-b]quinolin-6(7H)-one ***(5c)***

White crystals, yield 80%, m.p. 227-228 °C. IR: 3467, 3385 (NH_2); 3164 (NH); 1657 (C=O). ^{1}H NMR (500 MHz, DMSO-d_6): δ 0.97 (s, 3H, CH_3), 1.05 (s, 3H, CH_3), 2.06 (d, *J* = 16.0 Hz, 1H, CH), 2.27 (d, *J* = 16.0 Hz, 1H, CH), 2.51 (d, *J* = 14.0 Hz, 1H, CH), 2.62 (d, *J* = 18.0 Hz, 1H, CH), 5.51 (s, 1H, C_5-H), 6.15 (s, 1H, NH, D_2O-exchangeable), 7.28 (t, *J* = 8.0 Hz, 1H, Ar-H), 7.35-7.36 (m, 1H, Ar-H), 7.52-7.54 (m, 1H, Ar-H), 8.12 (s, 1H, Pyrimidine-H). ^{13}C NMR: δ 26.5, 28.6, 31.0, 31.6, 50.0, 93.9, 110.2, 128.6, 131.0, 134.5, 136.0, 156.8, 161.9, 162.5, 165.4, 195.7. Anal. Calcd. (Found) for $C_{19}H_{18}Cl_2N_4O$ (389.28): C, 58.62 (58.32); H, 4.66 (4.29); N, 14.39 (14.67).

6.1.4.4. 4-Amino-5-(2-chloro-6-fluorophenyl)-8,8-dimethyl-5,8,9,10-tetrahydropyrimido[4,5-b]quinolin-6(7H)-one ***(5d)***

White crystals, yield 79%, m.p. 254-257 °C. IR: 3468, 3387 (NH_2); 3157 (NH); 1658 (C=O). ^{1}H NMR (500 MHz, DMSO-d_6): δ 0.93 (s, 3H, CH_3), 1.05 (s, 3H, CH_3), 2.08 (d, *J* = 16.5 Hz, 1H, CH), 2.29 (d, *J* = 16.0 Hz, 1H, CH), 2.52 (d, *J* = 14.0 Hz, 1H, CH), 2.65 (d, *J* = 18.0 Hz, 1H, CH), 5.28 (s, 1H, C_5-H), 6.23 (s, 1H, NH, D_2O-exchangeable), 7.17 (s, 1H, Ar-H), 7.28-7.29 (m, 2H, Ar-H), 8.12 (s, 1H, Pyrimidine-H). ^{13}C NMR: δ 26.3, 28.6, 30.7, 31.8, 49.9, 94.2, 110.6 (d, *J* = 15.9 Hz), 115.1 (d, *J* = 24.0 Hz), 125.7, 126.2, 128.7, 129.9 (d, *J* = 10.3 Hz), 133.7, 156.7, 161.6, 162.6, 165.2, 195.7. EI-MS, *m/z*: 375.22 (12.91, M^++2), 374.25 (9.87, M^++1), 373.20 (38.92, M^+), 338.23 (100.00). Anal. Calcd. (Found) for $C_{19}H_{18}ClFN_4O$ (372.83): C, 61.21 (61.59); H, 4.87 (4.52); N, 15.03 (15.42).

6.1.4.5. 4-Amino-5-(2,6-difluorophenyl)-8,8-dimethyl-5,8,9,10-tetrahydropyrimido[4,5-b]quinolin-6(7H)-one ***(5e)***

White crystals, yield 86%, m.p. 275-277 °C. IR: 3445, 3332 (NH_2); 3134 (NH); 1659 (C=O). ^{1}H NMR (400 MHz, DMSO-d_6): δ 0.95 (s, 3H, CH_3), 1.07 (s, 3H, CH_3), 2.10 (d, *J* = 16 Hz, 1H, CH), 2.30 (d, *J* = 16.0 Hz, 1H, CH), 2.54-2.69 (m, 2H, CH_2), 5.22 (s, 1H, C_5-H), 6.58 (s, 1H, NH), 7.32 (t, *J* = 8.0 Hz, 1H, Ar-H), 7.51 (d, *J* = 8.0 Hz, 1H, Ar-H), 7.70 (d, *J* = 7.2 Hz, 1H, Ar-H), 8.12 (s, 1H, Pyrimidine-H). ^{13}C NMR: δ 27.0, 29.1, 32.2, 33.7, 50.4, 95.3, 111.9 (d, *J* = 25.0 Hz), 128.2 (d, *J* = 11.0 Hz), 129.8, 130.8 (d, *J* = 15.0 Hz), 132.5, 132.9, 141.3, 157.2 (d, *J* = 7.4 Hz), 161.9 (d, *J* = 7.1 Hz), 163.1, 163.2, 165.3, 196.2. EI-MS, *m/z*: 357.17 (1.46, M^++1), 356.21 (7.99, M^+), 55.15 (100.00). Anal. Calcd. (Found) for $C_{19}H_{18}F_2N_4O$ (356.14): C, 64.04 (64.41); H, 5.09 (5.43); N, 15.72 (15.40).

6.1.4.6. 4-Amino-5-(anthracen-9-yl)-8,8-dimethyl-5,8,9,10-tetrahydropyrimido[4,5-b]quinolin-6(7H)-one ***(5f)***

Yellow crystals, yield 83%, m.p. 234-236 °C. ^{1}H NMR (500 MHz, DMSO-d_6): δ 0.80 (s, 3H, CH_3), 1.05 (s, 3H, CH_3), 1.93 (d, *J* = 16.5 Hz, 1H, CH), 2.17 (d, *J* = 16.5 Hz, 1H, CH), 2.63-2.74 (dd, *J* = 17.9, 17.5 Hz, 2H, CH_2), 6.46 (s, 1H, C_5-H), 7.40-7.42 (m, 2H, Ar-H), 7.59 (t, *J* = 8.0 Hz, 1H, Ar-H), 7.72 (t, *J* = 8.0 Hz, 1H, Ar-H), 8.04-8.08 (m, 3H, Ar-H), 8.15 (d, *J* = 8.0 Hz, 1H, Ar-H), 8.60 (s, 1H, Pyrimidine-H), 9.12 (d, *J* = 9.0 Hz, 1H, Ar-H). ^{13}C NMR: δ 26.5, 28.5, 28.7, 31.6, 50.1, 98.0, 114.1, 122.8, 124.1, 125.2, 126.8, 127.3, 128.6, 130.6, 132.3, 134.6, 156.4, 160.8, 163.4, 195.9. EI-MS, *m/z*: 421.21 (59.01, M^++1), 419.71 (33.16, M^+), 167.51 (100.00). Anal. Calcd. (Found) for $C_{27}H_{24}N_4O$ (420.52): C, 77.12 (77.43); H, 5.75 (5.40); N, 13.32 (13.70).

6.1.5. Synthesis of 3-amino-4-imino-8,8-dimethyl-5-(substituted phenyl)-4,5,7,8,9,10-hexahydropyrimido[4,5-*b*]quinolin-6(3*H*)-ones 6a,b

Hydrazine hydrate 99% (5 mL, excess) in ethanol (10 mL) was added dropwise with vigorous stirring to a cold suspension (5-10 °C) of compound **4a,b** (0.005 mol) in ethanol (5 mL). The reaction mixture was stirred at room temperature for 3-5 h. The precipitated solid was filtered and crystallized from ethanol/water (3:1) to produce the pyrimidoquinolines **6a,b**.

6.1.5.1. 3-Amino-5-(2,3-dichlorophenyl)-4-imino-8,8-dimethyl-4,5,7,8,9,10-hexahydropyrimido[4,5-b]quinolin-6(3H)-one ***(6a)***

White powder, yield 96%, m.p. 206-207 °C. IR: 3304, 3285 (NH_2); 3196 (NH); 1655 (C=O). ^{1}H NMR (500 MHz, DMSO-d_6): δ 0.90 (s, 3H, CH_3), 1.03 (s, 3H, CH_3), 2.05 (d, *J* = 16.5 Hz, 1H,

CH), 2.27 (d, *J* = 16.0 Hz, 1H, CH), 2.51 (d, *J* = 18.0 Hz, 1H, CH), 2.61 (d, *J* = 18.0 Hz, 1H, CH), 5.08 (s, 1H, C_5-H), 5.66 (s, 2H, NH_2, D_2O-exchangeable), 6.56 (s, 1H, NH, D_2O-exchangeable), 6.73 (s, 1H, NH, D_2O-exchangeable), 7.28-7.45 (m, 3H, Ar-H), 8.06 (s, 1H, Pyrimidine-H). ^{13}C NMR: δ 26.5, 28.6, 31.8, 32.9, 50.0, 98.9, 112.1, 127.2, 128.2, 129.2, 130.7, 131.9, 142.3, 150.3, 152.1, 155.0, 164.1, 195.8. EI-MS, *m/z*: 408.00 (1.31, M^++4), 406.00 (1.90, M^++2), 404.00 (3.05, M^+), 77.10 (100.00). Anal. Calcd. (Found) for $C_{19}H_{19}Cl_2N_5O$ (404.30): C, 56.45 (56.80); H, 4.74 (4.41); N, 17.32 (17.60).

6.1.5.2. 3-Amino-5-(3,4-dichlorophenyl)-4-imino-8,8-dimethyl-4,5,7,8,9,10-hexahydropyrimido[4,5-b]quinolin-6(3H)-one ***(6b)***

White powder, yield 90%, m.p. 200-202 °C. IR: 3303, 3275 (NH_2); 3197 (NH); 1654 (C=O). ^{1}H NMR (500 MHz, DMSO-d_6): δ 0.91 (s, 3H, CH_3), 1.03 (s, 3H, CH_3), 2.10 (d, *J* = 16.5 Hz, 1H, CH), 2.28 (d, *J* = 16.0 Hz, 1H, CH), 2.57-2.63 (m, 2H, CH_2), 4.77 (s, 1H, C_5-H), 5.64 (s, 2H, NH_2, D_2O-exchangeable), 6.81 (s, 1H, NH, D_2O-exchangeable), 7.11-7.49 (m, 3H, Ar-H), 7.76 (s, 1H, NH, D_2O-exchangeable), 8.04 (s, 1H, Pyrimidine-H). ^{13}C NMR: δ 26.9, 29.1, 32.3, 39.4, 50.5, 90.4, 111.9, 124.1, 127.8, 129.2, 134.2, 136.4, 137.8, 150.2, 153.3, 155.5, 164.5, 196.3. EI-MS, *m/z*: 404.86 (16.64, M^++1), 379.68 (100.00). Anal. Calcd. (Found) for $C_{19}H_{19}Cl_2N_5O$ (404.30): C, 56.45 (56.71); H, 4.74 (4.39); N, 17.32 (17.59).

6.1.6. Synthesis of 5-(2,3-dichlorophenyl)-4-imino-8,8-dimethyl-3-(substituted benzylideneamino)-4,5,7,8,9,10-hexahydropyrimido[4,5-*b*]quinolin-6(3*H*)-ones 7a-d

A mixture of compound **6a** (2.02 g, 0.005 mol), the appropriate benzaldehyde (0.005 mol) and a catalytic amount of piperidine (0.5 mL) in ethanol (10 mL) was refluxed for 6-8 h. The mixture was concentrated, and the precipitated solid was filtered, washed several times with cold ethanol and crystallized from ethanol to yield the pyrimidoquinolines **7a-d**.

6.1.6.1. 3-(Benzylideneamino)-5-(2,3-dichlorophenyl)-4-imino-8,8-dimethyl-4,5,7,8,9,10-hexahydropyrimido[4,5-b]quinolin-6(3H)-one ***(7a)***

Dark yellow crystals, yield 85%, m.p. 226-227 °C. ^{1}H NMR (500 MHz, DMSO-d_6): δ 0.94 (s, 3H, CH_3), 1.06 (s, 3H, CH_3), 2.11 (d, *J* = 16.5 Hz, 1H, CH), 2.33 (d, *J* = 16.0 Hz, 1H, CH), 2.54 (d, *J* = 18.0 Hz, 1H, CH), 2.68 (d, *J* = 18.0 Hz, 1H, CH), 5.79 (s, 1H, C_5-H), 7.27 (d, *J* = 6.0 Hz, 1H, Ar-H), 7.39-7.46 (m, 4H, Ar-H), 7.71 (s, 3H, Ar-H), 8.12 (s, 1H, Pyrimidine-H), 8.34 (s, 1H, N=CH), 10.56 (s, 1H, NH, D_2O-exchangeable). ^{13}C NMR: δ 26.4, 28.7, 31.8, 32.1, 49.9, 96.0, 110.9, 126.6, 126.7, 128.9, 129.2, 129.8, 132.6, 133.4, 134.2, 134.9, 137.5, 144.7, 156.7, 158.4,

162.5, 164.5, 195.8. EI-MS, *m/z*: 492.19 (31.26, M^+), 222.00 (100.00). Anal. Calcd. (Found) for $C_{26}H_{23}Cl_2N_5O$ (492.40): C, 63.42 (63.09); H, 4.71 (4.31); N, 14.22 (14.60).

6.1.6.2. 3-((4-Chlorobenzylidene)amino)-5-(2,3-dichlorophenyl)-4-imino-8,8-dimethyl-4,5,7,8,9,10-hexahydropyrimido[4,5-b]quinolin-6(3H)-one ***(7b)***

Yellow crystals, yield 82%, m.p. 224-226 °C. ^{1}H NMR (500 MHz, DMSO-d_6): δ 0.89 (s, 3H, CH_3), 1.05 (s, 3H, CH_3), 2.18 (d, *J* = 16.0 Hz, 1H, CH), 2.34 (d, *J* = 16.0 Hz, 1H, CH), 2.58-2.67 (dd, *J* = 16.0, 16.0 Hz, 2H, CH_2), 5.76 (s, 1H, C_5-H), 7.11 (d, *J* = 8.0 Hz, 1H, Ar-H), 7.47-7.52 (m, 4H, Ar-H), 7.71 (d, *J* = 8.0 Hz, 2H, Ar-H), 8.18 (s, 1H, Pyrimidine-H), 8.38 (s, 1H, N=CH), 11.18 (s, 1H, NH, D_2O-exchangeable). ^{13}C NMR: δ 26.5, 28.5, 31.0, 32.0, 49.9, 97.2, 113.6, 127.9, 128.3, 129.0, 129.4, 130.0, 130.6, 130.8, 133.2, 134.2, 143.6, 144.4, 156.8, 158.3, 162.5, 164.3, 196.0. Anal. Calcd. (Found) for $C_{26}H_{22}Cl_3N_5O$ (525.09): C, 59.27 (59.52); H, 4.21 (4.61); N, 13.29 (13.60).

6.1.6.3. 3-((4-Bromobenzylidene)amino)-5-(2,3-dichlorophenyl)-4-imino-8,8-dimethyl-4,5,7,8,9,10-hexahydropyrimido[4,5-b]quinolin-6(3H)-one ***(7c)***

Yellow crystals, yield 78%, m.p. 293-295 °C. ^{1}H NMR (500 MHz, DMSO-d_6): δ 0.94 (s, 3H, CH_3), 1.06 (s, 3H, CH_3), 2.13 (d, *J* = 16.0 Hz, 1H, CH), 2.32 (d, *J* = 15.5 Hz, 1H, CH), 2.57 (d, *J* = 18.0 Hz, 1H, CH), 2.69 (d, *J* = 18.0 Hz, 1H, CH), 5.83 (s, 1H, C_5-H), 7.22 (t, *J* = 8.5 Hz, 1H, Ar-H), 7.45 (d, *J* = 7.0 Hz, 1H, Ar-H), 7.58-7.69 (m, 5H, Ar-H), 8.09 (s, 1H, Pyrimidine-H), 8.36 (s, 1H, N=CH), 10.57 (s, 1H, NH, D_2O-exchangeable), 12.19 (s, 1H, NH, D_2O-exchangeable). ^{13}C NMR: δ 26.5, 28.6, 31.8, 33.0, 49.9, 96.3, 111.1, 122.9, 127.4, 128.5, 129.5, 130.4, 131.9, 132.2, 132.7, 133.5, 141.0, 143.4, 156.8, 158.3, 162.5, 164.7, 195.8. EI-MS, *m/z*: 570.39 (31.68, M^+-1), 316.80 (100.00). Anal. Calcd. (Found) for $C_{26}H_{22}BrCl_2N_5O$ (571.30): C, 54.66 (54.45); H, 3.88 (3.61); N, 12.26 (12.60).

6.1.6.4. 5-(2,3-Dichlorophenyl)-4-imino-3-((4-(dimethylamino)benzylidene)amino)-8,8-dimethyl-4,5,7,8,9,10-hexahydropyrimido[4,5-b]quinolin-6(3H)-one ***(7d)***

Dark yellow crystals, yield 70%, m.p. 302-304 °C. ^{1}H NMR (500 MHz, DMSO-d_6): δ 0.94 (s, 3H, CH_3), 1.06 (s, 3H, CH_3), 2.12 (d, *J* = 16.5 Hz, 1H, CH), 2.32 (d, *J* = 16.5 Hz, 1H, CH), 2.56 (d, *J* = 18.0 Hz, 1H, CH), 2.68 (d, *J* = 18.0 Hz, 1H, CH), 2.95 (s, 6H, $N(CH_3)_2$), 5.89 (s, 1H, C_5-H), 6.75 (d, *J* = 9.0 Hz, 2H, Ar-H), 7.18-7.21 (t, *J* = 8.0 Hz, 1H, Ar-H), 7.44 (d, *J* = 7.0 Hz, 1H, Ar-H), 7.51 (d, *J* = 8.0 Hz, 2H, Ar-H), 7.68 (d, *J* = 7.5 Hz, 1H, Ar-H), 7.94 (s, 1H, Pyrimidine-H), 8.28 (s, 1H, N=CH), 10.21 (s, 1H, NH, D_2O-exchangeable). ^{13}C NMR: δ 26.5, 28.7, 31.8, 33.2, 42.7, 50.0, 95.3, 111.6, 111.9, 121.4, 127.3, 128.1, 129.0, 129.4, 130.5, 132.6, 141.3, 145.7, 151.3, 156.6, 158.3, 162.4, 164.7, 195.8. EI-MS, *m/z*: 535.84 (13.34, M^++1), 533.78 (3.90, M^+-

1), 258.58 (100.00). Anal. Calcd. (Found) for $C_{28}H_{28}Cl_2N_6O$ (535.47): C, 62.81 (62.51); H, 5.27 (5.55); N, 15.69 (15.83).

6.1.7. Synthesis of 1-(5-(2,3-dichlorophenyl)-4-imino-8,8-dimethyl-6-oxo-5,6,7,8,9,10-hexahydropyrimido[4,5-*b*]quinolin-3(4*H*)-yl)-3-(4-substituted phenyl)thioureas 8a,b

A mixture of **6a** (0.81 g, 0.002 mol) and the appropriate phenyl isothiocyanate (0.005 mol) in ethanol (10 mL) was refluxed for 3-4 h. The solvent was evaporated under reduced pressure, and the remained residue was crystallized from ethanol/water (1:1) to yield the thiourea derivatives **8a,b**.

6.1.7.1. 3-(4-Chlorophenyl)-1-(5-(2,3-dichlorophenyl)-4-imino-8,8-dimethyl-6-oxo-5,6,7,8,9,10-hexahydropyrimido[4,5-b]quinolin-3(4H)-yl)thiourea ***(8a)***

Pale green powder, yield 62%, m.p. 256-258 °C. ^{1}H NMR (500 MHz, DMSO-d_6): δ 0.93 (s, 3H, CH_3), 1.04 (s, 3H, CH_3), 2.06 (d, J = 15.5 Hz, 1H, CH), 2.28 (d, J = 16.0 Hz, 1H, CH), 2.52 (d, 18.0 Hz, 1H, CH), 2.64 (d, J = 17.0 Hz, 1H, CH), 5.10 (s, 1H, C_5-H), 6.64 (s, 2H, 2NH, D_2O-exchangeable), 7.36-7.46 (m, 3H, Ar-H), 7.68 (d, J = 8.5 Hz, 2H, Ar-H), 7.79 (d, J = 8.0 Hz, 2H, Ar-H), 8.09 (s, 1H, Pyrimidine-H), 9.39 (s, 1H, NH, D_2O-exchangeable), 9.97 (s, 1H, NH, D_2O-exchangeable). ^{13}C NMR: δ 26.4, 28.7, 31.7, 31.8, 49.9, 94.5, 111.1, 126.9, 127.0, 128.5, 129.5, 132.5, 133.1, 134.9, 138.8, 139.4, 151.3, 152.8, 156.7, 161.4, 162.7, 181.1, 195.7. EI-MS, *m/z*: 573.79 (9.85, M^+), 523.18 (100.00). Anal. Calcd. (Found) for $C_{26}H_{23}Cl_3N_6OS$ (573.92): C, 54.41 (54.79); H, 4.04 (4.36); N, 14.64 (14.89).

6.1.7.2. 1-(5-(2,3-Dichlorophenyl)-4-imino-8,8-dimethyl-6-oxo-5,6,7,8,9,10-hexahydropyrimido[4,5-b]quinolin-3(4H)-yl)-3-(4-methoxyphenyl)thiourea ***(8b)***

Pale yellow powder, yield 67%, m.p. 238-240 °C. ^{1}H NMR (500 MHz, DMSO-d_6): δ 0.93 (s, 3H, CH_3), 1.04 (s, 3H, CH_3), 2.06 (d, J = 16.0 Hz, 1H, CH), 2.28 (d, J = 16.0 Hz, 1H, CH), 2.51 (d, J = 18.0 Hz, 1H, CH), 2.64 (d, J = 17.5 Hz, 1H, CH), 3.76 (s, 3H, OCH_3), 5.10 (s, 1H, C_5-H), 6.70 (s, 1H, NH, D_2O-exchangeable), 6.98-7.15 (m, 4H, Ar-H), 7.36-7.38 (dd, J = 2.5, 8.5 Hz, 1H, Ar-H), 7.45 (d, J = 2.5 Hz, 1H, Ar-H), 7.77 (d, J = 8.0 Hz, 1H, Ar-H), 8.09 (s, 1H, Pyrimidine-H), 9.33 (s, 1H, NH, D_2O-exchangeable), 9.57 (s, 1H, NH, D_2O-exchangeable). ^{13}C NMR: δ 26.4, 28.7, 31.7, 32.2, 49.9, 55.3, 94.5, 111.1, 115.1, 126.9, 127.4, 129.5, 132.5, 133.1, 134.9, 137.1, 139.2, 156.7, 158.4, 161.4, 162.7, 164.8, 181.9, 195.7. EI-MS, *m/z*: 569.19 (54.98, M^+), 119.38 (100.00). Anal. Calcd. (Found) for $C_{27}H_{26}Cl_2N_6O_2S$ (569.51): C, 56.94 (57.23); H, 4.60 (4.93); N, 14.76 (14.95).

6.1.8. Synthesis of 9,9-dimethyl-12-(substituted phenyl)-8,9,10,12-tetrahydro-[1,2,4]triazolo[1',5':1,6]pyrimido[4,5-*b*]quinolin-11(7*H*)-ones 9a,b

A mixture of compound **6a,b** (0.002 mol) and triethyl orthoformate (10 mL) was refluxed for 8–10 h. The reaction mixture was cooled and diluted with cold ethanol (10 mL). The precipitated solid was filtered and crystallized from ethanol to yield the triazolopyrimidoquinolines **9a,b**.

6.1.8.1. 12-(2,3-Dichlorophenyl)-9,9-dimethyl-8,9,10,12-tetrahydro-[1,2,4]triazolo[1',5':1,6]pyrimido[4,5-b]quinolin-11(7H)-one ***(9a)***

White powder, yield 79%, m.p. 180-182 °C. ^{1}H NMR (500 MHz, DMSO-d_6): δ 1.04 (s, 3H, CH_3), 1.07 (s, 3H, CH_3), 2.21 (d, J = 16.5 Hz, 1H, CH), 2.32 (d, J = 16.0 Hz, 1H, CH), 2.67-2.79 (dd, J = 18.0, 18.0 Hz, 2H, CH_2), 5.25 (s, 1H, C_{12}-H), 7.32-7.34 (dd, J = 2.0, 2.0 Hz, 1H, Ar-H), 7.49 (d, J = 8.5 Hz, 1H, Ar-H), 7.58 (d, J = 2.5 Hz, 1H, Ar-H), 8.58 (s, 1H, Pyrimidine-H), 9.66 (s, 1H, Triazole-H). ^{13}C NMR: δ 26.9, 28.4, 32.1, 34.1, 50.0, 102.6, 111.5, 128.9, 129.6, 130.4, 130.5, 130.8, 141.0, 143.5, 151.7, 152.3, 156.8, 164.7, 196.1. EI-MS, *m/z*: 418.29 (2.81, M^++4), 416.25 (12.82, M^++2), 414.16 (23.78, M^+), 69.06 (100.00). Anal. Calcd. (Found) for $C_{20}H_{17}Cl_2N_5O$ (414.29): C, 57.98 (57.64); H, 4.14 (4.54); N, 16.90 (16.67).

6.1.8.2. 12-(3,4-Dichlorophenyl)-9,9-dimethyl-8,9,10,12-tetrahydro-[1,2,4]triazolo[1',5':1,6]pyrimido[4,5-b]quinolin-11(7H)-one ***(9b)***

White powder, yield 82%, m.p. 185-186 °C. ^{1}H NMR (500 MHz, DMSO-d_6): δ 1.02 (s, 3H, CH_3), 1.07 (s, 3H, CH_3), 2.22 (d, J = 16.0 Hz, 1H, CH), 2.32 (d, J = 16.5 Hz, 1H, CH), 2.69 (d, J = 18.0 Hz, 1H, CH), 2.77 (d, J = 17.5 Hz, 1H, CH), 5.25 (s, 1H, C_{12}-H), 7.32-7.34 (dd, J = 2.0, 2.0 Hz, 1H, Ar-H), 7.50 (d, J = 8.5 Hz, 1H, Ar-H), 7.58 (d, J = 2.0 Hz, 1H, Ar-H), 8.58 (s, 1H, Pyrimidine-H), 9.67 (s, 1H, Triazole-H). ^{13}C NMR: δ 26.9, 28.3, 32.0, 34.1, 49.9, 102.6, 111.4, 128.8, 129.6, 130.4, 130.5, 130.7, 140.9, 143.5, 151.6, 152.2, 156.8, 164.6, 195.9. EI-MS, *m/z*: 414.30 (0.09, M^+), 93.10 (100.00). Anal. Calcd. (Found) for $C_{20}H_{17}Cl_2N_5O$ (414.29): C, 57.98 (57.59); H, 4.14 (4.39); N, 16.90 (16.76).

6.2. Biology

All biological screening methods are presented in details in the Supplementary file.

Acknowledgments

We are immensely grateful to Holding Company for Biological Products and Vaccines (VACSERA), Egypt for performing the cytotoxicity, kinase profile, cell cycle analysis, cell apoptosis and Bax/Bcl-2 assays.

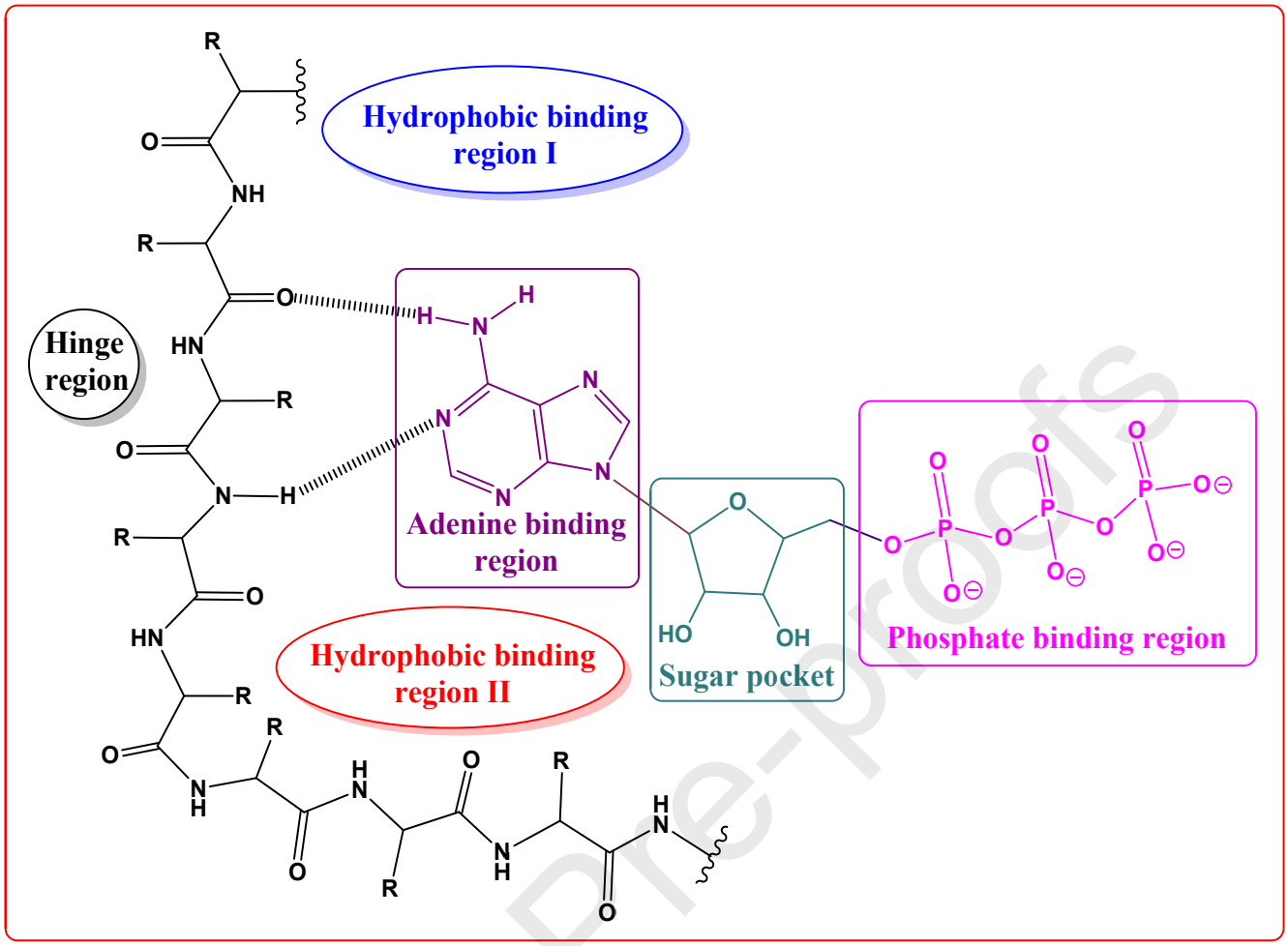

Fig. 1. The ATP-binding site of EGFR-TK.

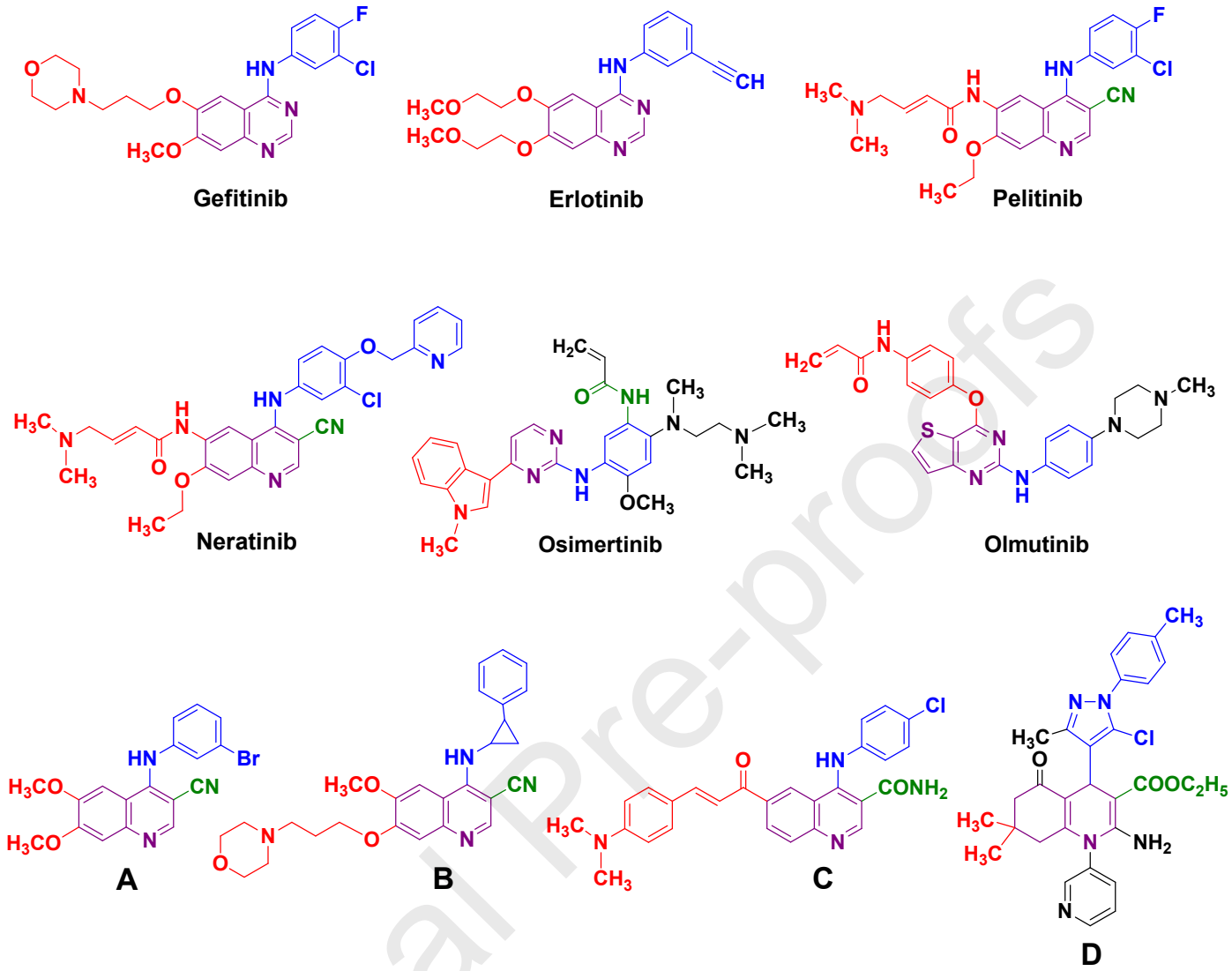

Fig. 2. Examples of first-generation (gefitinib and erlotinib), second-generation (pelitinib and neratinib) and third-generation (osimertinib and olmutinib) EGFR-TKIs, and quinolines **A-D** with reported antitumor and EGFR-TK inhibitory activities.

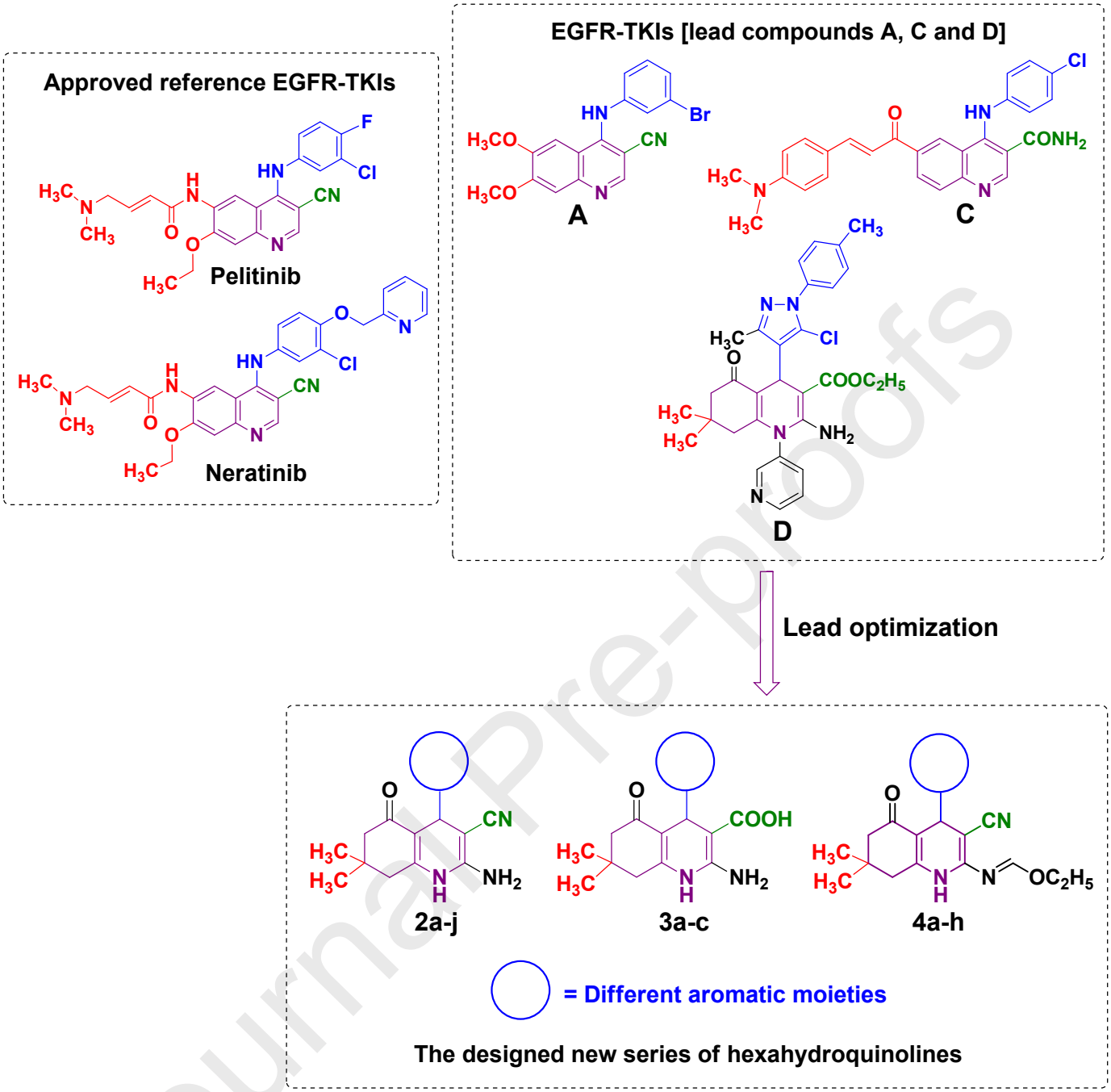

Fig. 3. The designed new series of hexahydroquinolines **2a-j**, **3a-c** and **4a-h** as prospective antitumor agents and EGFR-TKIs.

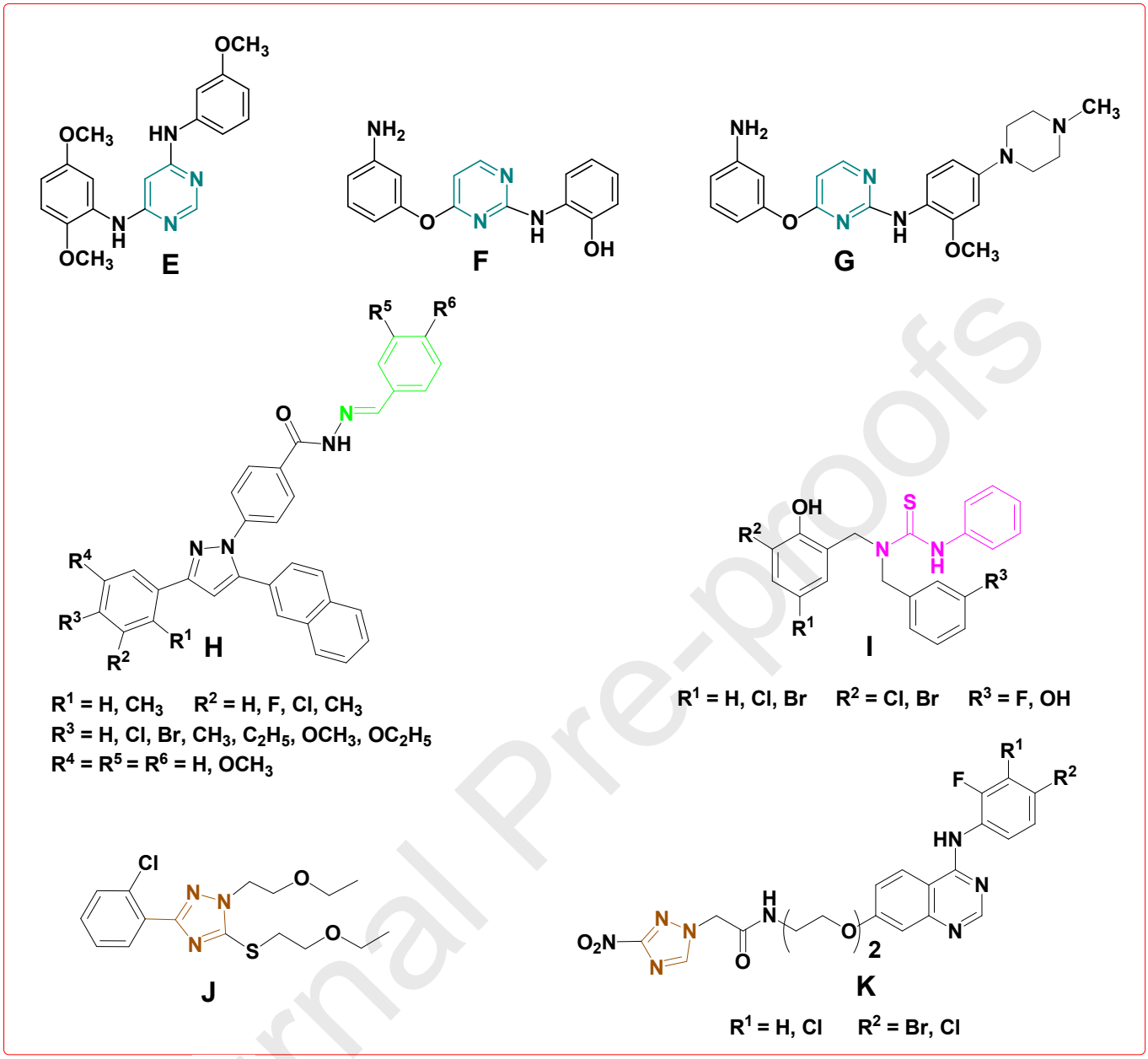

Fig. 4. Examples of pyrimidines **E-G**, benzylideneamines **H**, phenylthioureas **I** and [1,2,4]triazoles **J,K** with reported antitumor and EGFR-TK inhibitory activities.

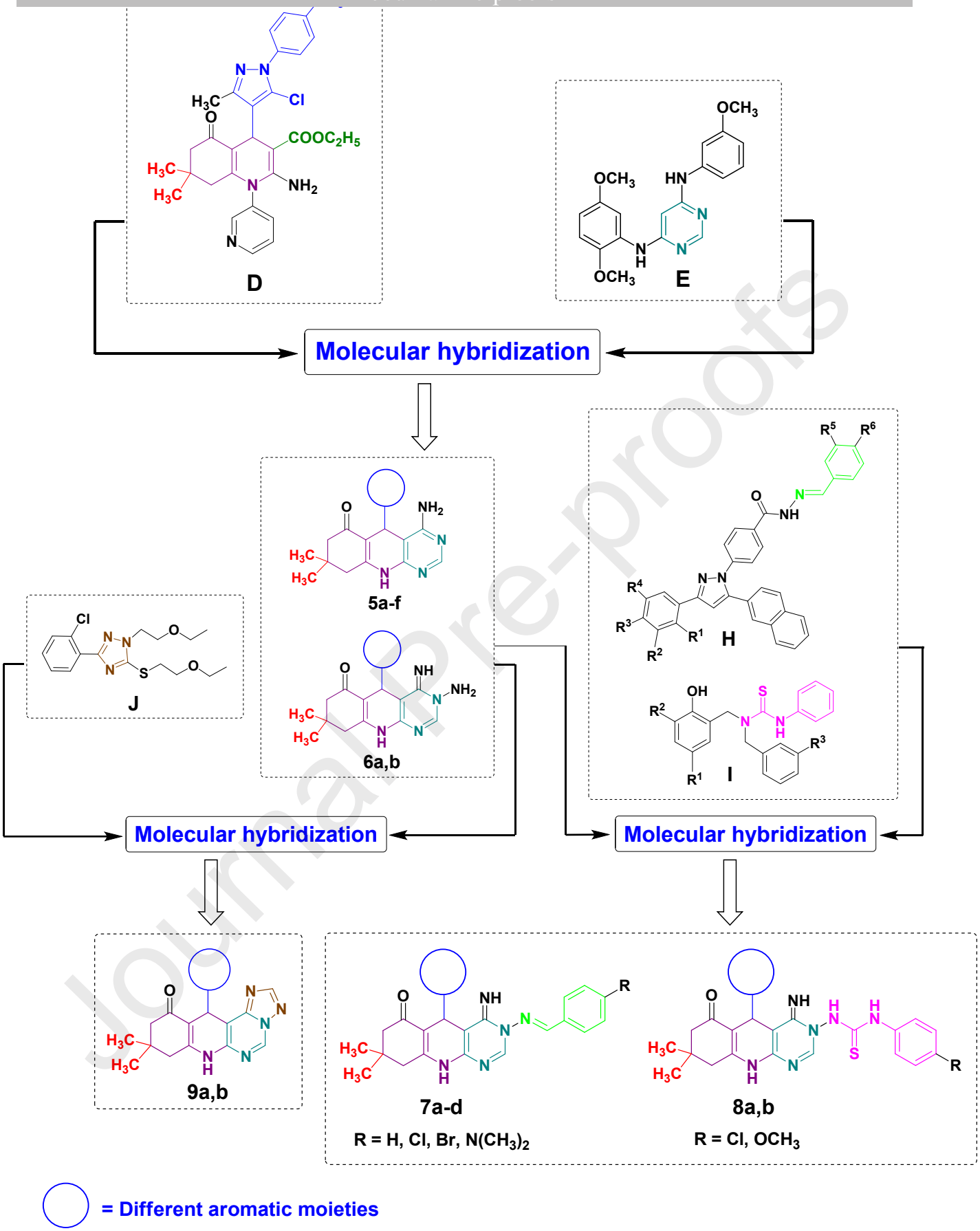

Fig. 5. The designed new hybrid compounds **5a-f, 6a,b, 7a-d, 8a,b** and **9a,b** as prospective antitumor agents and EGFR-TKIs.

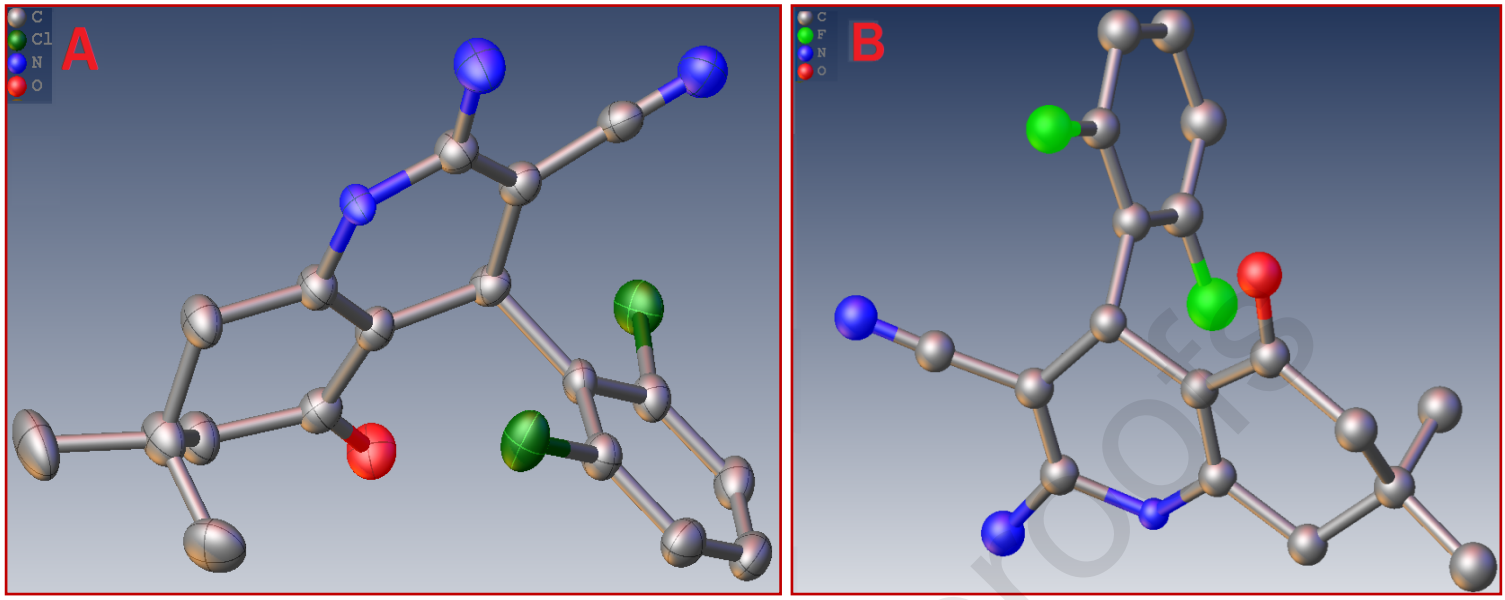

Fig. 6. The ORTEP plots of compounds **2c (A)** and **2f (B).**

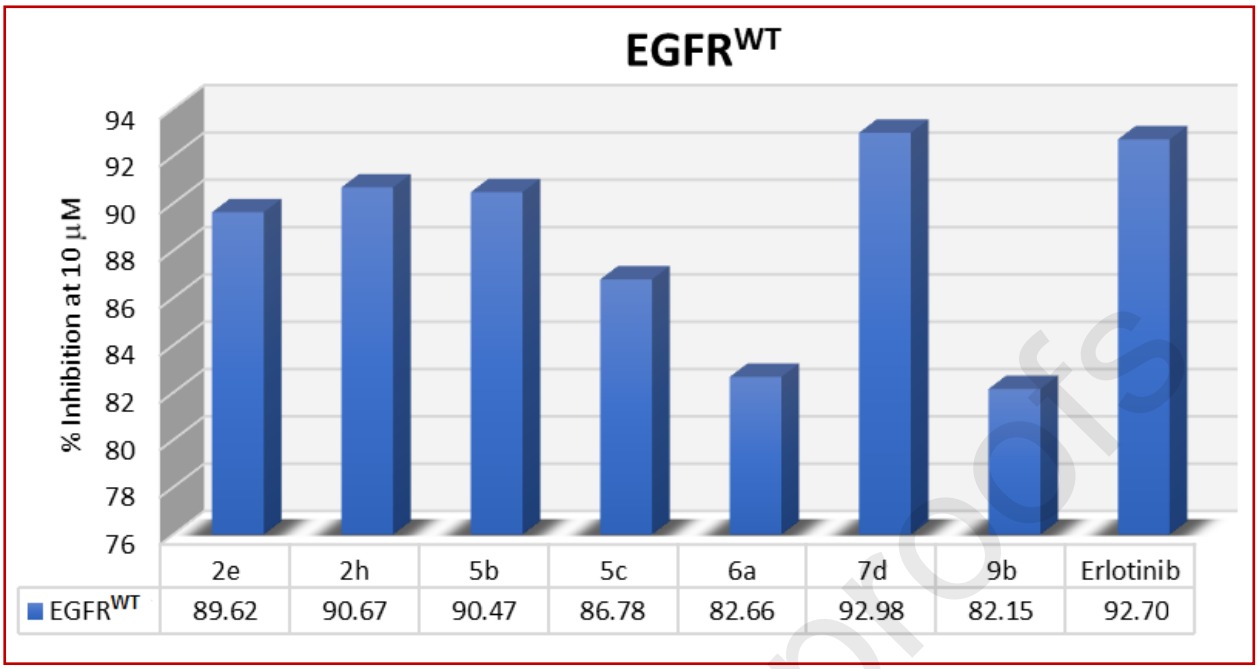

Fig. 7. % Inhibition of $EGFR^{WT}$ by compounds **2e, 2h, 5b, 5c, 6a, 7d** and **9b** (at 10 µM).

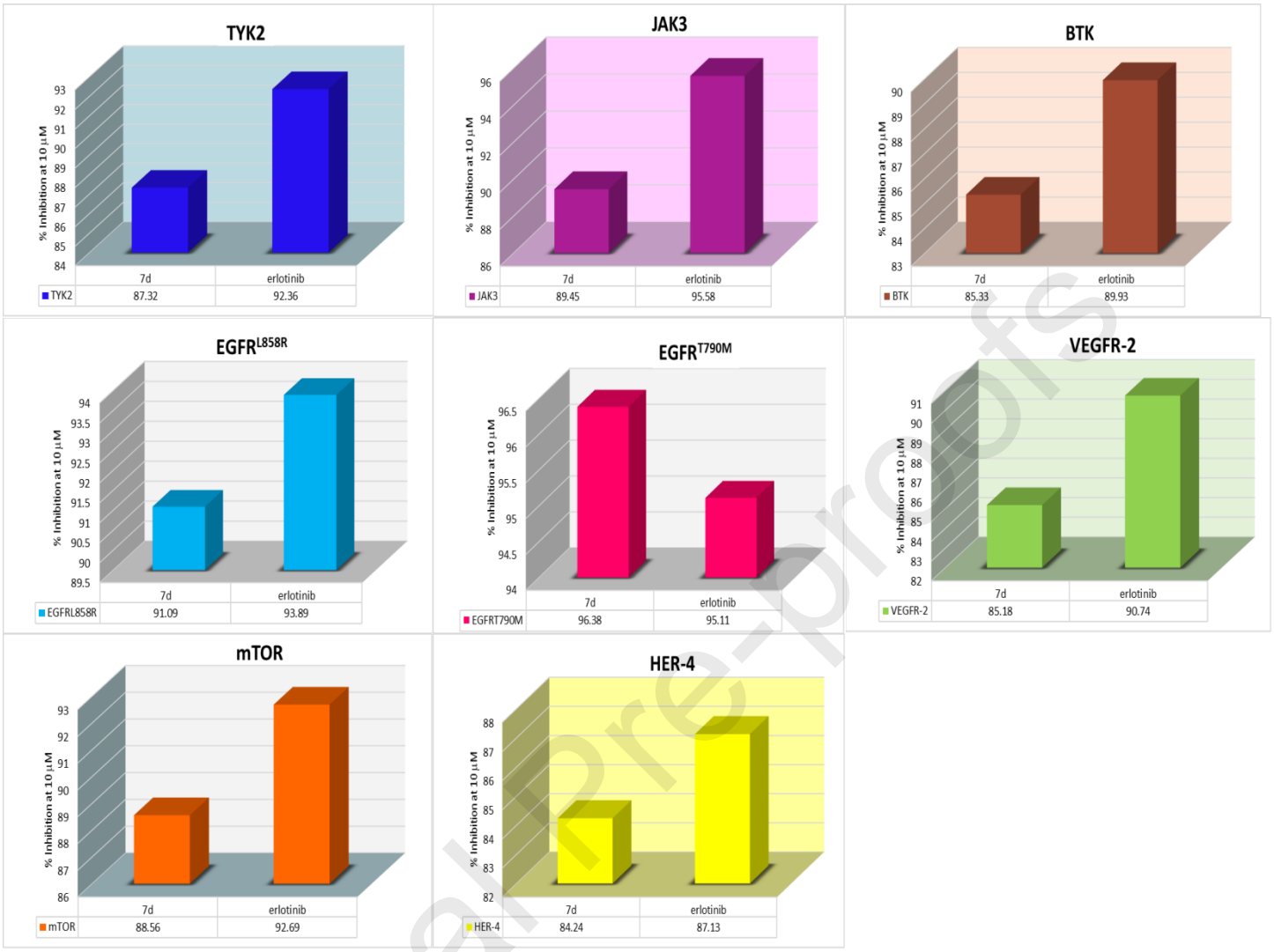

Fig. 8. % Inhibition of kinase activity induced by compound **7d** (at 10 µM).

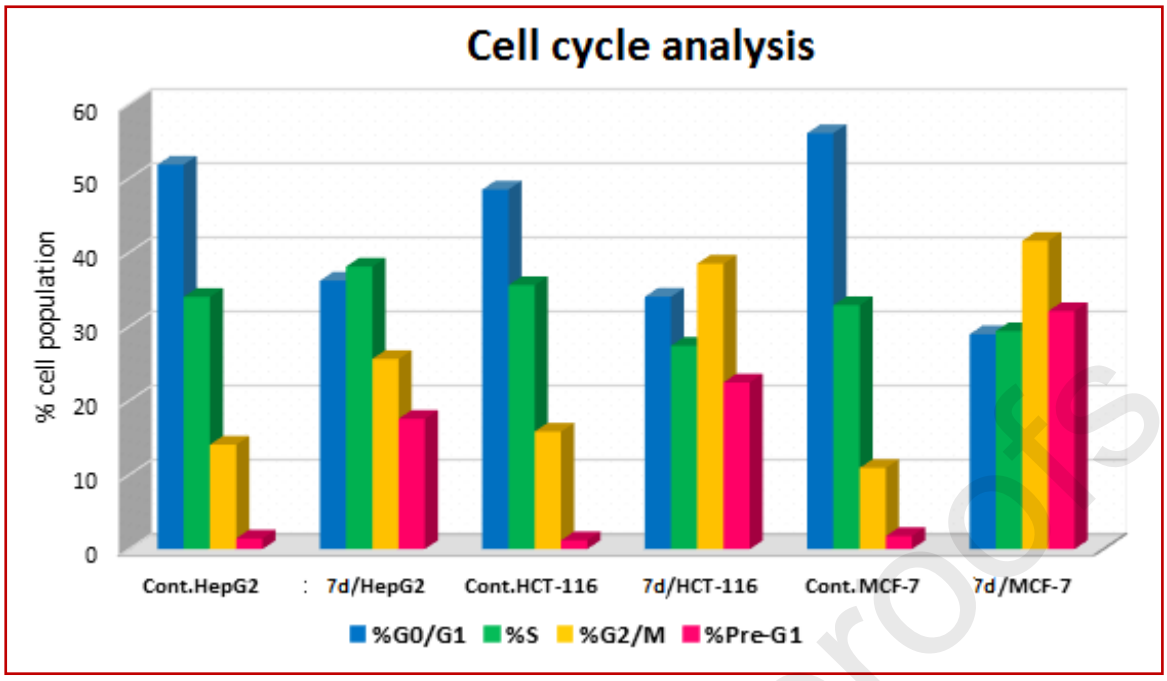

Fig. 9. Bar diagram showing % cell distribution in G0/G1, S, G2/M and Pre-G1 phases for HepG2, HCT-116 and MCF-7 cells treated with vehicle control and **7d** (at the IC_{50} of the corresponding cell line).

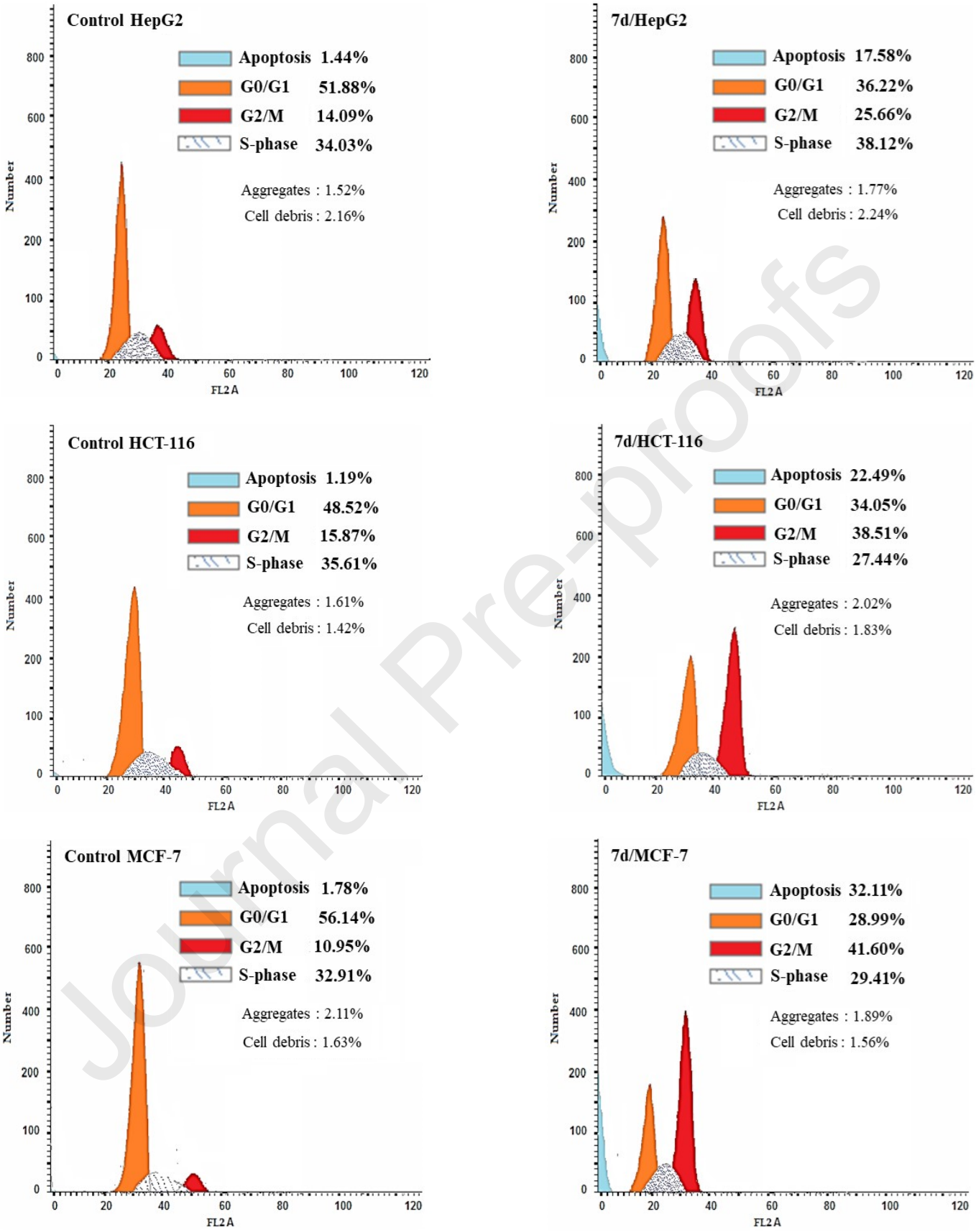

Fig. 10. Flow cytometry analysis of cell cycle phase distribution in HepG2, HCT-116 and MCF-7 cells after treatment with vehicle control and **7d** (at the IC_{50} of the corresponding cell line).

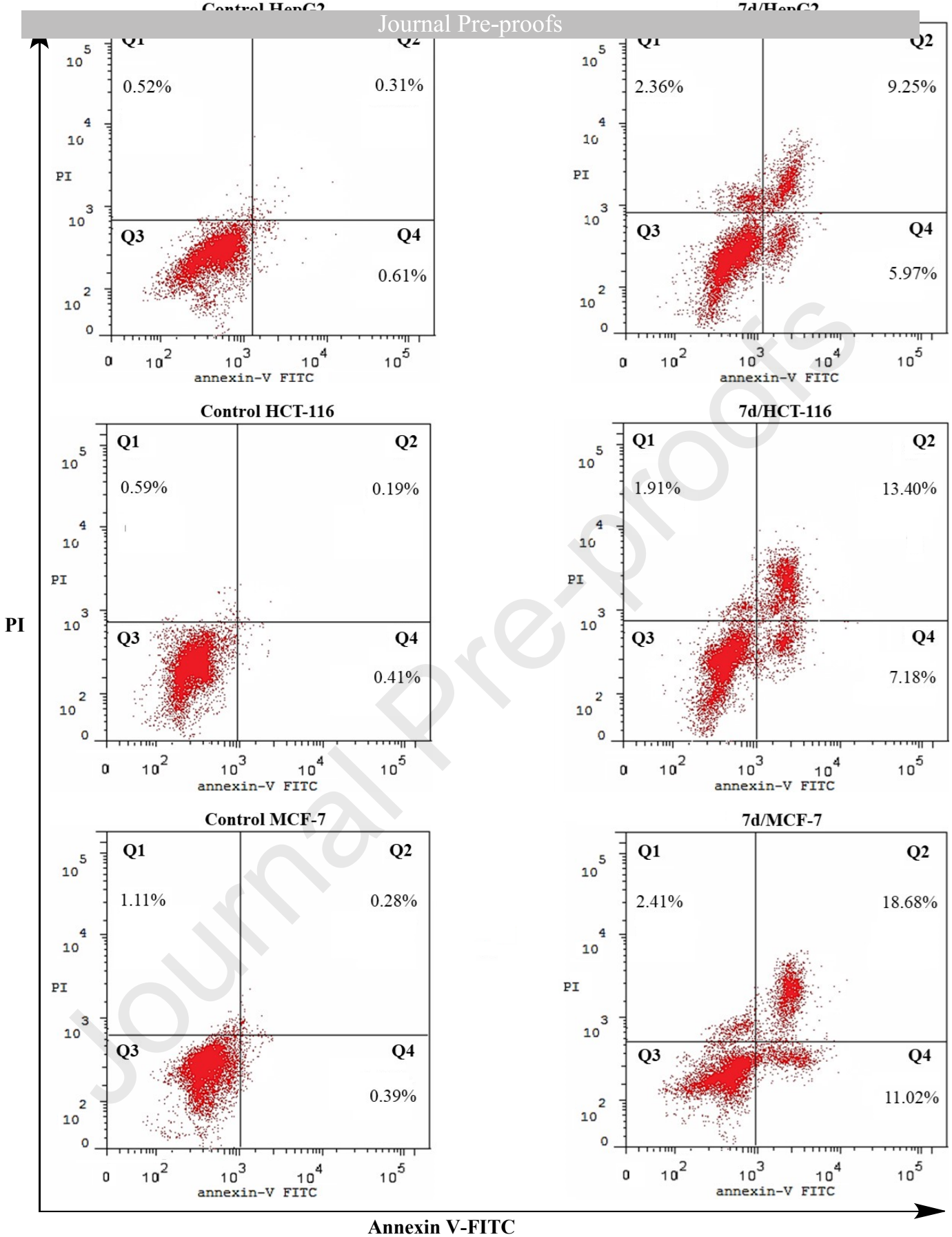

Fig. 11. Annexin V-FITC/PI double staining for detection of apoptosis in HepG2, HCT-116 and MCF-7 cells after treatment with **7d** (at the IC_{50} of the corresponding cell line). Q1 quadrant represents dead (necrotic) cells; Q2 quadrant represents late apoptosis; Q3 quadrant represents live cells; Q4 quadrant represents early apoptosis. Summation of early and late apoptosis represents total apoptosis.

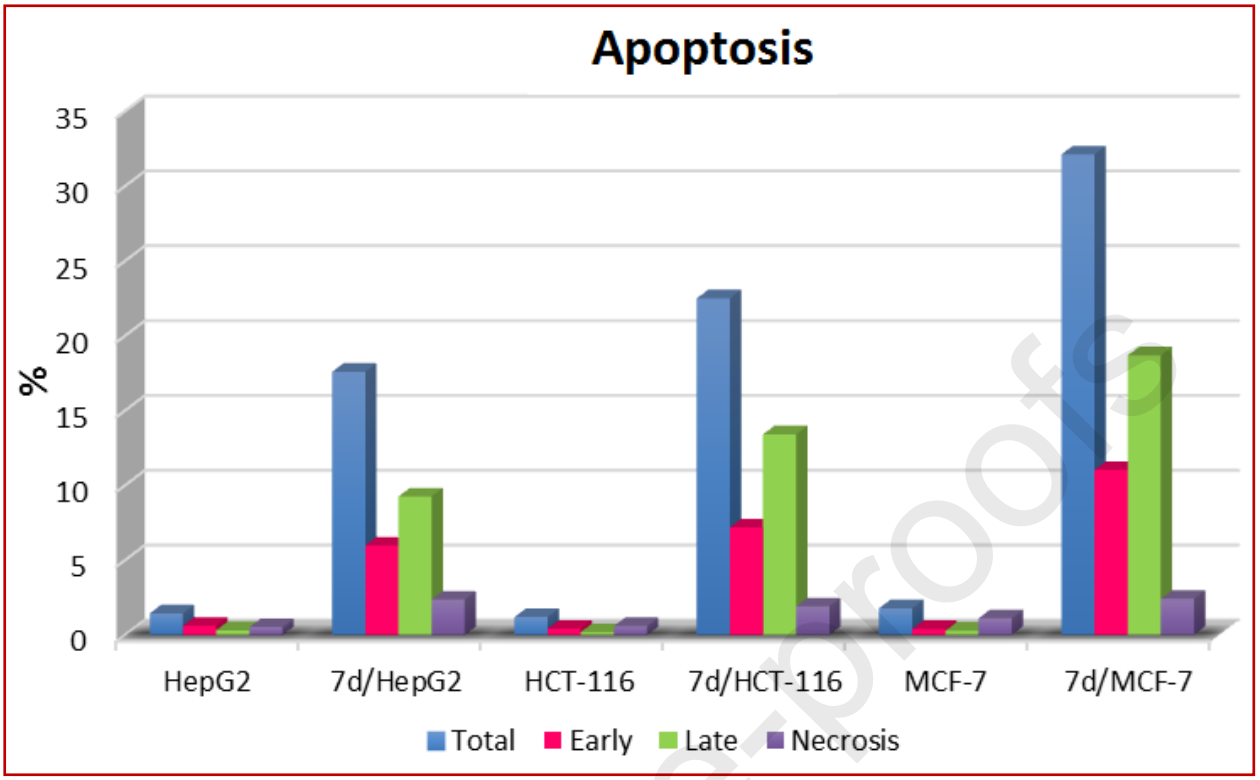

Fig. 12. Bar diagram showing % apoptosis in HepG2, HCT-116 and MCF-7 cells treated with vehicle control and **7d** (at the IC_{50} of the corresponding cell line).

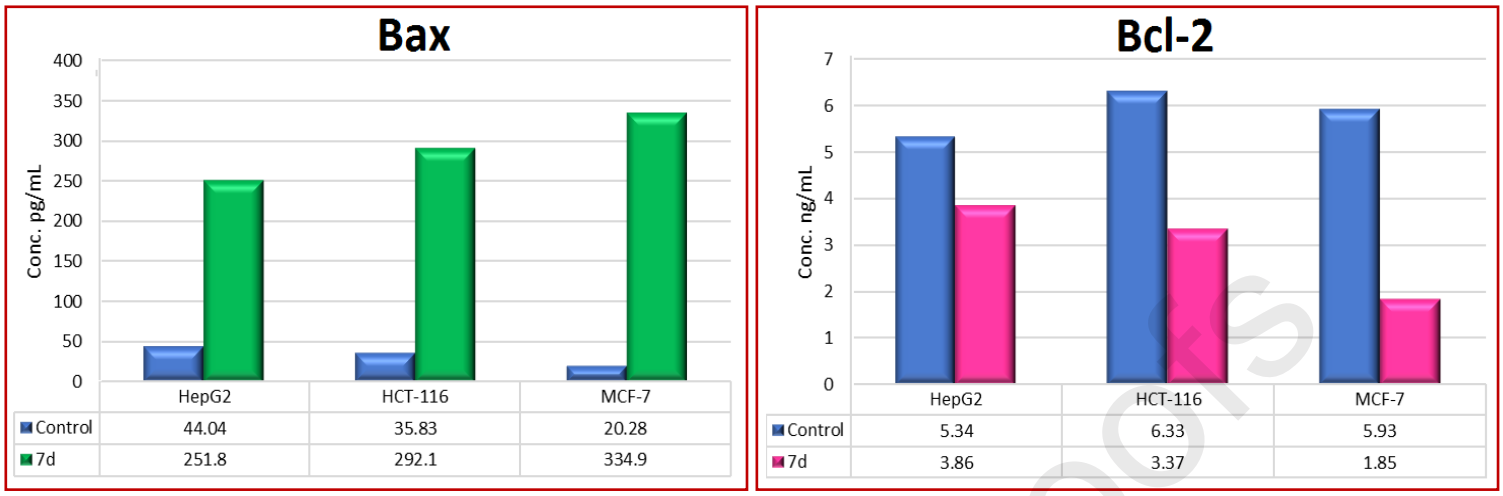

Fig. 13. Assessment of the effect of compound **7d** on Bax and Bcl-2 levels in HepG2, HCT-116 and MCF-7 cells.

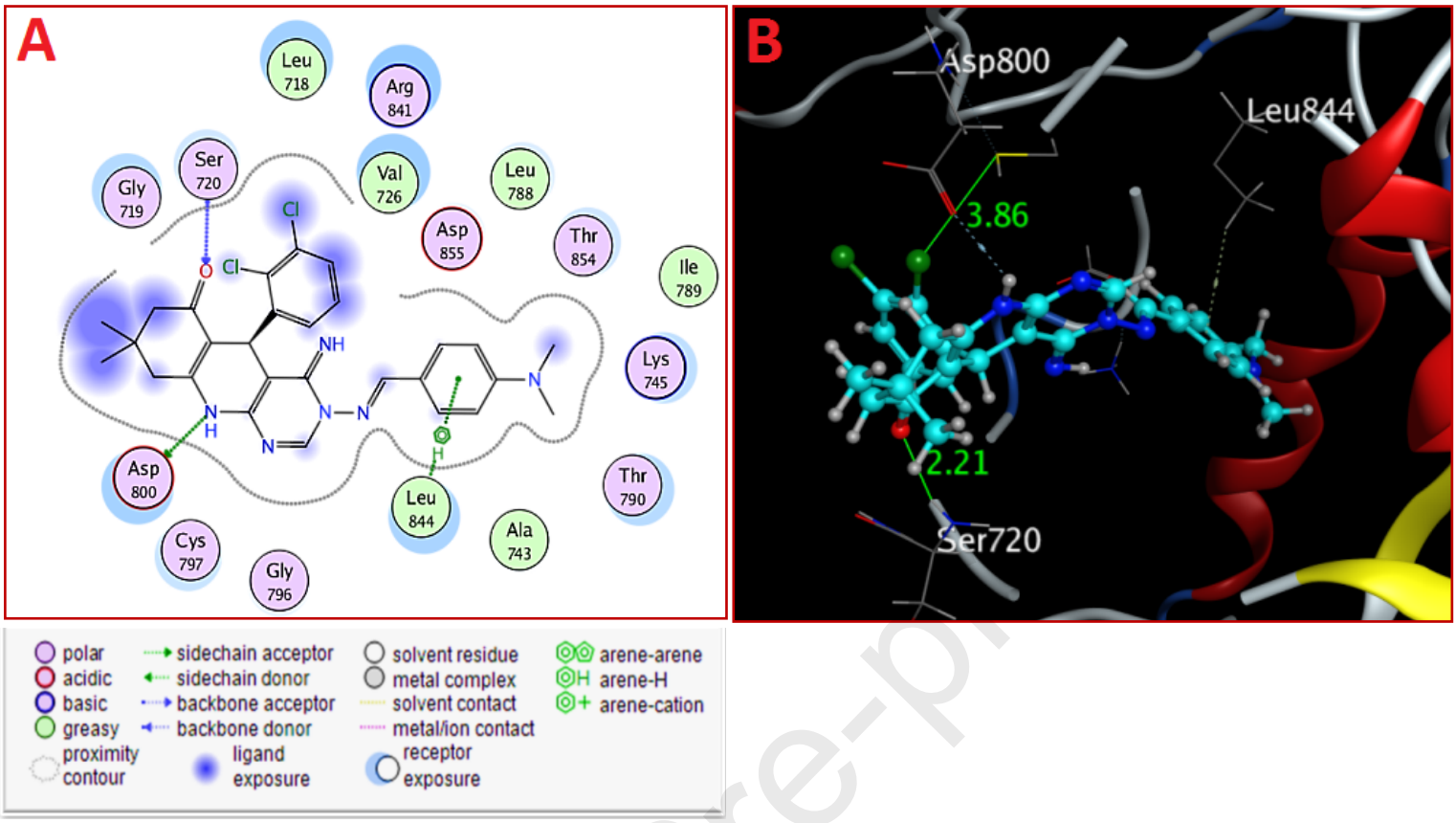

Fig. 14. (A) 2D Interaction of **7d** with the binding site of $EGFR^{WT}$. **(B)** 3D Interaction of **7d** with the binding site of $EGFR^{WT}$. Atoms are colored as follows: cyan for carbon, light gey for hydrogen, blue for nitrogen, red for oxygen and green for chlorine. (PDB code: 3W2S).

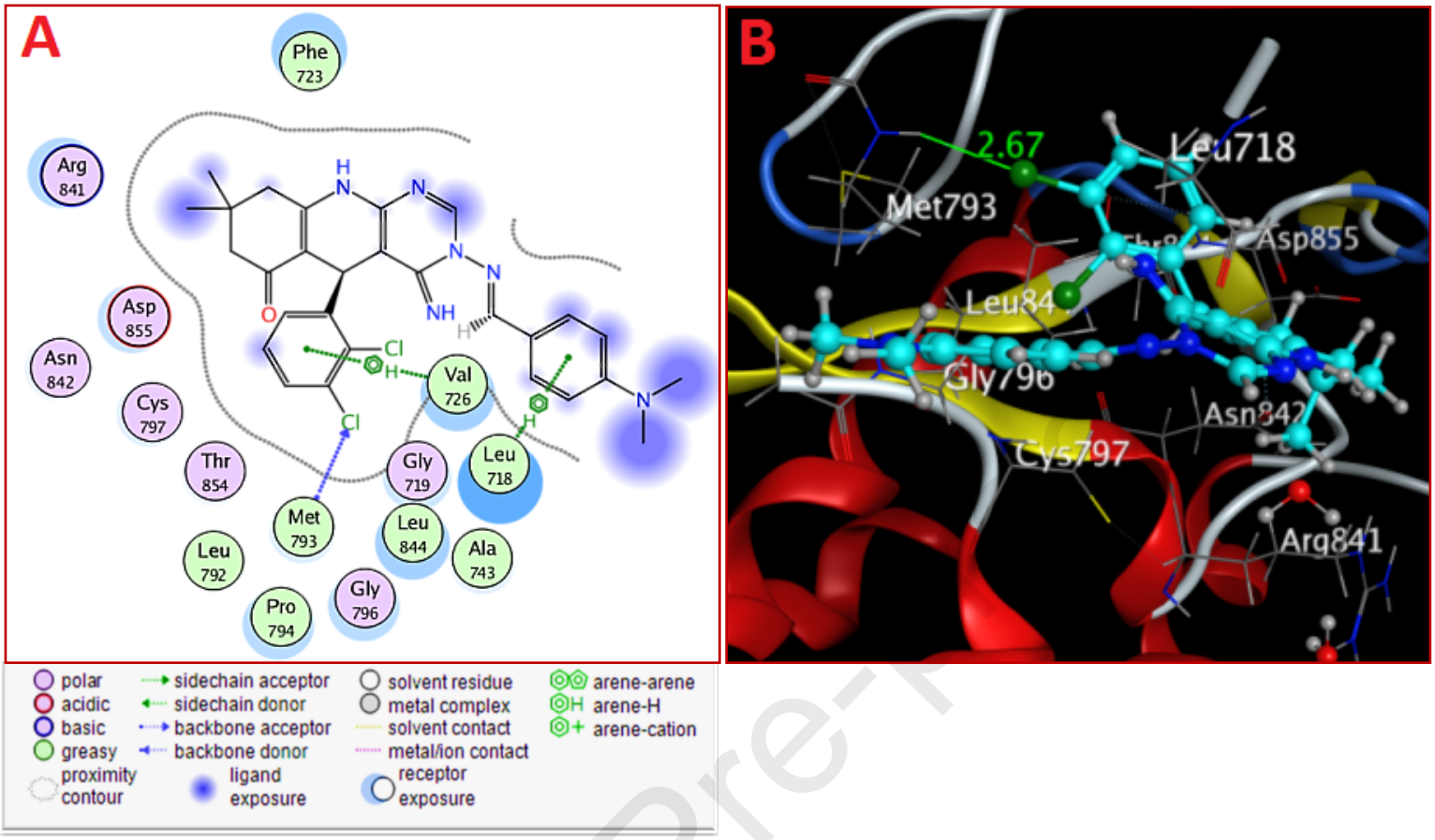

Fig. 15. (A) 2D Interaction of **7d** with the binding site of $EGFR^{L858R}$. **(B)** 3D Interaction of **7d** with the binding site of $EGFR^{L858R}$. Atoms are colored as follows: cyan for carbon, light gey for hydrogen, blue for nitrogen, red for oxygen and green for chlorine. (PDB code: 4LQM).

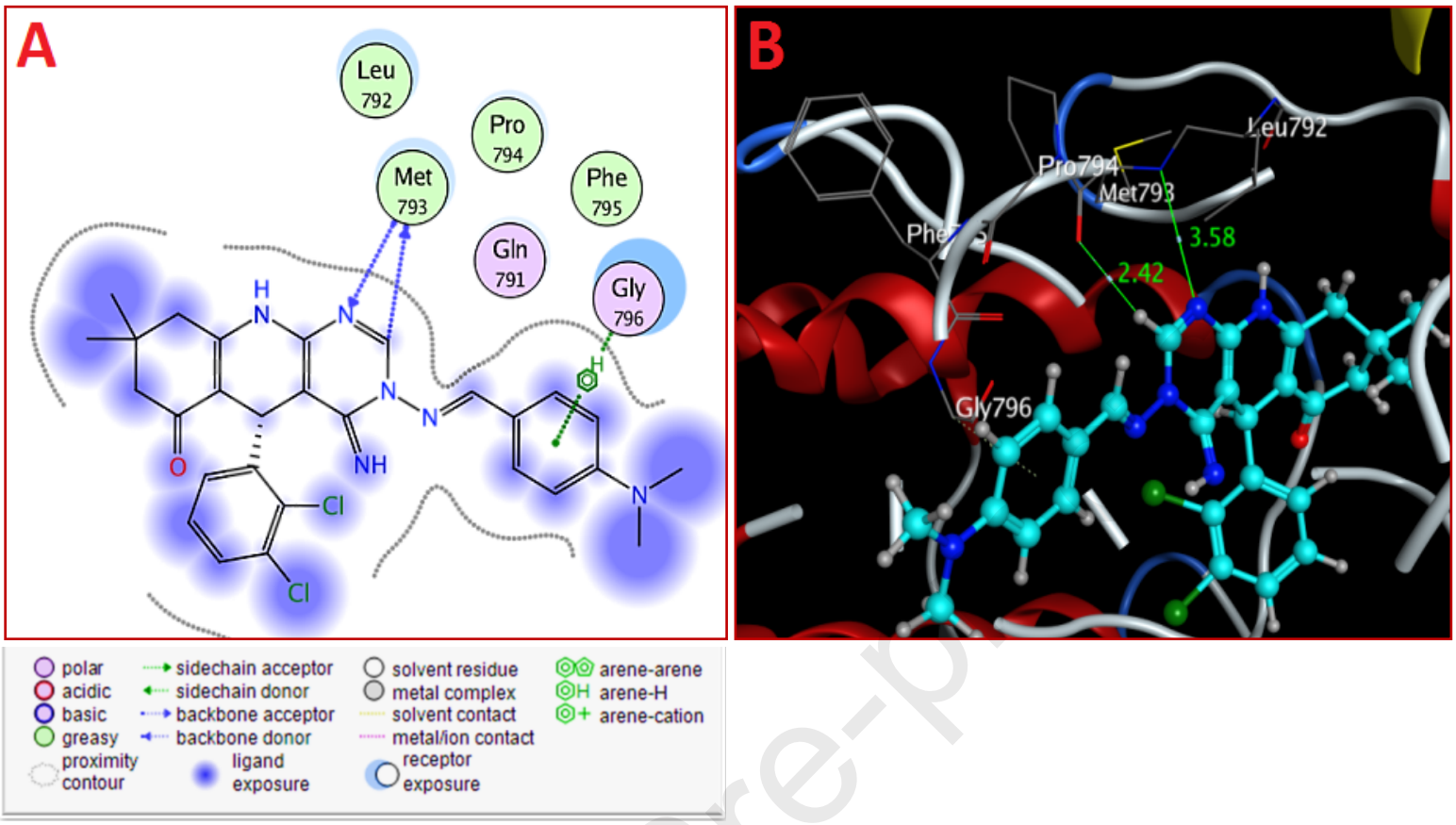

Fig. 16. (A) 2D Interaction of **7d** with the binding site of EGFR^{T790M}. **(B)** 3D Interaction of **7d** with the binding site of EGFR^{T790M}. Atoms are colored as follows: cyan for carbon, light gey for hydrogen, blue for nitrogen, red for oxygen and green for chlorine. (PDB code: 2JIV).

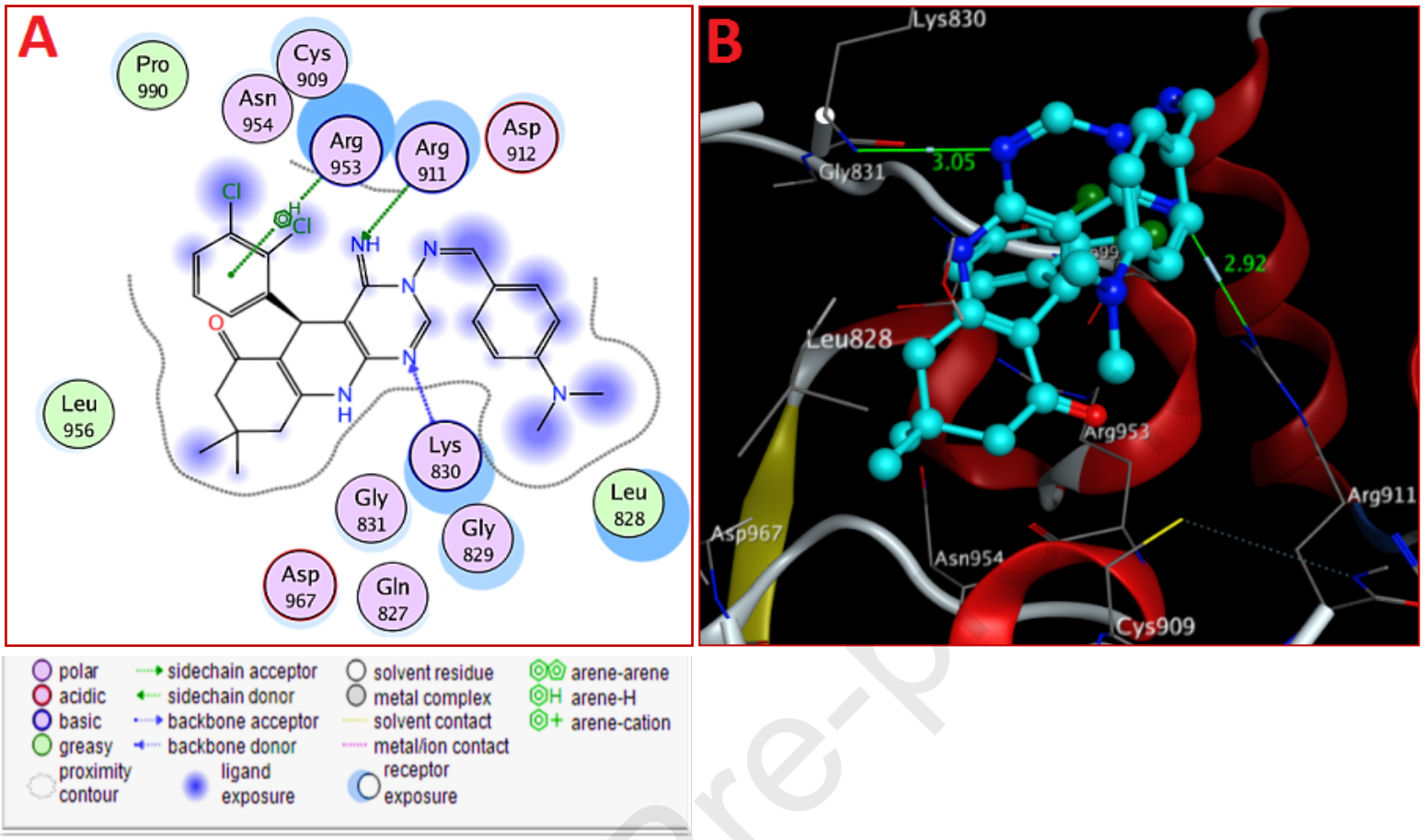

Fig. 17. (A) 2D Interaction of **7d** with the binding site of JAK3. **(B)** 3D Interaction of **7d** with the binding site of JAK3. Atoms are colored as follows: cyan for carbon, light gey for hydrogen, blue for nitrogen, red for oxygen and green for chlorine. (PDB code: 5TTV).

Table 1. Results of antitumor screening of the newly synthesized compounds.

Comp. No.	IC_{50} (μM)[a,b]			Comp. No.	IC_{50} (μM)[a,b]		
	HepG2	**HCT-116**	**MCF-7**		**HepG2**	**HCT-116**	**MCF-7**
2a	61.60±3.4	55.27±3.5	64.54±3.7	**4h**	14.29±1.2	**9.82±0.9**	14.32±1.2
2b	57.48±3.5	28.64±1.9	**10.86±0.9**	**5a**	63.69±3.7	56.37±3.6	81.98±4.5
2c	40.93±2.8	44.50±2.9	38.46±2.5	**5b**	**6.03±0.4**	**7.84±0.6**	**9.46±0.8**
2d	22.53±1.9	30.05±2.3	34.50±2.3	**5c**	**8.53±0.6**	**7.13±0.7**	**10.81±0.9**
2e	**8.13±0.7**	**6.81±0.3**	**8.20±0.4**	**5d**	17.12±1.5	16.05±1.4	20.61±1.6
2f	14.66±1.3	13.64±1.4	18.10±1.5	**5e**	25.06±2.3	23.71±1.8	29.17±2.3
2g	73.46±3.9	74.27±3.8	80.54±4.3	**5f**	19.50±1.7	14.91±1.3	24.08±1.9
2h	**10.35±1.0**	**8.00±0.6**	**8.89±0.7**	**6a**	**2.91±0.1**	**5.66±0.4**	**6.56±0.4**
2i	78.37±4.3	75.03±4.2	86.68±4.7	**6b**	59.18±3.2	62.39±3.9	72.19±4.0
2j	45.93±3.0	53.91±3.3	52.01±3.2	**7a**	26.53±2.1	19.32±1.6	21.84±1.8
3a	87.43±4.5	91.42±4.8	>100.00	**7b**	**9.50±0.8**	12.90±1.1	31.65±2.3
3b	49.53±3.3	53.52±3.5	69.32±3.8	**7c**	35.21±2.6	54.56±3.1	58.10±3.3
3c	70.65±3.8	59.70±3.6	88.46±4.7	**7d**	**4.46±0.2**	**5.27±0.5**	**3.25±0.2**
4a	38.11±2.9	32.65±2.3	52.78±3.4	**8a**	29.68±2.4	32.04±2.2	43.79±2.7
4b	29.34±2.6	19.18±1.6	33.83±2.5	**8b**	14.49±1.3	**8.27±0.7**	12.57±1.1
4c	41.65±3.0	38.60±2.5	57.82±3.5	**9a**	50.03±3.4	49.11±3.2	77.63±4.1
4d	12.48±1.4	**8.35±0.9**	13.60±1.4	**9b**	**6.18±0.5**	**3.85±0.2**	**9.13±0.9**
4e	35.84±2.8	42.97±2.7	46.01±3.1	**Doxorubicin**	4.50±0.2	5.23±0.3	4.17±0.2
4f	43.46±3.1	48.26±2.9	65.10±3.7	**Erlotinib**	8.19±0.4	11.21±0.6	4.16±0.2
4g	**10.17±0.9**	12.10±1.1	**7.92±0.6**	**Osimertinib**	8.44±0.5	8.89±0.6	9.72±0.6

[a]IC_{50} values = mean ± SD of three independent determinations.
[b]IC_{50} (μM): strong (1-10); moderate (11-50); weak (51-100); no activity (> 100).
Bold values represent the best results.

Table 2. Results of cytotoxicity against A431 and H1975 cancer cells, as well as WI38 and WISH normal cells.

Comp. No.	IC_{50} (μM)[a,b]			
	Cancer cells		Normal cells	
	A431	H1975	WI38	WISH
2e	9.82±1.0	7.13±0.6	86.40±4.2	57.49±3.3
2h	**6.43±0.5**	**2.89±0.3**	67.35±3.6	58.17±3.3
5b	7.89±0.6	8.75±0.6	55.08±3.2	19.78±1.7
5c	9.10±1.1	4.46±0.4	48.75±3.0	26.14±1.9
6a	10.62±1.5	12.31±1.7	39.26±2.5	29.53±2.3
7d	**4.96±0.3**	**1.32±0.2**	64.27±3.4	46.38±2.8
9b	9.67±1.3	10.11±1.3	51.49±3.1	63.37±3.5
Doxorubicin	2.73±0.2	4.19±0.2	6.72±0.5	3.18±0.2
Erlotinib	3.76±0.2	8.52±0.5	----	----
Osimertinib	5.63±0.3	0.69±0.1	----	----

[a]IC_{50} values = mean ± SD of three independent determinations.
[b]IC_{50} (μM): strong (1-20); moderate (21-50); weak (51-100); non-cytotoxic (> 100).
Bold values represent the best results.

Table 3. Cytotoxic selectivity against HepG2, HCT-116, MCF-7, A431 and H1975 cancer cells versus WI38 and WISH normal cells.

Comp. No.	SI[a]				
	Selectivity against HepG2 versus WI38 (WISH)	**Selectivity against HCT-116 versus WI38 (WISH)**	**Selectivity against MCF-7 versus WI38 (WISH)**	**Selectivity against A431 versus WI38 (WISH)**	**Selectivity against H1975 versus WI38 (WISH)**
2e	10.63 (7.07)	12.69 (8.44)	10.54 (7.01)	8.80 (5.85)	12.12 (8.06)
2h	6.51 (5.62)	8.42 (7.27)	7.58 (6.54)	11.65 (9.05)	23.30 (20.13)
5b	9.13 (3.28)	7.03 (2.52)	5.82 (2.09)	6.98 (2.51)	6.29 (2.26)
5c	5.72 (3.06)	6.84 (3.67)	4.51 (2.42)	5.36 (2.87)	10.93 (5.86)
6a	13.49 (10.15)	6.94 (5.22)	5.98 (4.50)	3.70 (2.78)	3.19 (2.40)
7d	**14.41 (10.40)**	12.19 (8.80)	**19.77 (14.27)**	**12.96 (9.35)**	**48.69 (35.14)**
9b	8.33 (10.25)	**13.37 (16.46)**	5.64 (6.94)	5.32 (6.55)	5.09 (6.27)
Doxorubicin	1.49 (0.71)	1.28 (0.61)	1.61 (0.76)	2.46 (1.16)	1.60 (0.65)

[a]SI: Selectivity index = IC_{50} calculated for normal cell/ IC_{50} calculated for cancer cell.
Bold values represent the highest SI toward each cancer cell line.

Table 4. $EGFR^{WT}$ inhibitory activity of the most potent antitumor compounds.

Comp. No.	IC_{50} (μM)[a]
	$EGFR^{WT}$
2e	0.153±0.003
2h	0.129±0.003
5b	0.143±0.003
5c	0.216±0.005
6a	0.347±0.007
7d	**0.083±0.002**
9b	0.459±0.009
Erlotinib	0.067±0.002
Osimertinib	0.480±0.009

[a]IC_{50} values = mean ± SD of three independent determinations.
Bold value represents the best result.

Table 5. Kinase profile assay of compound **7d** against eight human kinases.

Comp. No.	IC_{50} (μM)[a]							
	Tyrosine kinases contain SH2 Domain	**Tyrosine kinases contain SH2 and SH3 Domains**		**Other human protein or lipid kinases**				
	TYK2	**JAK3**	**BTK**	**$EGFR^{L858R}$**	**$EGFR^{T790M}$**	**VEGFR-2**	**mTOR**	**HER-4**
7d	0.089±0.002	**0.069±0.003**	0.183±0.006	**0.053±0.002**	**0.026±0.001**	0.150±0.005	0.166±0.005	0.298±0.009
Erlotinib	0.034±0.002	0.146±0.005	0.077±0.003	0.045±0.001	0.443±0.002	0.055±0.001	0.062±0.002	0.162±0.004
Osimertinib	**----**	**----**	**----**	0.025±0.001	0.022±0.001	**----**	**----**	**----**

[a]IC_{50} values = mean ± SD of three independent determinations.
Bold values represent the best results.

Table 6. Summary of residues involved in arene-H interaction, number of hydrogen bonds, residues involved in hydrogen bonding interaction and docking interaction energy (kcal/mol) of compound **7d** with $EGFR^{WT}$, $EGFR^{L858R}$, $EGFR^{T790M}$ and JAK3.

Enzyme	Residues involved in arene-H interaction	No. of H-bonds	Residues involved in H-bonding interaction	Docking interaction energy (kcal/mol)
$EGFR^{WT}$	Leu844	2	Asp800, Ser720	-6.73
$EGFR^{L858R}$	Leu718, Val726	1	Met793	-6.03
$EGFR^{T790M}$	Gly796	2	Met793	-6.82
JAK3	Arg953	2	Arg911, Lys830	-5.01

Table 7. Calculated Veber's and Lipinski's rule parameters for the new compounds.

Comp. No.	Molecular properties						
	TPSA[a]	Nrotb[b]	miLogP[c]	*n*HBD[d]	*n*HBA[e]	M. wt.	*n*Vs[f]
2a	78.91	1	2.83	3	4	362.26	0
2b	78.91	1	3.33	3	4	362.26	0
2c	78.91	1	2.83	3	4	362.26	0
2d	78.91	1	2.32	3	4	345.81	0
2e	78.91	1	1.83	3	4	329.35	0
2f	78.91	1	1.80	3	4	329.35	0
2g	78.91	2	3.84	3	4	369.47	0
2h	97.38	1	1.44	3	6	337.38	0
2i	78.91	1	3.23	3	4	343.43	0
2j	78.91	1	3.87	3	4	393.49	0
3a	92.42	2	2.79	4	5	381.26	0
3b	92.42	2	2.29	4	5	381.26	0
3c	92.42	2	1.26	4	5	348.35	0
4a	74.49	4	3.63	1	5	412.32	0
4b	74.49	4	4.13	1	5	418.32	0
4c	74.49	4	3.63	1	5	418.32	0
4d	74.49	4	3.12	1	5	401.87	0
4e	74.49	4	2.60	1	5	385.41	0
4f	74.29	5	4.64	1	5	425.53	0
4g	92.96	4	2.24	1	7	393.44	0
4h	74.49	4	4.67	1	5	449.55	0
5a	80.91	1	3.73	3	5	389.29	0
5b	80.91	1	3.75	3	5	389.29	0
5c	80.91	1	3.73	3	5	389.29	0
5d	80.91	1	3.21	3	5	372.83	0
5e	80.91	1	2.70	3	5	356.38	0
5f	80.91	1	4.76	3	5	420.52	0
6a	96.80	1	1.92	4	6	404.30	0
6b	96.80	1	1.95	4	6	404.30	0
7a	83.14	3	3.97	2	6	492.41	0
7b	83.14	3	4.65	2	6	526.86	1
7c	83.14	3	4.78	2	6	571.31	1
7d	86.38	4	4.07	2	7	535.48	1
8a	94.83	5	4.23	4	7	573.94	1
8b	104.06	6	3.60	4	8	569.52	1
9a	72.19	1	3.78	1	6	414.30	0
9b	72.19	1	3.75	1	6	414.30	0
Doxorubicin	207.70	5	-1.64	8	12	544.53	3
Erlotinib	74.75	10	2.79	1	7	393.44	0
Osimertinib	87.55	10	4.08	2	9	499.62	0

[a]TPSA: Topological polar surface area, [b]Nrotb: Number of rotatable bonds, [c]miLogP: The parameter of lipophilicity, [d]*n*HBD: Number of hydrogen bond donor sites, [e]*n*HBA: Number of hydrogen bond acceptor sites, [f]*n*Vs: Number of violations.

Table 8. *In silico* ADME properties of the new compounds.

Comp. No.	ADME properties			Comp. No.	ADME properties		
	BBB[a]	%PPB[b]	%HIA[c]		BBB[a]	%PPB[b]	%HIA[c]
2a	1.13	99.51	94.94	**4h**	0.13	94.66	97.22
2b	0.70	100.00	94.94	**5a**	1.13	95.50	95.32
2c	1.13	95.71	94.94	**5b**	0.69	99.56	95.32
2d	0.82	87.95	94.44	**5c**	1.13	92.09	95.32
2e	0.15	83.83	94.02	**5d**	0.89	86.67	94.77
2f	0.64	81.31	94.02	**5e**	0.75	87.23	94.40
2g	0.17	87.97	94.97	**5f**	0.12	92.05	96.43
2h	0.55	62.55	94.15	**6a**	1.55	86.90	88.79
2i	0.11	90.69	94.96	**6b**	1.45	89.96	88.79
2j	0.13	90.01	96.14	**7a**	4.93	88.79	93.09
3a	0.78	95.31	95.29	**7b**	6.08	96.02	93.65
3b	0.23	98.34	95.29	**7c**	6.24	100.00	93.94
3c	0.63	81.63	93.68	**7d**	3.35	84.97	93.37
4a	0.24	89.35	96.41	**8a**	4.26	94.80	92.98
4b	0.39	91.17	96.41	**8b**	2.71	89.10	91.88
4c	0.24	88.75	96.41	**9a**	1.05	90.58	96.72
4d	0.19	88.11	96.23	**9b**	0.37	91.39	96.72
4e	0.17	88.41	96.37	**Doxorubicin**	0.03	32.79	31.95
4f	0.05	91.22	96.42	**Erlotinib**	0.04	93.15	96.29
4g	0.24	71.26	97.09	**Osimertinib**	0.18	85.18	96.34

[a] BBB: Blood–brain barrier penetration, [b] %PPB: % Plasma protein binding, [c] %HIA: % Human intestinal absorption.

Table 9. *In silico* prediction of toxicity risks in human and drug-likeness of the new compounds.

Comp. No.	Toxicity risks in human			Drug-likeness
	Tumorigenicity	Irritancy	Mutagenicity	
2a	-	-	-	-3.42
2b	-	-	-	-3.42
2c	-	-	-	-3.42
2d	-	-	-	-4.93
2e	-	-	-	-6.69
2f	-	-	-	-6.69
2g	-	-	-	-3.00
2h	-	-	-	-3.44
2i	-	-	-	-6.17
2j	++	++	++	-7.77
3a	-	-	-	**1.35**
3b	-	-	-	**1.35**
3c	-	-	-	-0.43
4a	-	-	-	-4.68
4b	-	-	-	-4.68
4c	-	-	-	-4.68
4d	-	-	-	-6.18
4e	-	-	-	-6.47
4f	-	-	-	-4.25
4g	-	-	-	-4.73
4h	++	++	++	-9.01
5a	-	-	-	**0.66**
5b	-	-	-	**0.66**
5c	-	-	-	**0.66**
5d	-	-	-	-2.22
5e	-	-	-	-2.46
5f	++	++	++	-5.01
6a	-	-	-	**0.27**
6b	-	-	-	**0.27**
7a	-	-	-	**4.18**
7b	-	-	-	**4.90**
7c	-	-	-	**2.36**
7d	-	-	-	**3.30**
8a	-	-	-	**3.79**
8b	-	-	-	**2.08**
9a	-	-	-	**3.21**
9b	-	-	-	**3.21**
Doxorubicin	-	++	-	**7.19**
Erlotinib	-	-	-	-6.73
Osimertinib	+	+	++	-3.76

-low risk, + moderate risk, ++ high risk.
Bold values represent the best results.

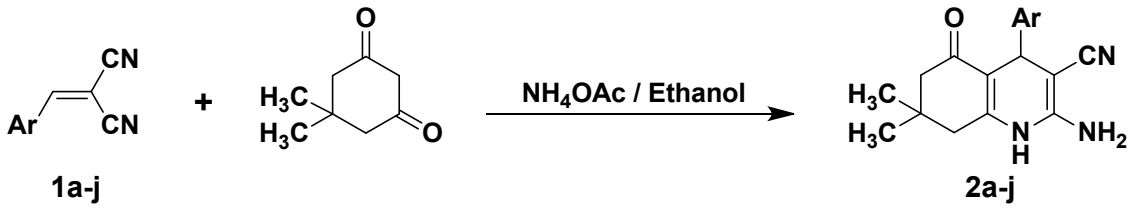

Comp. No.	Ar	Comp. No.	Ar
2a		2f	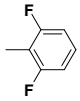
2b	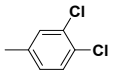	2g	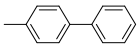
2c	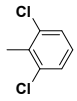	2h	
2d		2i	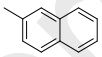
2e		2j	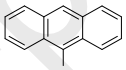

Scheme 1. Synthesis of compounds **2a-j.**

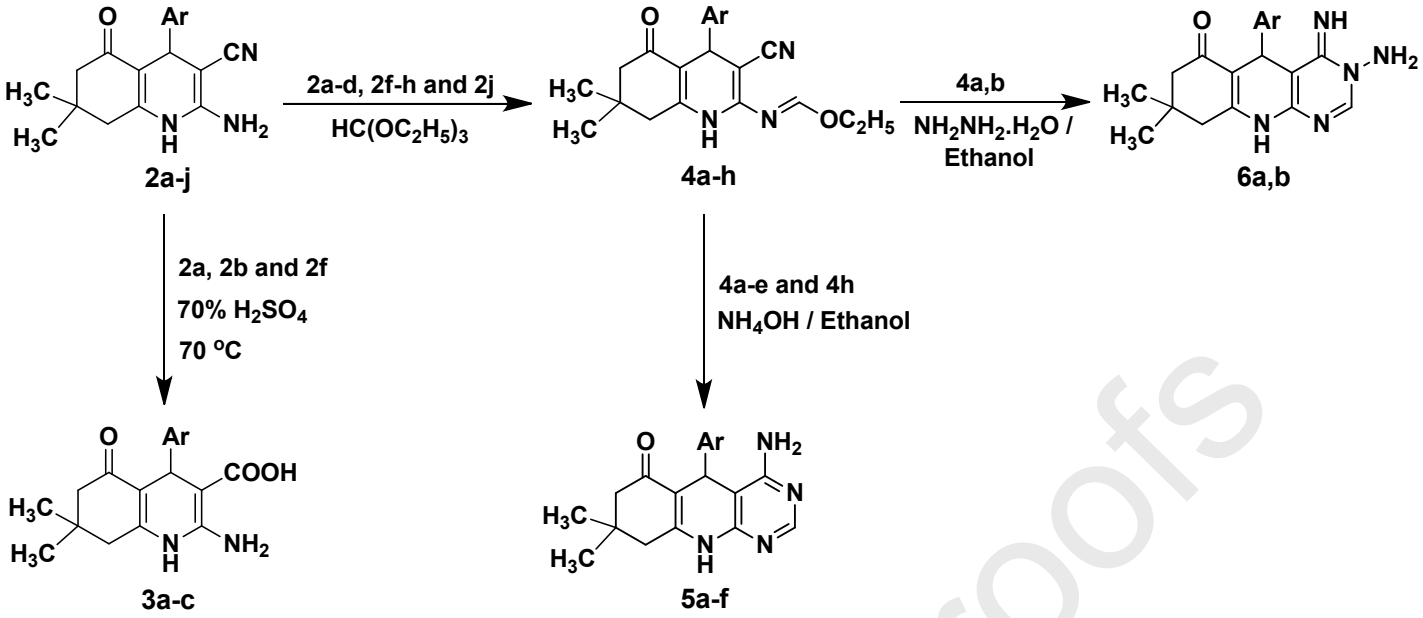

Comp. No.	Ar	Comp. No.	Ar	Comp. No.	Ar
3a		**4e**	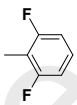	**5d**	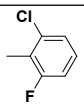
3b	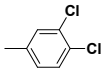	**4f**	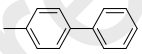	**5e**	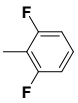
3c	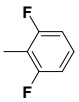	**4g**		**5f**	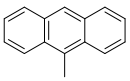
4a		**4h**	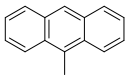	**6a**	
4b	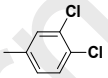	**5a**		**6b**	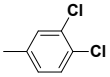
4c		**5b**	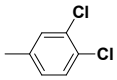	----	----
4d		**5c**	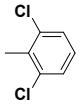	----	----

Scheme 2. Synthesis of compounds **3a-c, 4a-h, 5a-f** and **6a,b.**

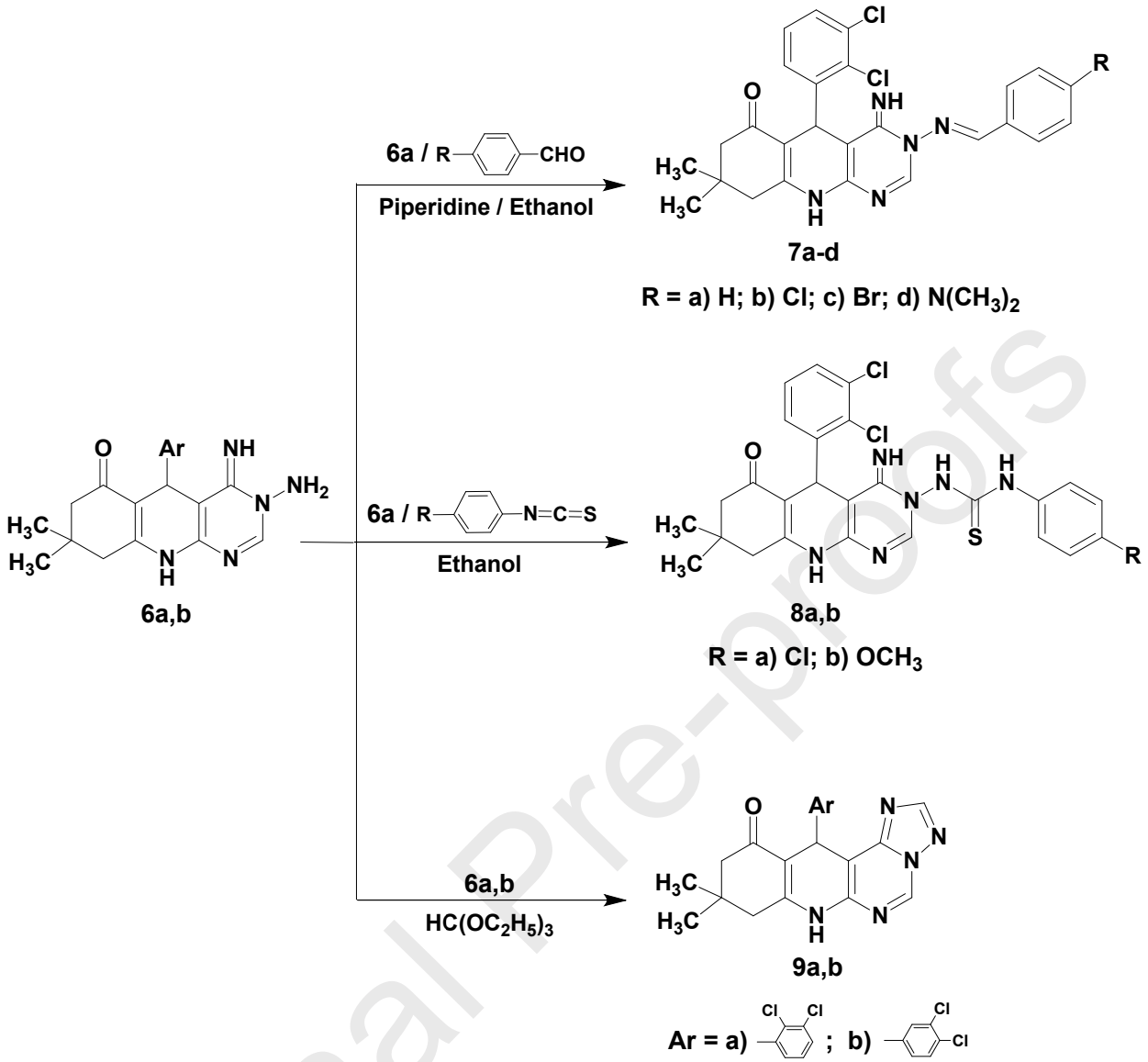

Scheme 3. Synthesis of compounds **7a-d, 8a,b** and **9a,b.**

References

[1] J. Ferlay, M. Colombet, I. Soerjomataram, C. Mathers, D.M. Parkin, M. Piñeros, A. Znaor, F. Bray, Estimating the global cancer incidence and mortality in 2018: GLOBOCAN sources and methods, Int. J. Cancer 144 (2019) 1941–1953.

[2] K. Westberg, G. Palmer, F. Hjern, T. Holm, A. Martling, Population-based study of surgical treatment with and without tumour resection in patients with locally recurrent rectal cancer, Br. J. Surg. 106 (2019) 790–798.

[3] Y. Zhao, J. Cao, A. Melamed, M. Worley, A. Gockley, D. Jones, H.T. Nia, Y. Zhang, T. Stylianopoulos, A.S. Kumar, F. Mpekris, M. Datta, Y. Sun, L. Wu, X. Gao, O. Yeku, M.G. del Carmen, D.R. Spriggs, R.K. Jain, L. Xu, Losartan treatment enhances chemotherapy efficacy and reduces ascites in ovarian cancer models by normalizing the tumor stroma, Proc. Natl. Acad. Sci. 116 (2019) 2210–2219.

[4] M. Wells, E. King, K. Toft, F. MacAulay, J. Patterson, N. Dougall, N. Hulbert-Williams, S. Boa, E. Slaven, J. Cowie, J. McGarva, P.G. Niblock, J. Philp, J. Roe, Development and feasibility of a swallowing intervention package (SiP) for patients receiving radiotherapy treatment for head and neck cancer-the SiP study protocol, Pilot Feasibility Stud. 2 (2016) 40, doi: 10.1186/s40814-016-0079-6.

[5] Y. Yarden, M.X. Sliwkowski, Untangling the ErbB signalling network, Nat. Rev. Mol. Cell Biol. 2 (2001) 127–137.

[6] N.E. Hynes, H.A. Lane, ERBB receptors and cancer: The complexity of targeted inhibitors, Nat. Rev. Cancer 5 (2005) 341–354.

[7] C.N. Prabhakar, Epidermal growth factor receptor in non-small cell lung cancer, Transl. Lung Cancer Res. 4 (2015) 110-118.

[8] M. Höpfner, A.P. Sutter, A. Huether, D. Schuppan, M. Zeitz, H. Scherüb, Targeting the epidermal growth factor receptor by gefitinib for treatment of hepatocellular carcinoma, J. Hepatol. 41 (2005) 1008-1016.

[9] C.-W. Huang, Y.-T. Chen, H.-L. Tsai, Y.-S. Yeh, W.-C. Su, C.-J. Ma, T.-N. Tsai, J.-Y. Wang, EGFR expression in patients with stage III colorectal cancer after adjuvant chemotherapy and on cancer cell function, Oncotarget 8 (2017) 114663–114676.

[10] D. Nguyen, S.X. Yang, Epidermal growth factor expression in breast cancer, J. Clin. Oncol. 23 (2005) 8118-8141.

[11] D. Fabbro, S. Ruetz, E. Buchdunger, S.W. Cowan-Jacob, G. Fendrich, J. Liebetanz, T. O'Reilley, P. Traxler, B. Chaudhari, H. Fretz, J. Zimmermann, T. Meyer, G. Carvatti, P. Furet, P.W. Manley, Protein kinases as targets for anticancer agents: From inhibitors to useful drugs, Pharmacol. Ther. 93 (2002) 79-98.

[12] Y. Yarden, The EGFR family and its ligands in human cancer: Signalling mechanisms and therapeutic opportunities, Eur. J. Cancer 37 (2001) 3–8.

[13] T.S. Mok, Y. Wu, S. Thongprasert, C. Yang, N. Saijo, P. Sunpaweravong, B. Han, B. Margono, Y. Ichinose, Y. Nishiwaki, Y. Ohe, J. Yang, B. Chewaskulyong, H. Jiang, E.L. Duffield, C.L. Watkins, A.A. Armour, M. Fukuoka, Gefitinib or carboplatin-paclitaxel, N. Engl. J. Med. 361 (2009) 947–957.

[14] F.A. Shepherd, J.R. Pereira, T. Ciuleanu, E.H. Tan, V. Hirsh, S. Thongprasert, D. Campos, S. Maoleekoonpiroj, M. Smylie, R. Martins, M. Dediu, D. Tu, D. Johnston, A. Bezjak, G. Clark, P. Santabárbara, L. Seymour, Erlotinib in previously treated non–small-cell lung cancer, N. Engl. J. Med. 353 (2005) 225–237.

[15] B. Ko, D. Paucar, B. Halmos, EGFR T790M: Revealing the secrets of a gatekeeper, Lung Cancer (Auckl). 8 (2017) 147-159.

[16] H.A. Yu, Analysis of tumor specimens at the time of acquired resistance to EGFR-TKI therapy in 155 patients with EGFR-mutant lung cancers, Clin. Cancer Res. 19 (2013) 2240–2247.

[17] T.T. Phan, B. Tran, S.T. Nguyen, T.T. Ho, H.T. Nguyen, V.T. Le, A.T. Le, EGFR plasma mutation in prediction models for resistance with EGFR TKI and survival of non-small cell lung cancer, Clin. Trans. Med. 8 (2019), doi: 10.1186/s40169-019-0219-8.

[18] K.K.W. To, D.C. Poon, Y. Wei, F. Wang, G. Lin, L. Fu, Pelitinib (EKB-569) targets the up-regulation of ABCB1 and ABCG2 induced by hyperthermia to eradicate lung cancer, Br. J. Pharmacol. 172 (2015) 4089-4106.

[19] M.A. Cherian, C.X. Ma, The role of neratinib in HER2-driven breast cancer, Fut. Oncol. 13 (2017) 1931-1943.

[20] M.J. Hochmair, A. Buder, S. Schwab, O.C. Burghuber, H. Prosch, W. Hilbe, A. Cseh, R. Fritz, M. Filipits, Liquid-biopsy-based identification of EGFR T790M mutation-mediated resistance to afatinib treatment in patients with advanced EGFR mutation-positive NSCLC, and subsequent response to osimertinib, Target Oncol. 14 (2019) 75-83.

[21] S.L. Greig, Osimertinib: First Global Approval, Drugs 76 (2016) 263–273.

[22] E.S. Kim, Olmutinib: First Global Approval, Drugs 76 (2016) 1153–1157.

[23] M.R.V. Finlay, M. Anderton, S. Ashton, P. Ballard, P.A. Bethel, M.R. Box, R.H. Bradbury, S.J. Brown, S. Butterworth, A. Campbell, C. Chorley, N. Colclough, D.A.E. Cross, G.S. Currie, M. Grist, L. Hassall, G.B. Hill, D. James, M. James, P. Kemmitt, T. Klinowska, G. Lamont, S.G. Lamont, N. Martin, H.L. McFarland, M.J. Mellor, J.P. Orme, D. Perkins, P. Perkins, G. Richmond, P. Smith, R.A. Ward, M.J. Waring, D. Whittaker, S. Wells, G.L. Wrigley, Discovery of a potent and selective EGFR inhibitor (AZD9291) of both sensitizing and T790M resistance mutations that spares the wild type form of the receptor, J. Med. Chem. 57 (2014) 8249–8267.

[24] P.A. Jänne, J.C.H. Yang, D.W. Kim, D. Planchard, Y. Ohe, S.S. Ramalingam, M.J. Ahn, S.W. Kim, W.C. Su, L. Horn, D. Haggstrom, E. Felip, J.H. Kim, P. Frewer, M. Cantarini, K.H. Brown, P.A. Dickinson, S. Ghiorghiu, M. Ranson, AZD9291 in EGFR inhibitor-resistant non-small-cell lung cancer, N. Engl. J. Med. 372 (2015) 1689–1699.

[25] M.L. Sos, H.B. Rode, S. Heynck, M. Peifer, F. Fischer, S. Klüter, V.G. Pawar, C. Reuter, J.M. Heuckmann, J. Weiss, L. Ruddigkeit, M. Rabiller, M. Koker, J.R. Simard, M. Getlik, Y. Yuza, T.H. Chen, H. Greulich, R.K. Thomas, D. Rauh, Chemogenomic profiling provides insights into the limited activity of irreversible EGFR inhibitors in tumor cells expressing the T790M EGFR resistance mutation, Cancer Res. 70 (2010) 868–874.

[26] A. Wissner, D. Berger, D. Boschelli, M. Floyd, L. Greenberger, B. Gruber, B. Johnson, N. Mamuya, R. Nilakantan, M. Reich, R. Shen, H. Tsou, E. Upeslacis, Y. Wang, B. Wu, F. Ye, N. Zhang, 4-Anilino-6,7-dialkoxyquinoline-3-carbonitrile inhibitors of epidermal growth factor receptor kinase and their bioisosteric relationship to the 4-anilino-6,7-dialkoxy-quinazoline inhibitors, J. Med. Chem. 43 (2000) 3244–3256.

[27] D. Ibrahim, D. Abou El Ella, A. El-Motwally, R. Aly, Molecular design and synthesis of certain new quinoline derivatives having potential anticancer activity, Eur. J. Med. Chem. 102 (2015) 115–131.

[28] C.B. Sangani, J.A. Makawana, X. Zhang, S.B. Teraiya, L. Lin, H.L. Zhu, Design, synthesis and molecular modeling of pyrazole-quinoline-pyridine hybrids as a new class of antimicrobial and anticancer agents, Eur. J. Med. Chem. 76 (2014) 549–557.

[29] Y. Zhang, H. Lv, L. Luo, Y. Xu, Y. Pan, Y. Wang, H. Lin, J. Xiong, P. Guo, J. Zhang, X. Li, F. Ye, Design, synthesis and pharmacological evaluation of *N*4, *N*6-disubstituted pyrimidine-4,6-diamine derivatives as potent EGFR inhibitors in non-small cell lung cancer, Eur. J. Med. Chem. 157 (2018) 1300–1325.

[30] G. Palareti, C. Legnani, B. Cosmi, E. Antonucci, N. Erba, D. Poli, S. Testa, A. Tosetto, Pyrimidine containing epidermal growth factor receptor kinase inhibitors: Synthesis and biological evaluation, Int. J. Lab. Hematol. 38 (2016) 42–49.

[31] H.C. Wang, X.Q. Yan, T.L. Yan, H.X. Li, Z.C. Wang, H.L. Zhu, Design, synthesis and biological evaluation of benzohydrazide derivatives containing dihydropyrazoles as potential EGFR kinase inhibitors, Molecules 21 (2016) 1012, doi: 10.3390/molecules21081012.

[32] H.Q. Li, T. Yan, Y. Yang, L. Shi, C.F. Zhou, H.L. Zhu, Synthesis and structure-activity relationships of *N*-benzyl-*N*-(X-2-hydroxybenzyl)-*N*′-phenylureas and thioureas as antitumor agents, Bioorg. Med. Chem. 18 (2010) 305–313.

[33] M.R. Aouad, H.M. Al-Mohammadi, F.F. Al-blewi, S. Ihmaid, H.M. Elbadawy, S.S. Althagfan, N. Rezki, Introducing of acyclonucleoside analogues tethered 1,2,4-triazole as anticancer agents with dual epidermal growth factor receptor kinase and microtubule inhibitors, Bioorg. Chem. 94 (2020) 103446, doi: 10.1016/j.bioorg.2019.103446.

[34] H. Wei, Y. Duan, W. Gou, J. Cui, H. Ning, D. Li, Y. Qin, Q. Liu, Y. Li, Design, synthesis and biological evaluation of novel 4-anilinoquinazoline derivatives as hypoxia-selective EGFR and VEGFR-2 dual inhibitors, Eur. J. Med. Chem. 181 (2019) 111552, doi: 10.1016/j.ejmech.2019.07.055.

[35] C.V. Junior, A. Danuello, V.dS. Bolzani, E.J. Barreiro, C.A.M. Fraga, Molecular hybridization: A useful tool in the design of new drug prototypes, Curr. Med. Chem. 14

(2007) 1829–1852.

[36] L.K. Gediya, V.C. Njar, Promise and challenges in drug discovery and development of hybrid anticancer drugs, Expert Opin. Drug Discov. 4 (2009) 1099–1111.

[37] B. Biersack, M. Zoldakova, K. Effenberger, R. Schobert, (Arene)Ru(II) complexes of epidermal growth factor receptor inhibiting tyrphostins with enhanced selectivity and cytotoxicity in cancer cells, Eur. J. Med. Chem. 45 (2010) 1972-1975.

[38] T. Fozing, C. Scheuer, S. Samnick, Synthesis and initial tumor affinity testing of iodine-123 labelled EGFR-affine agents as potential imaging probes for hormone-refractory prostate cancer, Eur. J. Med. Chem. 45 (2010) 3780-3786.

[39] J. Domarkas, F. Dudouit, C. Williams, Q. Qiyu, R. Banerjee, F. Brahimi, B.J. Jean-Claude, The combi-targeting concept: Synthesis of stable nitrosoureas designed to inhibit the epidermal growth factor receptor (EGFR), J. Med. Chem. 49 (2006) 3544-3552.

[40] E. Proschak, H. Stark, D. Merk, Polypharmacology by design: A medicinal chemist's perspective on multitargeting compounds, J. Med. Chem. 62 (2019) 420−444.

[41] M.A. Shaheen, A.A. El-Emam, N.S. El-Gohary, 1,4,5,6,7,8-Hexahydroquinolines and 5,6,7,8-tetrahydronaphthalenes: A new class of antitumor agents targeting the colchicine binding site of tubulin, Bioorg. Chem. 99 (2020) 103831, doi: 10.1016/j.bioorg.2020.103831.

[42] B. Şen, E.H. Akdere, A. Şavk, E. Gültekin, Ö. Paralı, H. Göksu, F. Şen, A novel thiocarbamide functionalized graphene oxide supported bimetallic monodisperse Rh-Pt nanoparticles (RhPt/TC@GO NPs) for Knoevenagel condensation of aryl aldehydes together with malononitrile, Appl. Catal. B Environ. 225 (2018) 148–153.

[43] D.S.W. Fan, Y. Wang, Q. Zhang, A. Kirchon, Z. Xiao, L. Zhang, F. Dai, R. Wang, Knoevenagel condensation on an aminofunctionalized metal-organic framework, Synfacts 14 (2018) 2137–2143.

[44] R. Malakooti, H. Mahmoudi, R. Hosseinabadi, S. Petrov, A. Migliori, Facile synthesis of pure non-monoclinic zirconia nanoparticles and their catalytic activity investigations for Knoevenagel condensation, RSC Adv. 3 (2013) 22353–22359.

[45] S. Atlas, M. Raihane, G.B. Kharas, P.G. Hendrickson, H. Kaddami, M. Arous, A. Kallel,

Novel copolymers of difluoro ring-substituted 2-phenyl-1,1-dicyanoethylenes with 4-fluorostyrene: Synthesis, structure and dielectric study, J. Macromol. Sci. A 49 (2012) 997–1010.

[46] K. Turpaev, M. Ermolenko, T. Cresteil, J.C. Drapier, Benzylidenemalononitrile compounds as activators of cell resistance to oxidative stress and modulators of multiple signaling pathways. A structure-activity relationship study, Biochem. Pharmacol. 82 (2011) 535–547.

[47] G.B. Kharas, S.M. Russell, R. Cisler, T.L. Capen, E.A. Chlupsa, L.A. Debellis, J.T.A. Duke, C.B. Frazier, A. Gora, E. Kamenetsky, A.S. Kurani, D.L. Kuta, A.L. Madison, P. Miramon, Novel copolymers of vinyl acetate and halogen ring-disubstituted 2-phenyl-1,1-dicyanoethylenes, J. Macromol. Sci. A 45 (2008) 261–264.

[48] X.S. Wang, Z.S. Zeng, Y.L. Li, D.Q. Shi, S.J. Tu, X.Y. Wei, Z.M. Zong, Simple procedure for the synthesis of arylmethylenemalononitrile without catalyst, Synth. Commun. 35 (2005) 1915–1920.

[49] M.B. El-Ashmawy, M.A. El-Sherbeny, N.S. El-Gohary, Synthesis and antitumor screening of new series of pyrimido[4,5-*b*]quinolines and [1,2,4]triazolo[2′,3′:3,4]pyrimido[6,5-*b*]quinolines, Med. Chem. Res. 22 (2013) 2724–2736.

[50] N.S. El-Gohary, S.S. Hawas, M.T. Gabr, M.I. Shaaban, M.B. El-Ashmawy, New series of fused pyrazolopyridines: Synthesis, molecular modeling, antimicrobial, antiquorum-sensing and antitumor activities, Bioorg. Chem. 92 (2019) 103109, doi. 10.1016/j.bioorg.2019.103109.

[51] O.I. Abd El-Salam, M.E.A. Zaki, M.M. Said, M. Abdulla, Synthesis, structural characterization of some pyrazolo[3,4-*d*]pyrimidine derivatives as anti-inflammatory agents, Egypt. J. Chem. 55 (2012) 529–547.

[52] T. Mosmann, Rapid colorimetric assay for cellular growth and survival: Application to proliferation and cytotoxicity assays, J. Immunol. Methods 65 (1983) 55-63.

[53] F. Denizot, R. Lang, Rapid colorimetric assay for cell growth and survival. Modifications to the tetrazolium dye procedure giving improved sensitivity and reliability, J. Immunol. Methods 89 (1986) 271–277.

[54] D. Gerlier, N. Thomasset, Use of MTT colorimetric assay to measure cell activation, J. Immunol. Methods 94 (1986) 57-63.

[55] Y.I. Jeong, D.H. Kim, C.W. Chung, J.J. Yoo, K.H. Choi, C.H. Kim, S.H. Ha, D.H. Kang, Doxorubicin-incorporated polymeric micelles composed of dextran-*b*-poly(DL-lactide-co-glycolide) copolymer, Int. J. Nanomedicine 6 (2011) 1415-1427.

[56] M.A. Sliwinskaa, G. Mosieniaka, K. Wolanina, A. Babika, K. Piwockaa, A. Magalskaa, J. Szczepanowskaa, J. Fronk, E. Sikora, Induction of senescence with doxorubicin leads to increased genomic instability of HCT116 cells, Mech. Ageing Dev. 130 (2009) 24-32.

[57] H. Taymaz-Nikerel, M.E. Karabekmez, S. Eraslan, B. Kırdar, Doxorubicin induces an extensive transcriptional and metabolic rewiring in yeast cells, Sci. Rep. 8 (2018) 13672, doi: 10.1038/s41598-018-31939-9.

[58] M.M. Gottesman, Mechanisms of cancer drug resistance, Annu. Rev. Med. 53 (2002) 615-627.

[59] T.R. Dunkern, I. Wedemeyer, M. Baumgärtner, G. Fritz, B. Kaina, Resistance of p53 knockout cells to doxorubicin is related to reduced formation of DNA strand breaks rather than impaired apoptotic signaling, DNA Repair (Amst) 2 (2003) 49-60.

[60] S. Machana, N. Weerapreeyakul, S. Barusrux, A. Nonpunya, B. Sripanidkulchai, T. Thitimetharoch, Cytotoxic and apoptotic effects of six herbal plants against the human hepatocarcinoma (HepG2) cell line, Chin. Med. 6 (2011) 39, doi: 10.1186/1749-8546-6-39.

[61] P. Prayong, S. Barusrux, N. Weerapreeyakul, Cytotoxic activity screening of some indigenous Thai plants, Fitoterapia. 79 (2008) 598 -601.

[62] H. Ma, S. Deacon, K. Horiuchi, The challenge of selecting protein kinase assays for lead discovery optimization, Expert Opin. Drug Discov. 3 (2008) 607–621.

[63] M.A.I. Elbastawesy, A.A. Aly, M. Ramadan, Y.A.M.M. Elshaier, B.G.M. Youssif, A.B. Brown, G.E.D.A. Abuo-Rahma, Novel pyrazoloquinolin-2-ones: Design, synthesis, docking studies, and biological evaluation as antiproliferative EGFR-TK inhibitors, Bioorg. Chem. 90 (2019) 103045, doi: 10.1016/j.bioorg.2019.103045.

[64] M.S. Abdelbaset, M. Abdel-Aziz, M. Ramadan, M.H. Abdelrahman, S.N.A. Bukhari, T.F.S. Ali, G.E.D.A. Abuo-Rahma, Discovery of novel thienoquinoline-2-carboxamide chalcone derivatives as antiproliferative EGFR tyrosine kinase inhibitors, Bioorg. Med. Chem. 27

(2019) 1076-1086.

[65] H. Lei, S. Fan, H. Zhang, Y.J. Liu, Y.Y. Hei, J.J. Zhang, A.Q. Zheng, M. Xin, S.Q. Zhang, Discovery of novel 9-heterocyclyl substituted 9*H*-purines as L858R/T790M/C797S mutant EGFR tyrosine kinase inhibitors, Eur. J. Med. Chem. 186 (2019) 111888, doi: 10.1016/j.ejmech.2019.111888.

[66] Y. Zhang, L. Chen, H. Xu, X. Li, L. Zhao, W. Wang, B. Li, X. Zhang, 6,7-Dimorpholinoalkoxy quinazoline derivatives as potent EGFR inhibitors with enhanced antiproliferative activities against tumor cells, Eur. J. Med. Chem. 147 (2018) 77–89.

[67] C.S. Devi, D.A. Kumar, S.S. Singh, N. Gabra, N. Deepika, Y.P. Kumar, S. Satyanarayana, Synthesis, interaction with DNA, cytotoxicity, cell cycle arrest and apoptotic inducing properties of ruthenium(II) molecular "light switch" complexes, Eur. J. Med. Chem. 64 (2013) 410–421.

[68] K.K.W. Lo, T.K.M. Lee, J.S.Y. Lau, W.L. Poon, S.H. Cheng, Luminescent biological probes derived from ruthenium(II) estradiol polypyridine complexes, Inorg. Chem. 47 (2008) 200–208.

[69] Y.C. Li, Y.S. Tyan, H.M. Kuo, W.C. Chang, T.C. Hsia, J.G. Chung, Baicalein induced *in vitro* apoptosis undergo caspases activity in human promyelocytic leukemia HL-60 cells, Food Chem. Toxicol. 42 (2004) 37–43.

[70] R.S.Y. Wong, Apoptosis in cancer: From pathogenesis to treatment, J. Exp. Clin. Cancer Res. 30 (2011) 87, doi: 10.1186/1756-9966-30-87.

[71] A. Shamas-Din, J. Kale, B. Leber, D.W. Andrews, Mechanisms of action of Bcl-2 family proteins, Cold Spring Harbor Perspect. Biol. 5 (2013) 008714, doi: 10.1101/cshperspect.a008714.

[72] K.J. Campbell, S.W.G. Tait, Targeting BCL-2 regulated apoptosis in cancer, Open Biol. 8 (2018) 180002, doi: 10.1098/rsob.180002.

[73] https://www.rcsb.org/structure/3W2S.

[74] https://www.rcsb.org/structure/4LQM.

[75] https://www.rcsb.org/structure/2JIV.

[76] https://www.rcsb.org/structure/5TTV.

[77] MOE 2014.0901 of Chemical Computing Group. Inc. https://www.chemcomp.com/.

[78] R.U. Kadam, N. Roy, Recent trends in drug-likeness prediction: A comprehensive review of *in silico* methods, Ind. J. Pharm. Sci. 69 (2007) 609–615.

[79] C.A. Lipinski, Lead- and drug-like compounds: The rule-of-five revolution, Drug Discov. Today Technol. 1 (2004) 337–341.

[80] D.F. Veber, S.R. Johnson, H.Y. Cheng, B.R. Smith, K.W. Ward, K.D. Kopple, Molecular properties that influence the oral bioavailability of drug candidates, J. Med. Chem. 45 (2002) 2615–2623.

[81] https://www.molinspiration.com/cgi-bin/properties.

[82] https://preadmet.bmdrc.kr.

[83] https://www.organic-chemistry.org/prog/peo/.

[84] Ajay, G.W. Bemis, M.A. Murcko, Designing libraries with CNS activity, J. Med. Chem. 42 (1999) 4942–4951.

[85] O. Ursu, A. Rayan, A. Goldblum, T. Opera, Understanding drug-likeness, WIREs Comput. Mol. Sci. 1 (2011) 760-781.

[86] S. Tu, J. Zhang, X. Zhu, Y. Zhang, Q. Wang, J. Xu, B. Jiang, R. Jia, J. Zhang, F. Shi, One-pot synthesis of hexahydroquinolines *via* a four-component cyclocondensation under microwave irradiation in solvent free conditions: A green chemistry strategy, J. Heterocycl. Chem. 43 (2006) 985–988.

[87] A. Amoozadeh, S. Rahmani, M. Bitaraf, F.B. Abadi, E. Tabrizian, Nano-zirconia as an excellent nano support for immobilization of sulfonic acid: A new, efficient and highly recyclable heterogeneous solid acid nanocatalyst for multicomponent reactions, New J. Chem. 40 (2016) 770–780.

[88] E. Tabrizian, A. Amoozadeh, A unique approach to magnetization of metal oxides: Nano-Fe_3O_4,TDI, TiO_2 as a highly efficient, magnetically separable and recyclable heterogeneous nanocatalyst, Catal. Sci. Technol. 6 (2016) 6267–6276.

Captions of Figures, Tables and Schemes

Fig. 1. The ATP-binding site of EGFR-TK.

Fig. 2. Examples of first-generation (gefitinib and erlotinib), second-generation (pelitinib and neratinib) and third-generation (osimertinib and olmutinib) EGFR-TKIs, and quinolines **A-D** with reported antitumor and EGFR-TK inhibitory activities.

Fig. 3. The designed new series of hexahydroquinolines **2a-j**, **3a-c** and **4a-h** as prospective antitumor agents and EGFR-TKIs.

Fig. 4. Examples of pyrimidines **E-G**, benzylideneamines **H**, phenylthioureas **I** and [1,2,4]triazoles **J,K** with reported antitumor and EGFR-TK inhibitory activities.

Fig. 5. The designed new hybrid compounds **5a-f, 6a,b, 7a-d, 8a,b** and **9a,b** as prospective antitumor agents and EGFR-TKIs.

Fig. 6. The ORTEP plots of compounds **2c (A)** and **2f (B)**.

Fig. 7. % Inhibition of $EGFR^{WT}$ by compounds **2e, 2h, 5b, 5c, 6a, 7d** and **9b** at concentration of 10 μM.

Fig. 8. % Inhibition of kinase activity induced by compound **7d (**at 10 μM).

Fig. 9. Bar diagram showing % cell distribution in G0/G1, S, G2/M and Pre-G1 phases for HepG2, HCT-116 and MCF-7 cells treated with vehicle control and **7d** (at the IC_{50} of the corresponding cell line) for 24 h.

Fig. 10. Flow cytometry analysis of cell cycle phase distribution in HepG2, HCT-116 and MCF-7 cells after treatment with vehicle control and **7d** (at the IC_{50} of the corresponding cell line) for 24 h.

Fig. 11. Annexin V-FITC/PI double staining for detection of apoptosis in HepG2, HCT-116 and MCF-7 cells after treatment with **7d** (at the IC_{50} of the corresponding cell line) for 24 h. Q1 quadrant represents dead (necrotic) cells; Q2 quadrant represents late apoptosis; Q3 quadrant represents live cells; Q4 quadrant represents early apoptosis. Summation of early and late apoptosis represents total apoptosis.

Fig. 12. Bar diagram showing % apoptosis in HepG2, HCT-116 and MCF-7 cells treated with vehicle control and **7d** (at the IC_{50} of the corresponding cell line) for 24 h.

Fig. 13. Assessment of the effect of compound **7d** on Bax and Bcl-2 levels in HepG2, HCT-116 and MCF-7 cells.

Fig. 14. (A) 2D Interaction of **7d** with the binding site of $EGFR^{WT}$. **(B)** 3D Interaction of **7d** with the binding site of $EGFR^{WT}$. Atoms are colored as follows: cyan for carbon, light gey for hydrogen, blue for nitrogen, red for oxygen and green for chlorine. (PDB code: 3W2S).

Fig. 15. (A) 2D Interaction of **7d** with the binding site of $EGFR^{L858R}$. **(B)** 3D Interaction of **7d** with the binding site of $EGFR^{L858R}$. Atoms are colored as follows: cyan for carbon, light gey for hydrogen, blue for nitrogen, red for oxygen and green for chlorine. (PDB code: 4LQM).

Fig. 16. (A) 2D Interaction of **7d** with the binding site of $EGFR^{T790M}$. **(B)** 3D Interaction of **7d** with the binding site of $EGFR^{T790M}$. Atoms are colored as follows: cyan for carbon, light gey for hydrogen, blue for nitrogen, red for oxygen and green for chlorine. (PDB code: 2JIV).

Fig. 17. (A) 2D Interaction of **7d** with the binding site of JAK3. **(B)** 3D Interaction of **7d** with the binding site of JAK3. Atoms are colored as follows: cyan for carbon, light gey for hydrogen, blue for nitrogen, red for oxygen and green for chlorine. (PDB code: 5TTV).

Table 1. Results of antitumor screening of the newly synthesized compounds.

Table 2. Results of cytotoxicity against A431 and H1975 cancer cells, as well as WI38 and WISH normal cells.

Table 3. Cytotoxic selectivity against HepG2, HCT-116, MCF-7, A431 and H1975 cancer cells versus WI38 and WISH normal cells.

Table 4. $EGFR^{WT}$ inhibitory activity of the most active antitumor compounds.

Table 5. Kinase profile assay of compound **7d** against eight human kinases.

Table 6. Summary of hydrophobic interaction, number of hydrogen bonds, residues involved in hydrogen bonding interaction and docking interaction energy (kcal/mol) of compound **7d** with $EGFR^{WT}$, $EGFR^{L858R}$, $EGFR^{T790M}$ and JAK3.

Table 7. Calculated Veber's and Lipinski's rule parameters for the new compounds.

Table 8. *In silico* ADME properties of the new compounds.

Table 9. *In silico* prediction of toxicity risks in human and drug-likeness of the new compounds.

Scheme 1. Synthesis of compounds **2a-j.**

Scheme 2. Synthesis of compounds **3a-c, 4a-h, 5a-f** and **6a,b.**

Scheme 3. Synthesis of compounds **7a-d, 8a,b** and **9a,b.**

The authors declare that they have no known competing financial interests or personal relationships that could have appeared to influence the work reported in this paper.

Design, synthesis and biological evaluation of new series of hexahydroquinoline and fused quinoline derivatives as potent inhibitors of wild-type EGFR and mutant EGFR (L858R and T790M)

Mennatallah A. Shaheen, Ali A. El-Emam, Nadia S. El-Gohary

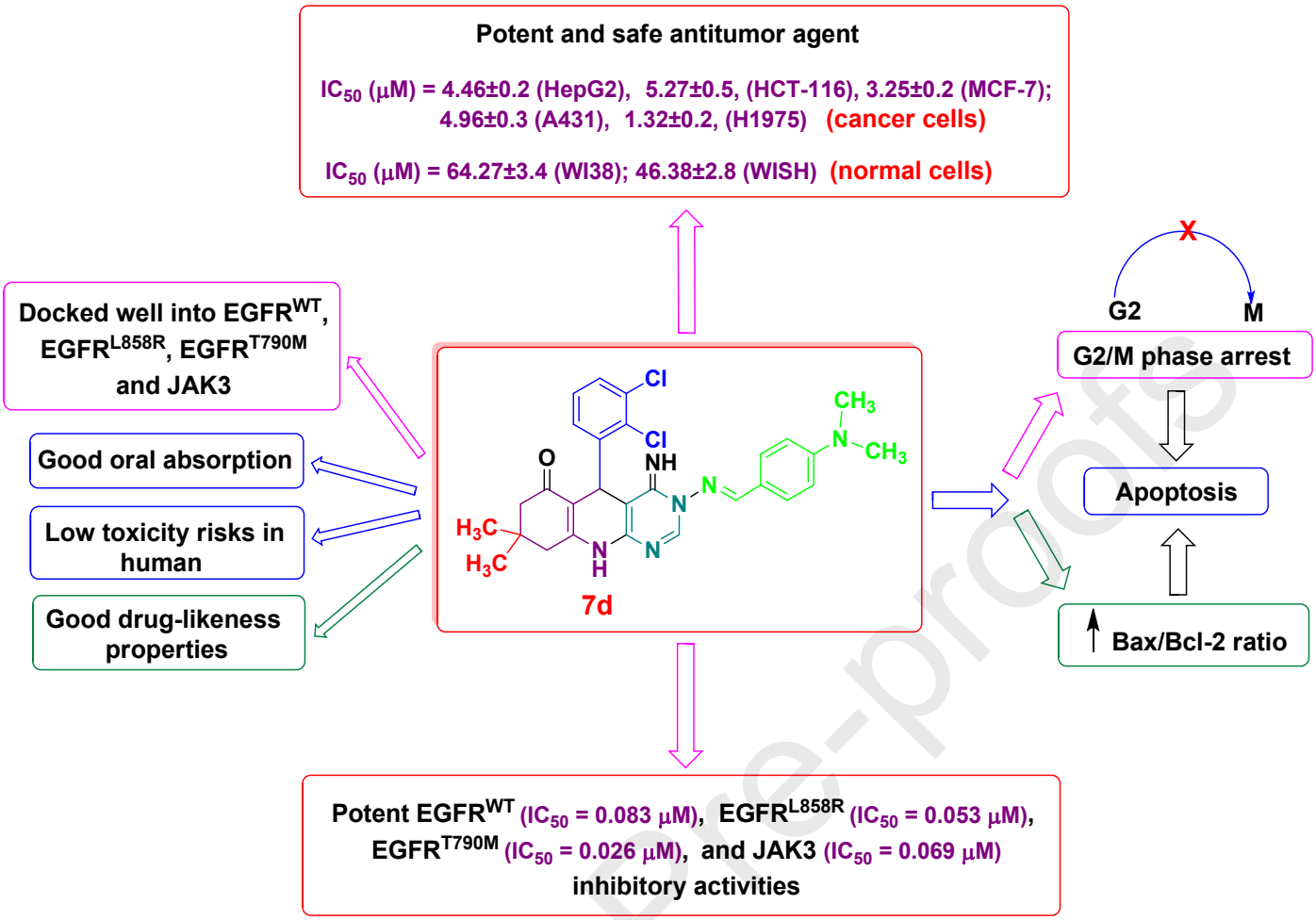

- New hexahydroquinolines and fused quinolines were prepared.
- The new analogs were screened for their antitumor activity
- Analog **7d** showed potent and safe antitumor activity
- Analog **7d** showed obvious inhibition of $EGFR^{WT}$, $EGFR^{T790M}$, $EGFR^{L858R}$ and JAK3
- Analog **7d** induced cell cycle arrest in G2/M and pre-G1 phases
- Analog **7d** induced cell death through apoptosis supported by increased Bax/Bcl-2 ratio